STUDY OF BIOPOLYMER GELS BASED ON POLYHYDROXYALKONATES

A THESIS SUBMITTED TO THE

SAVITRIBAI PHULE PUNE UNIVERSITY

FOR THE DEGREE OF

DOCTOR OF PHILOSOPHY (Ph.D.)

IN

CHEMICAL ENGINEERING

BY

Prashant A. Patil

Dr. ASHISH LELE

(RESEARCH GUIDE)

Dr. JYOTI JOG

(RESEARCH CO-GUIDE)

POLYMER SCIENCE AND ENGINEERING DIVISION
CSIR-NATIONAL CHEMICAL LABORATORY
PUNE - 411008 (INDIA)

SEPTEMBER 2018

CERTIFICATE

This is to certify that the work presented in the thesis entitled "**Study of biopolymer gels based on Polyhydroxyalkonates**" by **Mr. Prashant A. Patil**, submitted for the degree **Doctor of Philosophy** in **Chemical Engineering** was carried out under my supervision at the Polymer Science and Engineering Division, CSIR-National Chemical Laboratory, Pune, 411008, India. Such material as has been obtained from other sources has been duly acknowledged in the thesis.

Dr. Ashish Lele **Dr. Jyoti P. Jog**

(Research Guide) **(Research Co-Guide)**

Date:

Place: CSIR-NCL, Pune

DECLARATION

I hereby declare that the work presented in the thesis entitled "**Study of biopolymer gels based on Polyhydroxyalkonates",** submitted for Ph.D. Degree in **Chemical Engineering** to the Savitribai Phule Pune University, has been carried out under the supervision of **Dr. Ashish Lele and Dr. Jyoti P. Jog** at the Polymer Science and Engineering Division, CSIR-National Chemical Laboratory, Pune. The work is original and has not been submitted in part or in full by me for any degree or diploma to this or any other University.

Mr. Prashant A. Patil

(**Research Student)**

Date:

Place: CSIR-NCL, Pune

Dedicated to my beloved parents

ACKNOWLEDGEMENTS

It gives immense pleasure to thank my mentor Dr. Ashish Lele and Dr. Jyoti Jog for their motivation, suggestions, and invaluable guidance during my PhD. I am also thankful to them for giving me freedom for doing research.

I would like to express my gratitude to Dr. Harshwardhan Pol, Mr. Vivek Borkar, Dr. Anuya Nisal, Dr Neelima Bulakh, Mrs. Sangeeta Hambhir, Mrs Poorvi Purohit, Dr. V Premnath and Dr. K Guruswamy and Dr. Ashish Orpe for help, inspiration and moral support. I would like to thank Dr. Suresh Bhat for suggestions on light scattering experiments.

I am thankful to my colleagues Sameer, Dr. Amruta Kulkarni, Dr. Kalyani Chikhalikar, Dr. Samrudhi Kamble, Dr. Deepti Marathe, Dr. Indravardhan, Aniket, Ramendra, Dr. Manoj, Akash, Dr. Venugopal, Dr. Somyajyoti Chatterji, Dr. Seena Joseph, Dr. Shailesh Nagarkar, Dr. Chirag Kalelkar, K J Kiran, Fayis, Dr. Chetan, Amol, Dr. Lily, Dr. Santosh, Dr. Rajendra, and Bharitiji for their help and encouragement. Thank you all for making this journey memorable.

I would like to thank my special friends Kishor Desale, Manoj Ghodmare, Prashant Baviskar, Bhupal Patil, Bhupendra Mali, Sandip Patil and Bipin Rokade for support and encouraging me. I would like to thank Anshu and Priyal for happy and lively moments.

A special thanks to Abhijeet, Vinayak, Swapnil and Sagar for cheering me.

I would like to express my gratitude to K D Deshpande Sir, Sanjay sir, Avinash sir, and DIRC team for support and assistance during my stay in NCL.

I am thankful to Dr. Sunita Barve and CSIR-NCL- KRC Library group for help and support.

I would like to thank staff and students from PSE and PAML lab for creating such a friendly research environment.

I am thankful to Council of Scientific and Industrial research for SRF funding.

I would like to thank Chavan madam, Savitribai Phule Pune University, for her generous help in the administrative matter.

I am thankful to PAM cricket team and NCL colony cricket team players for the sporty and healthy environment during my stay in NCL.

I would like to express my gratitude to Poonam tai, Tushar Zope, Jitendra, Sapna, Prath, Pranit and Atharva for continuous support and encouragement during my research. Finally, I would like to thank my wife Dr. M Dhanalakshmi for her patience and moral support. I am thankful to her for always standing with me in sun and shower.

Prashant Patil

Table of contents

List of figures

List of tables

List of Abbreviations

PHB	Poly(3-hydroxybutyrate)
PHBV	Poly(3-hydroxybutyrate co 3-hydroxy valarate)
SEM	Scanning electron microscope
DSC	Differential scanning calorimetry
3-D	Three dimensional
HAP	Hydroxyapatite
TRMS	Time resolved mechanical spectroscopy
TIPS	Thermally induced phase separation
DLS	Dynamic light scattering
UCST	Upper critical solution temperature

List of symbols

n	Relaxation exponent
G'	Storage modulus
G"	Loss modulus
G(t)	Relaxation modulus
n	Relaxation exponent
S	Strength of gel
n	Avrami index
t	Time
λ	Relaxation time
γ	Strain
δ	Damping factor
ω	Angular frequency
q	Scattering vector
θ	Scattering angle
λ	Wavelength of laser
n	Refractive index
N_{mu}	Mutation number
λ_{mu}	Mutation time
G(t)	Modulus at time t
G(P)	Plateau modulus

Gt_i	Initial modulus,
X(t)	Crystalline fraction
ϕ	Cooling rate
T	Temperature
Z	Rate
$^{g}_{1}(\tau)$	Electric field correlation function
D	Diffusion coefficient
η	Viscosity
ΔH_f	Heat of fusion
K_b	Boltzman constant
ε	Elongation

ABSTRACT

PHBV is naturally occurring biopolymer synthesized by bacteria. PHBV's biocompatibility and biodegradability makes it an attractive tissue engineering material. There are various methods reported in the literature for making scaffolds; a few examples are electrospinning, particle leaching, phase inversion, and thermally induced phase separation method (TIPS). Thermally induced phase separation process is used for the preparation of microporous scaffolds. In this work, we have undertaken fundamental studies on understanding the TIPS process for PHBV/solvent systems, which can, in future be used to tailor-make scaffolds of controlled morphology from PHBV. PHBV shows a thermoreversible sol-gel transition in chlorobenzene. The kinetics of thermally induced phase separation, morphology and final properties of the phase-separated structure formed during gelation are dependent on various processing parameters such as the concentration of the polymer, quench rate, and quench temperature, and solvents. Hence in order to relate the structure formed during gelation, it is imperative to study the kinetics of phase separation/gelation process. This work is a fundamental study to probe isothermal and nonisothermal gelation kinetics mainly using rheology and dynamic light scattering techniques.

Kinetics of gelation shows three stages of gelation. First stage (I) of gelation consists of initial induction phase and incipient gelation. First stage of gelation analyzed for induction phase. Induction times scales as exponentially indicating predominantly nucleation and growth event. Incipient gelation phase analyzed for Winter Chambon criteria for gel point detection. Time resolved mechanical spectroscopy technique used for determination of the sol-gel transition. At gel point,

the damping factor becomes independent of frequency. The relaxation exponent close to 0.6 suggests the gelation occur before the crossover point G' and G". The second rapid gelation phase (II) was studied using an equation similar to the Avrami equation. The Avrami exponent close to 3 and 4 suggests 3-dimensional growth of the structure. The effect of quench temperature and concentration on the formation of the structure was presented.

Nonisothermal gelation kinetics analyzed for initial incipient gelation (I) analyzed for Winter Chambon criteria to determine so-gel transition. The gel strength is higher in non-isothermal conditions suggests the gels formed under nonisothermal conditions are stiffer. Heating and cooling cycle, suggest hysteresis indicating first order process. The effect of heating and cooling rate gels suggest a degree of undercooling for structure formation increases with cooling rate. The rapid gelation stage (II) under nonisothermal condition analyzed using equation similar to modified Avrami equation. The Avrami exponent close to 3 suggesting 3-dimensional growth of the network.

The dynamic light scattering on sol-gel transition was studied under isothermal condition. The autocorrelation function during different stages of gelation monitored. In the initial sol state autocorrelation function decays faster. In rapid gelation stage (II), autocorrelation function shows delay in the autocorrelation function. In the third stage of gelation, the phase gets arrested and no significant change in autocorrelation function was observed.

Chapter 1

Introduction

1.1 Introduction

Poly(3-hydroxybutyrate-co-3-hydroxy valerate) or PHBV is a biodegradable and biocompatible polymer belonging to the generic group of aliphatic polyesters called Polyhydroxyalkonates (PHA), which are produced by microorganisms under unbalanced growth conditions[1]. A few examples of PHA's are Poly(3-hydroxybutyrate) (PHB), Poly(3-hydroxyvalerate) (PHV) Copolymer of Poly(3-hydroxy butyrate valerate co 3-hydroxy valerate) (PHBV), Poly(3-hydroxy Octanaote) (PHO) and Poly3-hydroxyhexonate (PHBHHx). Among all of these, PHBV is the most widely produced and studied copolymer. PHBV is synthesized as an energy reserve material by numerous micro-organisms such as Escherichia Coli, Paracoccusdenitrificans, Ralstoniaeutropha, H halmonas, E eturopha, A. eutrophus, A. latus, A. faecalis, A. ruhlandii and A. aquamarinus. It can be produced at a larger scale using aerobic and anaerobic fermentation processes [2–4]. PHBV is considered to be a possible alternative to synthetic non-biodegradable polymers made from petroleum [5]. The structure of PHBV is shown in figure 1.1

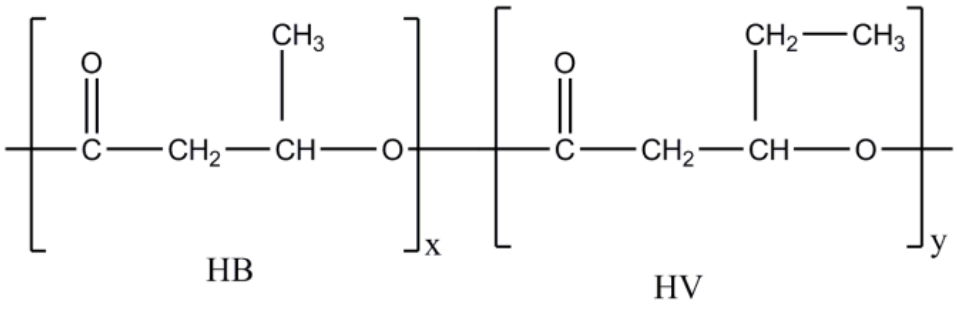

Figure 1.1 Chemical structure of PHBV

Poly(3-hydroxy butyrate) or PHB is an electrically active and optically active biopolymer[6]. Mechanically stretched PHB chains are rich in shear piezoelectricity. It is a semi-crystalline polymer with a high melting temperature and a high degree of crystallinity. PHB is insoluble in water but is soluble in chlorinated hydrocarbons[7]. It has good barrier properties. The reported values of Young's modulus and tensile strength of PHB are comparable to polypropylene (PP)**.** The addition of hydroxyvalerate (HV) to PHB increases impact strength, toughness, and ductility but

reduces stiffness and tensile strength relative to the PHB homopolymer. The PHBV bio degraded in order of PHBV 40 > PHBV 20 > PHBV 3 and PHB[8]. PHAs, PHBV is also thermally unstable and has a narrow processing window[9] and expensive. Table 1.1 shows thermal and mechanical properties of PHBV.

Table 1.1 Thermal and mechanical properties of PHBV (source: eXPRESS Polymer Letters Vol.8, No.11 (2014) 791–808)

Product	**Thermal properties**			**Mechanical properties**		
	Tm [^{o}C]	X_{cr} [%]	Tc [^{o}C]	E [GPa]	σ [MPa]	ε (%)
Biomer P209	-	30-40	-	0.84-1.20	15-20	600-1200
Biomer P226	-	60-70	-	1.14-1.90	24-27	6-9
Biomer P240	-	60-70	-	1.85	28	11
BIOCYCLE 1000	170-175	-	117	2.2 (Flex)	32	4.0
BIOCYCLE 18BC-1	165-170	-	117	2.4 (Flex)	25	2.2
BIOCYCLE 189C-1	165-170	-	121	2.6 (Flex)	30	2.2
BIOCYCLE189D-1	154-170		125	3.8 (Flex)	36	2.0
ENMAT Y1000	170-176	-	-	2.8-3.5	39	2
MirelP4001	-	-	110	1.90 (Flex)	20	5
MirelP4010	-	-	-	1.45 (Flex)	10	10
MirelP5001	-	-	-	0.30-0.4	20	404-463
MirelP5004	170	-	-	-	25-30	400-500
MirelM2100	170	-	-	-	-	-
Mirel M2200	165-170	30-60	-	-	-	-
Mirel M4100	160-170	40-60	-	-	-	-
	164-166	27-45	-		-	-

1.2 Application of PHBV

Commercially available Polyhydroxyalkonates are listed in Table 1.2. PHA was initially explored for applications in food packaging[10], its high cost is the most important limiting factor for such large volume applications. Therefore, PHBV is increasingly explored for high-value biomedical applications. It has been used to develop many biomedical products such as sutures, suture fasteners, rivets, screws, bone plates and surgical mesh etc[11–13]. PHBV also is used in formulations for controlled release of drugs and for making biodegradable scaffolds in tissue engineering applications[14–17].

Table 1.2 Commercially available polyhydroxyalkanoate, supplier and products[18] (source: eXPRESS Polymer Letters Vol.8, No.11 (2014) 791–808)

Commercial name	Producer	Country	Product
Biomer	Biomer	Germany	Biomer P209 Biomer P226 Biomer P240
Minerv-PHA	Bio-On	Italy	Minerv-PHA
Biogreen	Mistshubishi Gas	Japan	Biogreen
Biocycle	PHB Industrial	Brazil	BIOCYCLE 1000 BIOCYCLE 18BC-1 BIOCYCLE 189C-1 BIOCYCLE189D-1
Ecogen	Tianan Biological Materials Polyone	China	ENMAT Y1000 ENMAT Y1000P ENMAT Y3000 ENMAT Y3000P

Mirel	Metabolix	USA	Mirel P4001 Mirel P4010 Mirel P5001 Mirel P5004 Mirel M2100 Mirel M2200 Mirel M4100
Nodax	P&G chemicals	USA/Japan	Nodax™
Metabolix	Telles LLC	USA	Mvera™ B5011 Mvera™ B5010
Jiangsu Nantian	Jiangsu Nantian Group	China	P(3HB)
Goodfellow	Goodfellow Cambridge Ltd	UK	Polyhydroxyalkaonates- Biopolymer (PHA) PHBV (PHB98/PHV2%) Polyhydroxyalkaonates/polyhydroxyvalarate 12% Biopolymer (PHB88/PHV12)
Tepha (86)	Tepha INC	USA	P(4HB)

In this thesis, we have used PHBV 2% HV supplied from Goodfellow, UK.

1.3 Gels

Gelation of polymer solutions is of great practical and theoretical interest today. The gel is a state of matter between solid and liquid[19]. It consists of a sample spanning a network of microstructural motifs that are held together by attractive or repulsive forces. In several systems, gels are formed due to incomplete phase separation. In such gels, there are at least two phases: a liquid continuous phase and the gelator as a dispersed or co-continuous phase. Though a gel contains large amounts of a liquid, it

is characterized by the dynamically arrested state in which structural motifs forming a network structure in the gel exhibit highly retarded motions. Gels are typically classified into two broad categories: Type I gel (physical gel) and Type II gel (chemical gel). In Type I gels, the network structure is formed by secondary forces such as van der waal forces, hydrogen bonding, ionic interactions and hydrophobic interactions. These gels have temporary associations between chains. They are reversible in nature and sensitive to environmental changes such as temperature, pH, light, and electric field, etc. Yogurt, jelly, agar gels are the typical examples of such gels. Type II gels i.e., chemical gels involve the formation of covalent bonds and always results in a strong gel. Covalently cross-linked molecular networks of polymers that are swollen in the liquid are good examples of these gels.

Recently, polymer gels, hydrogels and organogels have increasingly attracted attention of researchers because of their diverse applications in food, pharmaceuticals, cosmetics and biomedical industry[20–22]. Many biopolymers form gels in aqueous or organic solutions. Network formation during gelation is a kinetic process and there is considerable theoretical and experimental interest in understanding the mechanism and kinetics of these processes. Such understanding can be used to tailor the microstructure of the gels and hence their properties. In this thesis we have investigated thermoreversible gels formed from PHBV solutions in organic solvents. In particular, this thesis reports on detailed investigations of the gelation kinetics of PHBV gels in chlorobenzene using rheological and light scattering techniques. Such gels, upon complete removal of the solvent, are expected to have biomedical applications in tissue engineering and drug delivery vehicles.

1.3.1 Sol-gel transition (Winter-Chambon Criteria)

Thermoreversible gelation is a process by which sol-to-gel or the reverse process occurs upon changing the temperature. One of the critical properties of a thermoreversible gel is its sol-gel transition temperature. Alternatively, one may define a gelation time for an isothermal gelation process. The gelation temperature or the gelation time can be thought of as the “gel point” that unambiguously defines conversion of sol into gel. A simplistic way to determine the gel point of a thermoreversible gel is the “vial inversion” method wherein a vial containing a sample is inverted at different temperatures during gelation. The temperature (or time) at which the sample does not flow is crudely taken as the gel point. More rigorously,

gel point is determined rheologically in a temperature-sweep (or time-sweep) dynamic oscillatory experiment in which the viscoelastic moduli of the sample are measured at a constant strain amplitude and frequency in an imposed oscillatory shear experiment while simultaneously ramping the temperature at an appropriate heating/cooling rate (or holding isothermal and marching in time). It is then assumed that the temperature (or time) at which the storage modulus (G') crosses over loss modulus (G") is the gelation temperature of the system. However, it turns out that the gelation point determined in this manner is a function of frequency. Hence the crossover point is not an unambiguously defined gel point of the system. Winter and Chambon proposed an experimental methodology to determine the gel point unambiguously. They performed dynamic mechanical experiments on PDMS while it was undergoing cross-linking[23]. The utilized a chemistry that allowed for the crosslinking reaction to be quenched at different times during the dynamic mechanical test. Frequency sweep tests were performed at selected times before and after the crossover point observed in an isothermal time-sweep test (see figure 1.2 a). The corresponding frequency sweep data is shown in figure 1.2 b).

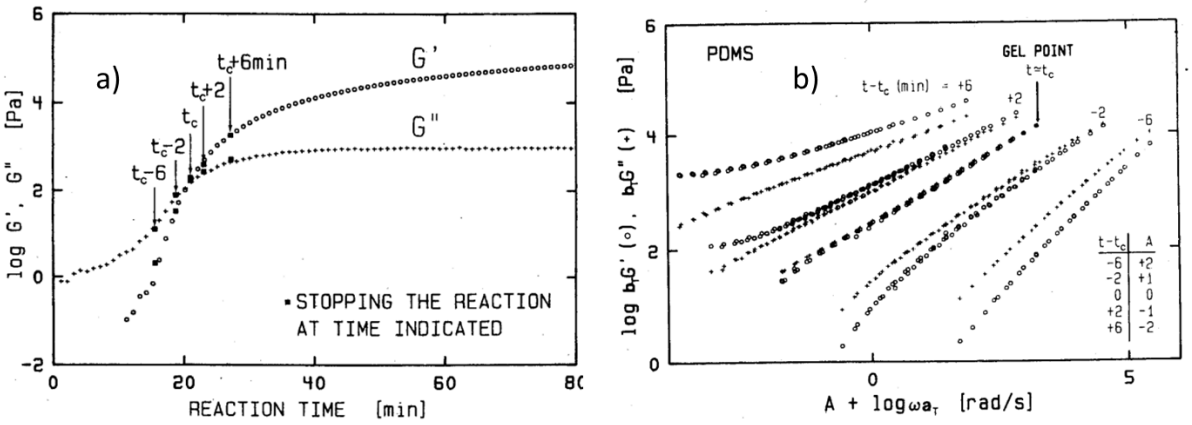

Figure 1.2 Dynamic mechanical test on PDMS gel (reprinted with permission from H H Winter and F Chambon, "Analysis of liner viscoelasticity of crosslinking polymer at gel point", Journal of rheology, 30(2)1986, 367-382. Copy right 1986. The society of rheology.)

The frequency sweep data before the crossover shows G" > G' indicating liquid-like behavior. For this gel it turns out that the frequency sweep data at the crossover time shows congruency of moduli. After the crossover point, the system shows G' > G".

Thus, at the gel point,

$$G' \sim G'' \sim \omega^n$$

Since, G' and G'' are related by Krammer-Kronig relation:

$$G'(\omega) = \frac{2}{\pi}\int_0^\infty \frac{G''(x)}{1-(\frac{x}{\omega})^2}\frac{dx}{x}$$

This leads to the conclusion that damping factor must be constant in a multi-frequency test at gel point i.e., the damping factor must be independent of frequency at the true gel point. The figure 1.3 shows the damping factor as a function of time for different frequency[24].

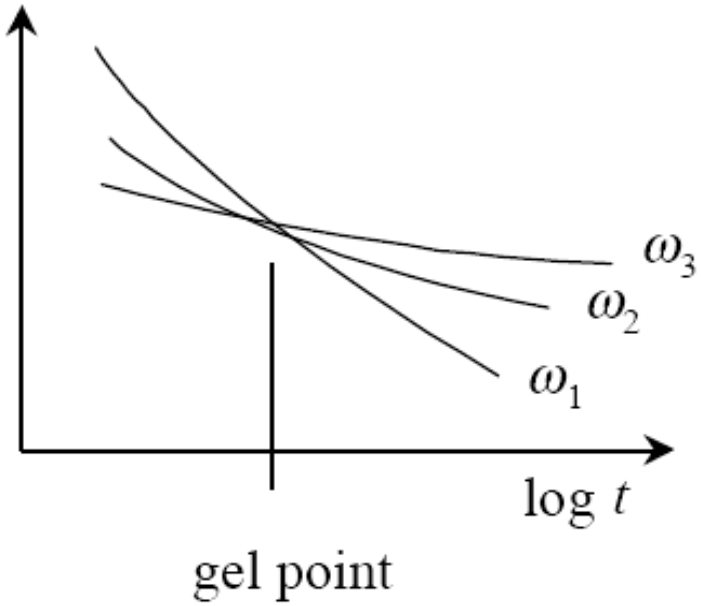

Figure 1.3 Damping factor Vs. time.

At the gel point the damping factor must be given by

$$\tan\delta = \tan(\frac{n\pi}{2})$$

This is unique criteria was found to be obeyed by physical as well as chemical gels. The congruency of moduli at the gel point also leads to the conclusion that the stress relaxation modulus must have a power-law time dependence given by

$$G(t) = St^{-n},$$

where, G(t) = relaxation modulus, S = Strength of gel ($Pa.s^{1/n}$) and n is relaxation exponent. This is the constitutive equation of the gel.

Structure formation during thermoreversible gelation is a kinetic process and depends on state variables and processing parameters such as the concentration of polymer, quench rate, quench temperature and nature of solvent. There is considerable theoretical and experimental interest in understanding the mechanism and kinetics of gelation processes. Such understanding can be used to tailor the structure and hence the properties of gels. Hence, to understand how structure forms during gelation, it is imperative to study the kinetics of phase separation/gelation process.

1.4 Thermally induced phase separation (TIPS; also called Temperature-induced phase separation).

Scaffold-based tissue engineering is an exciting and emerging field in recent years[25]. The primary role of a scaffold in tissue engineering is to provide support for cells to adhere and grow. Polymers have been widely used as biomaterials for the fabrication of scaffolds. Biocompatible and biodegradable natural polymers such as silk, Polyhydroxybutyrate, chitosan, gelatin and collagen has been successfully used to make scaffolds for tissue engineering applications[26–28]. The main requirements of a scaffold material are listed below

- Three-dimensional structures.
- Biocompatible and biodegradable.
- High surface area.
- High porosity and interconnected pores to allow cell migration and transfer of nutrition and metabolic waste.
- Adequate mechanical strength.

- Non-toxicity to the cells.
- Appropriate degradation rate to match the rate of new tissue formation.
- Positive interaction with cells to promote enhanced cell adhesion, growth, migration and differentiation.

Many fabrication methods are available to make polymer scaffolds. Some examples are 3-D printing [29,30], solvent casting[31,32], particulate–leaching, drawing, template synthesis, phase separation, self-assembly, freeze drying[33,34] and electrostatic spinning[35–37] (electrospinning). TIPS technique is an easily implementable method to fabricate porous polymer scaffolds[38–40].

In the TIPS process, temperature is the driving force for phase separation into polymer rich and polymer lean phase. If the polymer is semi-crystalline, phase separation is often followed by crystallization of the polymer from the polymer-rich phase. A typical polymer-solvent phase diagram is shown in figure1.4. At a high temperature above the binodal line, the polymer solution is homogeneous. Binodal curve separates the homogeneous phase from the metastable phases on the phase diagram. When the polymer solution is quenched below the binodal line, the polymer phase separates into two phases, a polymer rich and polymer lean phase. The area between the binodal and spinodal curve is a metastable state, where the two phases are in equilibrium. The spinodal curve separates the metastable state and unstable state. Once phase separation is initiated, it continues until the polymer-rich phase becomes immobilized by gelation, glass transition, or crystallization. Once this occurs, the structure is effectively frozen into place, and the solvent can be removed from the film. Scaffold morphology is controlled by the mechanism of the initial phase separation, the kinetics of domain growth following phase separation, and the exact way in which the solidification process interrupts domain growth.

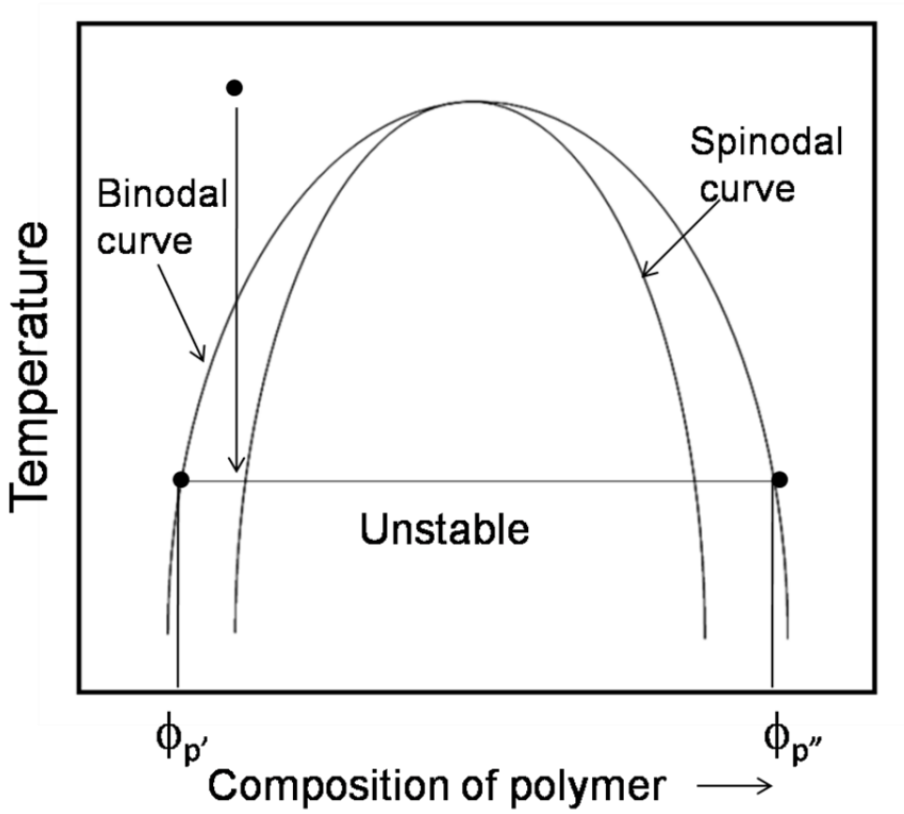

Figure 1.4 Polymer solvent phase diagram showing upper critical solution temperature

The main advantages of the TIPS process are listed below.

- Scaffolds have highly porous and interconnected foam structure, which is suitable for cell growth and proliferation.
- Scaffolds of complex shape and large size can be made with relative ease.
- A wide range of polymers can be processed into scaffolds.
- Bioactive materials can be incorporated in the scaffolds.

The main drawback of the TIPS process is the fact that residual solvent can be left in the scaffolds, which could be highly cytotoxic. Therefore, removal of traces of residual solvent is important.

1.5 Literature review

1.5.1 Literature review on PHB/PHBV

PHA was first discovered in 1925 by Lemoigne et al. Between 1950 and 1960 Baptist and coworkers at W. R.Grace and Co. USA produced sufficient quantities of PHB for commercial evaluation. However, low yield of fermentation products and isolation of the polymer was expensive. In 1970, ICI produces upto 70% of dry cell weight of PHB using large-scale fermentation process with optimized conditions. It was later discovered that the properties of PHB are much improved by producing PHBV. In, 1990, the first product of Biopol, a biodegradable shampoo bottle, was made by Wella AG, Darmstadt. Since then the use of PHBV in food packing and biomedical applications has gradually increased[41].

1.5.2 Literature review on PHB/PHBV gels

Andrij Pich et al reported thermoreversible gelation of biodegradable polyester poly (3-hydroxybutyrate-co-3-hydroxyvalerate) (PHBV) in toluene[42]. Interestingly, hot PHBV solutions became transparent gels after cooling to room temperature. This physical gelation process was followed by light scattering and viscosity measurements for solutions of different PHBV concentrations. It was found that gelation temperature increases with increasing polymer concentration in toluene. PHBV films were prepared on solid substrates by gelation process followed by solvent removal. PHBV concentration in the solution was observed to influence the surface morphology of obtained films. Homogeneous PHBV films with increased surface roughness can be obtained by means of this technique. Hydrolytic degradation studies indicated that surface morphology of PHBV layers changes considerably with degradation time.

Recently, Brian J. Sobieskiet al. studied a biodegradable thermally reversible gel made from poly[(R)-3- hydroxybutyrate-co-(R)-3-hydroxyhexanoate] (PHBHx) in dimethylformamide (DMF) solutions[43]. The polymer concentrations were 2, 3, 4, 5,7,10 and 15%. SEM images revealed that microscopic phase separation occurred between the polymer and the solvent, resulting in a network of PHBHx ribbons and fibrils, less than a micrometer in width and thickness, suspended in the solvent. As the concentration of the polymer increases, the morphology of the system did not change, but the polymer regions increased in density.

Bordi et al. measured thermal and dielectric properties of poly(3-hydroxybutyrate) in dimethyl formamide at a concentration of 10 g L^{-1}. The behavior of the gel permittivity and conductivity, compared with those of the solvent as well as of the solution at higher temperatures, confirmed the presence of a melting process in the system upon heating[44]. The heat evolved in this process, as well as the frequency range of the permittivity and conductivity, indicated the presence of polymeric moieties, organized in crystalline supra molecular clusters.

1.5.3 PHBV scaffolds

There are several reports on PHB scaffolds prepared by different techniques but only a few using the TIPS process. The key research papers are summarized below.
Naznin Sultana and Min Wang etal reported that poly(hydroxybutyrate-co-valerate) (PHBV)-/Hydroxyapatite (HA) scaffolds prepared by TIPS process had osteoconductive property, which is useful for bone tissue engineering. HA-PHBV scaffolds were prepared by using an emulsion freezing/freeze-drying technique[45]. The scaffolds were highly porous and had interconnected porous structures. The incorporation of HA nanoparticles also helps to enhance compressive mechanical properties of the scaffolds.

In 2013, Jun Wu et al reported scaffolds of poly(hydroxybutyrate-co-hydroxyvalerate) (PHBV)/ Bioglass (BG). They showed that the incorporation of BG into PHBV can improve the hydrophilicity of the composites[46]. They compared the effects of PHBV scaffolds and PHBV/BG composite scaffolds on the properties of engineered cartilage *in vivo*. Rabbit articular chondrocytes were seeded into PHBV scaffolds and PHBV/BG scaffolds. Short-term *in vitro* culture followed by long-term *in vivo* transplantation were performed to evaluate the difference in cartilage regeneration between the cartilage layers grown on PHBV and PHBV/BG scaffolds. The results showed that the incorporation of BG into PHBV efficiently improved both the hydrophilicity of the composites and the percentage of adhered cells and promoted cell migration into the inner part the constructs. With prolonged incubation time *in vivo*, the chondrocyte-scaffold constructs in the PHBV/BG group formed thicker cartilage-like tissue with better bio mechanical properties and a higher cartilage matrix content than the constructs in the PHBV/BG group. These results indicate that

PHBV/BG scaffolds can be used to prepare better-engineered cartilage than pure PHBV.

Recently, Takashi Tsujimoto et al. demonstrated fabrication of biodegradable porous materials from bacterial polyester, poly(3-hydroxybutyrate-co-3-hydroxyhexanoate) (P3HB3HHx) via thermally induced phase separation[47]. P3HB3HHx monoliths with topological porous structure were prepared by dissolution of P3HB3HHx in dimethyl sulfoxide (DMSO) at 85 ^{o}C and subsequent quenching. The microstructure of the resulting P3HB3HHx monoliths was changed by the P3HB3HHx concentration of the polymer solution. Differential scanning calorimetry and polarized optical microscopy analysis revealed that the P3HB3HHx monoliths crystallized during phase separation and subsequent aging. The mechanical properties, such as compression modulus and stress of the monoliths depended on the 3-hydroxyhexanoate content of P3HB3HHx.

Wei Huang et al. studied scaffolds by embedding poly (b-hydroxybutyrate-co-b-hydroxyvalerate) (PHBV) microspheres into poly (L-lactic-coglycolic acid) (PLGA) matrix. The morphology of the hybrid scaffold was rougher than that of pure PLGA scaffold, which had no significant effect on the cell behavior. The *in vitro* evaluation suggested that the model is suitable as a scaffold for engineering bone tissue and has the potential for further applications in drug delivery system.

Ruiz1, É B Hermida et al. studied the porous scaffolds of poly(3-hydroxybutyrate-co-3-hydroxyvalerate) prepared by three different techniques: salt leaching (SL), emulsion solvent evaporation (ESE) and temperature induced phase separation (TIPS)[48]. For SL, partially fused sieved grains of sodium chloride (106-355 μm) were used as a porogen. In case of ESE, aqueous emulsions prepared from a solution of PHBV in chloroform allowed formation of flexible films. The content of surfactant was used to control pore size. For scaffolds made by TIPS, the pore size was found to decrease on increasing cooling rate, and the morphology of the interconnected structure could be controlled by changing the temperature gradient.

Chao Li et al. investigated poly (L-lactide-co-ε-caprolactone) (PLCL) / poly (β-hydroxybutyrate-co-β-hydroxyvalerate) microsphere scaffolds for cartilage tissue engineering[49]. Microspheres were fabricated by using an emulsion solvent evaporation method. Compressive modulus, surface topography and porosity of the composite scaffolds were studied. The *in vitro* and *in vivo* chondrogenesis within the chondrocyte-laden scaffolds was investigated by examining the proliferation of

chondrocytes and the deposition of glycosaminoglycan (GAG) and type II collagen. The incorporation of PLCL within PHBV microspheres showed no significant effects on adhesion at 6h. *In vitro* cartilage formation and proliferation of the chondrocytes at both 2 weeks and 4 weeks, as well as total contents of GAG and type II collagen excreted increased significantly with time. The incorporation of PHBV microspheres not only enhanced the compressive modulus of PLCL scaffolds but could also serve as scaffolding structures for cartilaginous tissue formation.

1.5.4 Degradation studies of PHBV

Degradation studies on PHBV have been reported by many researchers. Degradation agents studied include enzymes, temperature, air, soil and heat. The key papers are summarized below.

Yoshihiro Aoyagi et al. investigated thermal degradation of poly[(R)-3-hydroxybutyrate] (PHB), poly[e-caprolactone] (PCL), and poly[(S)-lactide] (PLA) under both isothermal and non-isothermal conditions[50]. They reported time evolution of weight loss and number–average degree of polymerization, reflecting the different degradation mechanisms. Thermo-gravimetric analysis showed that PHB is degraded by random chain scission (cis-elimination), while PCL is degraded by unzipping depolymerization from the hydroxyl end of the polymer chains. In contrast, the thermal degradation behavior of PLA was very complex.

A. Spyros and R. Kimmich et al. studied enzymatic degradation of poly(3-hydroxybutyrate), PHB, and poly(3-hydroxybutyrate-co-23%-3-hydroxyvalerate), PHBV by depolymerase B from Pseudomonas lemoignei[51]. Degradation samples were prepared by melt pressing. Degradation studies were performed in buffer solutions of double-distilled water containing 50 mM Tris-HCl, pH 8.0, 1 mM CaCl2, and a depolymerase B concentration of 3 µg/mL without shaking.

Deroine Morgan et al. demonstrated the natural degradation and biodegradation of poly(3-hydroxybutyrate-co-3-hydroxyvalerate) (PHBV) films in different marine environments. PHBV films were kept in seawater for 180 days and percent degradation was calculated by weight loss of the PHBV film.

Idayu Muhamad et al. studied the hydrolytic degradation of poly-β-(hydroxybutyrate) PHB, poly-β-(hydroxybutyrate-co-β-valerate) (PHBV) and

PHBV/cellulose triacetate blend in different pH at 37 °C. PHBV showed similar degradation trend to PHB in the higher alkaline medium[52]. In the presence of cellulose triacetate, the water uptake in the blend and permeability increased which favored the hydrolytic degradation especially in lower pH medium. The degradation rate was slow in acidic hydrolytic medium but increased when the pH of the medium was increased from pH 7.4 to pH 13.

Hui Liu et al. demonstrated the influence of hydroxyvalerate composition of PHBV copolymer on bone cell viability and *in vitro* degradation[53]. Degradation was studied by monitoring time-dependent changes in mass and chemical composition of the micro porous films. The mass loss of PHBV film upon 19 weeks of exposure to pH 7.4 phosphate buffer medium was found to range from 2.8% to 9.2% with a strong dependence on the original composition of the co polyester film and morphology. The NMR results showed a significant decrease in the mol % of HV content in the degraded PHBV film.

Luis Cabedo et al. studied the degradation of polyhydroxybutyrate-co-valerate during processing with clay-based nanofillers. PHBV was processed with trilayered clays using different mixing methods, and the effect of processing time, clay type, and clay content on polymer molecular weight and composite morphology was studied[54]. Molecular weight (Mw) of PHBV was found to decrease by 38% after extrusion processing and was further reduced in the presence of montmorillonite (MMT). However, when PHBV was processed with kaolinite as the additive, no further reduction in polymer molecular weight was observed.

1.5. Summary

PHBV is naturally occurring biopolymer synthesized by bacteria. This polymer has potential application in biomedical, packaging. The biocompatible and biodegradability makes it an attractive tissue engg. material. TIPS process can be efficiently used to prepare micro porous scaffolds. PHBV scaffolds can be prepared via TIPS processes. The various processing parameters such as sol-gel transition quench temperature and quench rate and concentration. Rheological techniques can be used to study the sol-gel transition and kinetics of gelation.

1.6 References:

1. Mohanty, A. K., Misra, M. & Drzal, L. T. Sustainable bio-composites from renewable resources: opportunities and challenges in the green materials world. *Journal of Polymers and the Environment* **10,** 19–26 (2002).

2. Khanna, S. & Srivastava, A. K. Statistical media optimization studies for growth and PHB production by Ralstonia eutropha. *Process Biochemistry* **40,** 2173–2182 (2005).

3. Gouda, M. K., Swellam, A. E. & Omar, S. H. Production of PHB by a Bacillus megaterium strain using sugarcane molasses and corn steep liquor as sole carbon and nitrogen sources. *Microbiological research* **156,** 201–207 (2001).

4. Valappil, S. P. *et al.* Large-scale production and efficient recovery of PHB with desirable material properties, from the newly characterised Bacillus cereus SPV. *Journal of Biotechnology* **132,** 251–258 (2007).

5. Yu, L., Dean, K. & Li, L. Polymer blends and composites from renewable resources. *Progress in polymer science* **31,** 576–602 (2006).

6. Shelton, J. R., Agostini, D. E. & Lando, J. B. Synthesis and characterization of poly-β-hydroxybutyrate. II. Synthesis of d-poly-β-hydroxybutyrate and the mechanism of ring-opening polymerization of β-butyrolactone. *Journal of Polymer Science Part A-1: Polymer Chemistry* **9,** 2789–2799 (1971).

7. Hahn, S. K., Chang, Y. K., Kim, B. S. & Chang, H. N. Optimization of microbial poly (3-hydroxybutyrate) recover using dispersions of sodium hypochlorite solution and chloroform. *Biotechnology and Bioengineering* **44,** 256–261 (1994).

8. Weng, Y.-X., Wang, X.-L. & Wang, Y.-Z. Biodegradation behavior of PHAs with different chemical structures under controlled composting conditions. *Polymer Testing* **30,** 372–380 (2011).

9. Qiu, Z., Ikehara, T. & Nishi, T. Miscibility and crystallization behaviour of biodegradable blends of two aliphatic polyesters. Poly (3-hydroxybutyrate-co-hydroxyvalerate) and poly (butylene succinate) blends. *Polymer* **44,** 7519–7527 (2003).

10. Sreekanth, M. S., Vijayendra, S. V. N., Joshi, G. J. & Shamala, T. R. Effect of carbon and nitrogen sources on simultaneous production of α-amylase and green food packaging polymer by Bacillus sp. CFR 67. *Journal of food science and technology* **50,** 404–408 (2013).

11. Grage, K. *et al.* Bacterial polyhydroxyalkanoate granules: biogenesis, structure, and potential use as nano-/micro-beads in biotechnological and biomedical applications. *Biomacromolecules* **10,** 660–669 (2009).

12. Valappil, S. P., Misra, S. K., Boccaccini, A. R. & Roy, I. Biomedical applications of polyhydroxyalkanoates, an overview of animal testing and in vivo responses. *Expert Review of Medical Devices* **3,** 853–868 (2006).

13. Boccaccini, A. R. *et al.* Polymer/bioactive glass nanocomposites for biomedical applications: a review. *Composites science and technology* **70,** 1764–1776 (2010).

14. Murphy, W. L., Dennis, R. G., Kileny, J. L. & Mooney, D. J. Salt fusion: an approach to improve pore interconnectivity within tissue engineering scaffolds. *Tissue engineering* **8,** 43–52 (2002).

15. Duan, B. *et al.* Three-dimensional nanocomposite scaffolds fabricated via selective laser sintering for bone tissue engineering. *Acta biomaterialia* **6,** 4495–4505 (2010).

16. Rezwan, K., Chen, Q. Z., Blaker, J. J. & Boccaccini, A. R. Biodegradable and bioactive porous polymer/inorganic composite scaffolds for bone tissue engineering. *Biomaterials* **27,** 3413–3431 (2006).

17. Huang, W., Shi, X., Ren, L., Du, C. & Wang, Y. PHBV microspheres–PLGA matrix composite scaffold for bone tissue engineering. *Biomaterials* **31,** 4278–4285 (2010).

18. Bugnicourt, E., Cinelli, P., Lazzeri, A. & Alvarez, V. A. Polyhydroxyalkanoate (PHA): Review of synthesis, characteristics, processing and potential applications in packaging. (2014).

19. Poon, W. C. K. The physics of a model colloid–polymer mixture. *Journal of Physics: Condensed Matter* **14,** R859 (2002).

20. Hoffman, A. S. Hydrogels for biomedical applications. *Advanced drug delivery reviews* **64,** 18–23 (2012).

21. Ahmed, E. M. Hydrogel: Preparation, characterization, and applications: A review. *Journal of advanced research* **6,** 105–121 (2015).

22. Liu, K. L., Zhu, J. & Li, J. Elucidating rheological property enhancements in supramolecular hydrogels of short poly [(R, S)-3-hydroxybutyrate]-based amphiphilic triblock copolymer and α-cyclodextrin for injectable hydrogel applications. *Soft Matter* **6,** 2300–2311 (2010).

23. Chambon, F. & Winter, H. H. Stopping of crosslinking reaction in a PDMS polymer at the gel point. *Polymer Bulletin* **13,** 499–503 (1985).

24. Winter, H. H. Can the gel point of a cross-linking polymer be detected by the G′–G ″crossover? *Polymer Engineering & Science* **27,** 1698–1702 (1987).

25. Peltola, S. M., Melchels, F. P., Grijpma, D. W. & Kellomäki, M. A review of rapid prototyping techniques for tissue engineering purposes. *Annals of medicine* **40,** 268–280 (2008).

26. Nisal, A. *et al.* Silk fibroin micro-particle scaffolds with superior compression modulus and slow bioresorption for effective bone regeneration. *Scientific reports* **8,** 7235 (2018).

27. Sahoo, S., Toh, S. L. & Goh, J. C. A bFGF-releasing silk/PLGA-based biohybrid scaffold for ligament/tendon tissue engineering using mesenchymal progenitor cells. *Biomaterials* **31,** 2990–2998 (2010).

28. Chong, E. J. *et al.* Evaluation of electrospun PCL/gelatin nanofibrous scaffold for wound healing and layered dermal reconstitution. *Acta biomaterialia* **3,** 321–330 (2007).

29. Leukers, B. *et al.* Hydroxyapatite scaffolds for bone tissue engineering made by 3D printing. *Journal of Materials Science: Materials in Medicine* **16,** 1121–1124 (2005).

30. Lam, C. X. F., Mo, X. M., Teoh, S.-H. & Hutmacher, D. W. Scaffold development using 3D printing with a starch-based polymer. *Materials Science and Engineering: C* **20,** 49–56 (2002).

31. Sin, D. *et al.* Polyurethane (PU) scaffolds prepared by solvent casting/particulate leaching (SCPL) combined with centrifugation. *Materials Science and Engineering: C* **30,** 78–85 (2010).

32. Suh, S. W. *et al.* Effect of different particles on cell proliferation in polymer scaffolds using a solvent-casting and particulate leaching technique. *ASAIO journal* **48,** 460–464 (2002).

33. O'Brien, F. J., Harley, B. A., Yannas, I. V. & Gibson, L. Influence of freezing rate on pore structure in freeze-dried collagen-GAG scaffolds. *Biomaterials* **25,** 1077–1086 (2004).

34. Wu, X. *et al.* Preparation of aligned porous gelatin scaffolds by unidirectional freeze-drying method. *Acta biomaterialia* **6,** 1167–1177 (2010).

35. Dhanalakshmi, M., Lele, A. K. & Jog, J. P. Electrospinning of Nylon11: Effect of processing parameters on morphology and microstructure. *Materials Today Communications* **3,** 141–148 (2015).

36. Yang, F., Murugan, R., Wang, S. & Ramakrishna, S. Electrospinning of nano/micro scale poly (L-lactic acid) aligned fibers and their potential in neural tissue engineering. *Biomaterials* **26,** 2603–2610 (2005).

37. Zhong, S. *et al.* An aligned nanofibrous collagen scaffold by electrospinning and its effects on in vitro fibroblast culture. *Journal of Biomedical Materials Research Part A: An Official Journal of The Society for Biomaterials, The Japanese Society for Biomaterials, and The Australian Society for Biomaterials and the Korean Society for Biomaterials* **79,** 456–463 (2006).

38. La Carrubba, V., Pavia, F. C., Brucato, V. & Piccarolo, S. PLLA/PLA scaffolds prepared via Thermally Induced Phase Separation (TIPS): tuning of properties and biodegradability. *International Journal of Material Forming* **1,** 619–622 (2008).

39. Chen, J.-S., Tu, S.-L. & Tsay, R.-Y. A morphological study of porous polylactide scaffolds prepared by thermally induced phase separation. *Journal of the Taiwan Institute of Chemical Engineers* **41,** 229–238 (2010).

40. Zhang, H., Liu, X., Yang, M. & Zhu, L. Silk fibroin/sodium alginate composite nano-fibrous scaffold prepared through thermally induced phase-separation (TIPS) method for biomedical applications. *Materials Science and Engineering: C* **55,** 8–13 (2015).

41. Kaplan, D. L. Introduction to biopolymers from renewable resources. in *Biopolymers from renewable resources* 1–29 (Springer, 1998).

42. Pich, A., Schiemenz, N., Boyko, V. & Adler, H.-J. P. Thermoreversible gelation of biodegradable polyester (PHBV) in toluene. *Polymer* **47,** 553–560 (2006).

43. Sobieski, B. J. *et al.* Thermally reversible physical gels of poly [(R)-3-hydroxybutyrate-co-(R)-3-hydroxyhexanoate]: Part 1 gelation in dimethylformamide. *Polymer* **131,** 217–223 (2017).

44. Bordi, F., Cametti, C., Cesàro, A. & Paradossi, G. Dielectric properties of poly (3-hydroxybutyrate) gels in dimethylformamide. *Polymer* **37,** 3501–3507 (1996).

45. Sultana, N. & Wang, M. Fabrication of HA/PHBV composite scaffolds through the emulsion freezing/freeze-drying process and characterisation of the scaffolds. *Journal of Materials Science: Materials in Medicine* **19,** 2555 (2008).

46. Wu, J., Xue, K., Li, H., Sun, J. & Liu, K. Improvement of PHBV scaffolds with bioglass for cartilage tissue engineering. *PloS one* **8,** e71563 (2013).

47. Tsujimoto, T., Hosoda, N. & Uyama, H. Fabrication of porous poly (3-hydroxybutyrate-co-3-hydroxyhexanoate) monoliths via thermally induced phase separation. *Polymers* **8,** 66 (2016).

48. Ruiz, I., Hermida, É. B. & Baldessari, A. Fabrication and characterization of porous PHBV scaffolds for tissue engineering. in *Journal of Physics: Conference Series* **332,** 012028 (IOP Publishing, 2011).

49. Li, C. *et al.* Poly (L-lactide-co-caprolactone) scaffolds enhanced with poly (β-hydroxybutyrate-co-β-hydroxyvalerate) microspheres for cartilage regeneration. *Biomedical Materials* **8,** 025005 (2013).

50. Aoyagi, Y., Yamashita, K. & Doi, Y. Thermal degradation of poly [(R)-3-hydroxybutyrate], poly [ε-caprolactone], and poly [(S)-lactide]. *Polymer Degradation and Stability* **76,** 53–59 (2002).

51. Spyros, A., Kimmich, R., Briese, B. H. & Jendrossek, D. H NMR Imaging Study of Enzymatic Degradation in Poly (3-hydroxybutyrate) and Poly (3-hydroxybutyrate-co-3-hydroxyvalerate). Evidence for Preferential Degradation of the Amorphous Phase by PHB Depolymerase B from Pseudomonas lemoignei. *Macromolecules* **30,** 8218–8225 (1997).

52. Muhamad, I. I., Lee, K. J. & Noor, M. A. M. Comparing the Degradation of Poly-β-(hydroxybutyrate), Poly-β–(hydroxybutyrate-co-valerate)(PHBV) and PHBV/Cellulose Triacetate Blend. *Malaysian Polymer Journal* **1,** 39–46 (2006).

53. Liu, H., Pancholi, M., Stubbs Iii, J. & Raghavan, D. Influence of hydroxyvalerate composition of polyhydroxy butyrate valerate (PHBV) copolymer on bone cell viability and in vitro degradation. *Journal of applied polymer science* **116,** 3225–3231 (2010).

54. Cabedo, L., Plackett, D., Giménez, E. & Lagarón, J. M. Studying the degradation of polyhydroxybutyrate-co-valerate during processing with clay-based nanofillers. *Journal of applied polymer science* **112,** 3669–3676 (2009).

Chapter 2

Objectives

2 Objectives

PHBV is naturally occurring bio-compatible and biodegradable polymer with wide application in tissue engineering. There are various techniques used for tissue engineered scaffold such as electrospinning and temperature induced phase separation (TIPS). The latter technique is widely used for the preparation of scaffolds and involves separation of polymer-rich phase from a homogeneous solution phase upon change in temperature. PHBV shows UCST type of behavior and forms gels in few solvents such DMF, DMSO, chlorobenzene, and toluene. At high temperature, the polymer solution is homogeneous. As solutions cool down, solid-liquid or liquid-liquid phase separation occurs depending upon the quench temperature. Thus, the TIPS process can be used to make scaffolds from PHBV. The structure and final properties of scaffold prepared via this techniques are depends on the kinetics of phase separation and structure formation, quench temperature and concentration of the polymer. Present work is a fundamental study to develop more insight in the TIPS process and accompanying sol-gel transition kinetics.

The main aims of the present work are listed below

- To study the sol-gel transition kinetics under isothermal conditions.
- To study the sol-gel transition kinetics under non-isothermal conditions.
- To study dynamics of structure formation during sol-gel transition.

We have used rheology as the main tool to probe the sol gel transition kinetics under isothermal and non-isothermal gelation kinetics.

2.1 Isothermal gelation kinetics

Kinetics of sol-gel transition under isothermal conditions were studied using rheology. There are three stages in gelation of which we have analyzed the first two

stages. First stage of gelation consists of initial induction phase and incipient gelation. The first stage is that of induction of a new phase during first order transition. The incipient gelation stage sample spanning network is formed. This was analyzed by the Winter-Chambon criteria to detect gel point. The second rapid gelation stage in which the network structure builds rapidly was analyzed by Avrami model.

2.2 Non-isothermal gelation kinetics

Gelation kinetics under non-isothermal conditions, which are more representative of the TIPS process, were also analyzed using the Winter-Chambon criteria. Similarly, the rapid gelation kinetics were analyzed using a modified Avrami model.

2.3 Dynamic light scattering

Dynamic light scattering experiments were performed during the sol-gel transition. The network structure scatters light and thereby gives information about its dynamics in solution. From the fluctuations of scattered light intensity the length scale of the network was calculated as a function of gelation time using Stokes-Einstein equation.

Chapter 3

Sol -Gel transition kinetics of PHBV gel under isothermal conditions

This chapter presents analysis of different stages of gelation under isothermal conditions. The first stage of gelation namely, the induction phase, is analyzed in the context of classical nucleation theory. The first stage of incipient structure build-up, is analyzed using Winter Chambon criteria for gel point detection. The second gelation stage namely, the rapid network build-up stage, is analyzed using a treatment similar to Avrami equation for phase transition. The effects of quench temperature and polymer concentration on the formation of network structure during gelation are presented in this chapter.

3.1 Introduction

Poly(hydroxybutyrate-co-valerate) copolymer in certain solvents show UCST type of phase behavior, and consequently upon changing temperature, displays thermo-reversible sol-gel transition. This process, also called Temperature-Induced-Phase-Separation or TIPS, is one of the methods used for preparation of scaffolds for tissue engineering. The critical process parameters of TIPS which can be used to tailor the structure and properties of scaffolds are quench temperature, gel time and quench rate. However, first, the effects of these parameters on TIPS must be understood. Rheology is a powerful technique to probe the sol-gel transition kinetics. Various rheological techniques are used to probe these transitions. Small amplitude oscillatory shear is perhaps the most commonly used technique. The small amplitude is chosen in order the retain the structure formed during gelation. Gelation kinetics has been studied for gels using dynamic rheometry under isothermal conditions [1] [2]. In literature, isothermal time test has been performed on various biopolymer gels such K-Carignan [3], gelatin gels [4]. In this chapter, we present rheological measurements that were used to probe the sol-gel transition kinetics of PHBV solutions under isothermal conditions. The effect of concentration and quench temperature were studied. In particular, analysis of the first three stages of sol-gel transition is presented.

3.2 Materials and methods

3.2.1. Materials

Polyhydroxybutyratevalerate (PHBV) random block copolymer (Mw=4,10,000 g/mol) was procured from Good Fellow, UK. The HV content is 2%. The melting point of PHBV is 160 ^{o}C and glass transition is 1^{o}C. The solvent chlorobenzene was procured from Merck Chemicals, India.

3.2.2 Gel preparation

Initially, we investigated the gelation of PHBV in different solvents and found that PHBV formed gels in chlorobenzene, dimethylformamide, dichlorobenzene, dimethyl sulphoxide, dichlorobenzene, and toluene. Of these, we chose to work with

chlorobenzene because of the easily accessible temperature range in which sol-gel transition occurred and also the reasonable translucency of the gel, which enabled microscopy and light scattering studies that are presented later in the thesis. Consequently, PHBV solutions with 0.4, 1, 3, 6, 10% w/v concentrations were prepared in chlorobenzene in a hot oil bath maintained at 130 ^{o}C and upon cooling these solutions to room temperature, translucent gels were formed. The prepared gels were stored in culture tube at low temperature.

3.2.3 Rheology

Rheological properties of PHBV gels were studied using a Anton Paar MCR 301 stress-controlled rheometer (Anton Paar) with a cup and bob geometry. The diameter of cup and bob was 18.08 and 16.66 mm respectively. Material is sheared between narrow gap of cup and bob. Rheological parameters such as storage modulus, loss modulus and damping factor, etc. were determined using the in-built software of the rheometer. We performed strain sweep test, frequency sweep test, isothermal time test and time resolved mechanical spectroscopy test on PHBV gels. The details of these tests are given below.

3.2.4 Strain sweep test:

Strain sweep experiments are performed in order to determine the linear viscoelastic regime of the strain. The gel was melted in the gap between the cup and bob and cooled at the rate of 2 ^{o}C/ min to 25 ^{o}C, after which a hold time of 45 minutes was given to form the gel. Oscillatory strain sweep test with angular frequency 10 rad/ s and strain amplitude ranging from 0.01 to 100% was performed on the PHBV gel.

3.2.5 Frequency sweep test:

PHBV gel was loaded in a cup and heated to 110 ^{o}C to convert it into sol. The sol was cooled at 10 ^{o}C/min to 20 ^{o}C and held at this temperature for 15 min. Frequency sweep test was carried out at constant strain amplitude of 0.05% and angular frequency ranging from 0.01 to 628 rad/s.

3.2.6 Isothermal time test:

The time-dependent evolution of storage and loss modulus under isothermal

conditions was measured at a constant frequency of 10 rad/s and constant oscillatory strain in LVE regime of 0.05% at various (26 °C to 50 °C) temperatures. The experimental protocol for isothermal time test is shown in figure 3.1

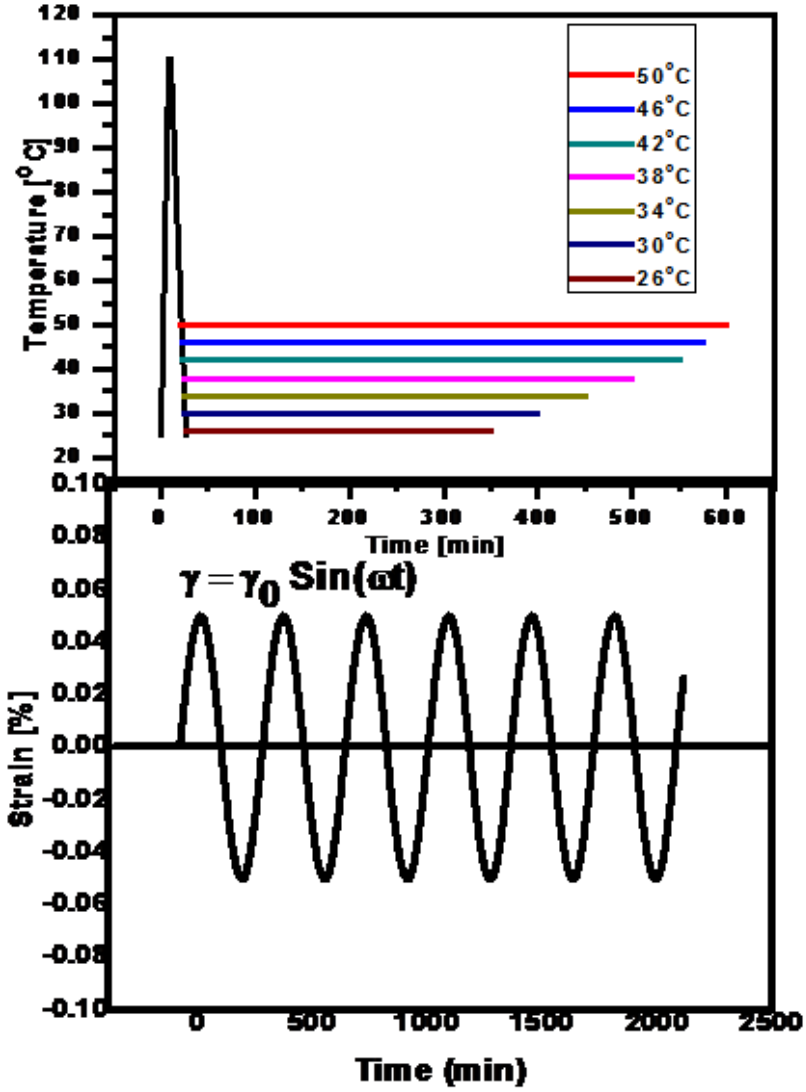

Figure 3.1 Experimental protocol for Isothermal time test

3.2.7 Time resolved mechanical spectroscopy (TRMS)

For TRMS test, gel was melted in the cup at 110 °C and cooled rapidly at 10 °C/min to 60 °C. Short duration oscillatory frequency sweep test with frequency ranging from 10 rad/s to 60 rad/s at 0.15% strain was performed on the sample. This frequency sweep test is repeated one after the another consecutively till the material completely transformed from the sol state to gel state.

3.2.8 Scanning electron microscope

An environmental SEM from Leica-440 was used to image the microstructure of

the gel. A small piece of gel was first converted to sol at high temperature. A drop of sol was sandwiched between two coverslips and freely cooled to room temperature to form gel. The gel was preserved for two weeks before doing SEM. The sample was then mounted on SEM sample holder and micrographs were imaged at 30 kV under low vacuum conditions that allowed imaging of the gel without having to remove the solvent.

3.3. Results and Discussion

3.3.1 Thermoreversible gelation in PHBV

The solution of polyhydroxybutyratevalerate copolymer in chlorobenzene shows an upper critical solution temperature (UCST) type of phase behavior. At high temperature (130 ^{o}C) solutions are homogeneous, and upon cooling to room temperature, phase separation occurs creating a polymer rich phase and a polymer lean phase. However, phase separation does not proceed completely to give a solid polymer precipitate. Instead, as phase separation occurs, the system gets structurally arrested. As a result, PHBV shows sol to gel transition on cooling and a gel to sol transition on heating. At an elementary level, the sol-gel transition can be seen via tube inversion method shown in figure 3.2 .

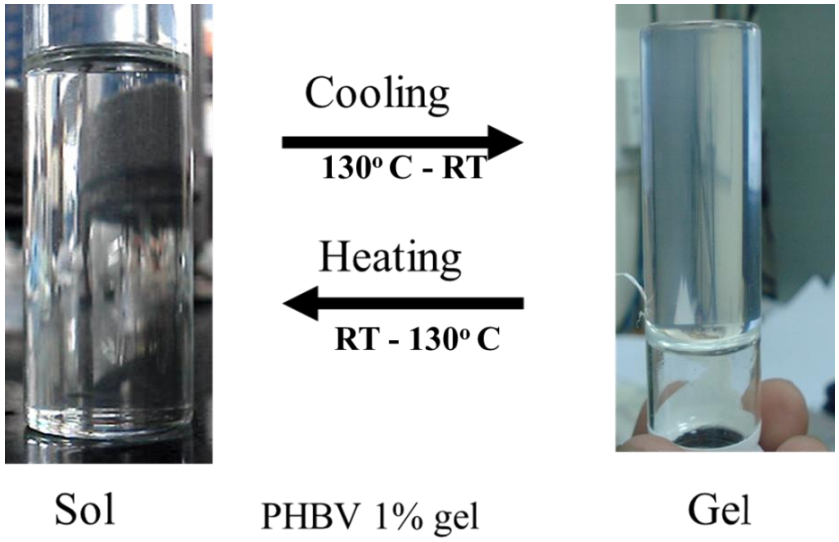

Figure 3.2 Sol -gel transition of 1% PHBV solution in chlorobenzene

As can be seen in figure 3.2, a clear solution of PHBV in chlorobenzene at 130 ^{o}C turns into a translucent gel upon free cooling to room temperature. The gel can support its weight and hence does not flow upon inversion of the tube. Upon re-heating the gel forms sol reversibly.

3.3.2 Scanning electron microscopy

Environmental scanning electron micrograph of PHBV 1% gel is shown in figure 3.3. The SEM micrograph shows a percolated fractal network structure of the gel.

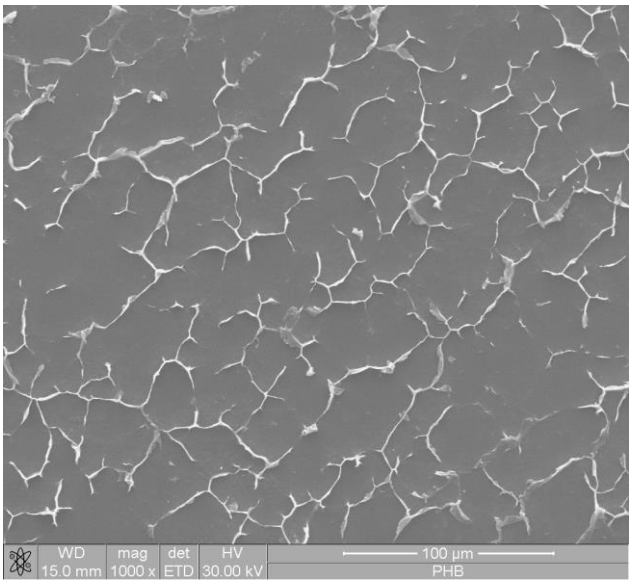

Figure 3.3 Scanning electron micrograph of network structure formed during gelation

3.3.3 Strain sweep test

Strain sweep experiments were performed in order to determine the linear viscoelastic regime of the strain. Figure 3.4 (a) shows the strain sweep test of PHBV 0.4% gels. Both G′ and G″ showed strain-independent response until a strain of 1%, after which the G′ showed considerable strain softening, while the G″ showed a maximum before softening. The 1% strain indicates the limit of linear viscoelastic regime. Strain amplitudes larger than this limit breaks the network formed during gelation. The pronounced peak of G" in stain sweep is an indication of soft solid nature of the gel, which is to be expected. Many different soft solids show similar rheology [5 6] Storage modulus as a function of strain for different concentration is shown in figure 3.4 (b). The strain demarking the end of linear viscoelastic regime decreases with increase in concentration. The strain in linear regime 0.05% was selected for all further dynamic rheology experiments.

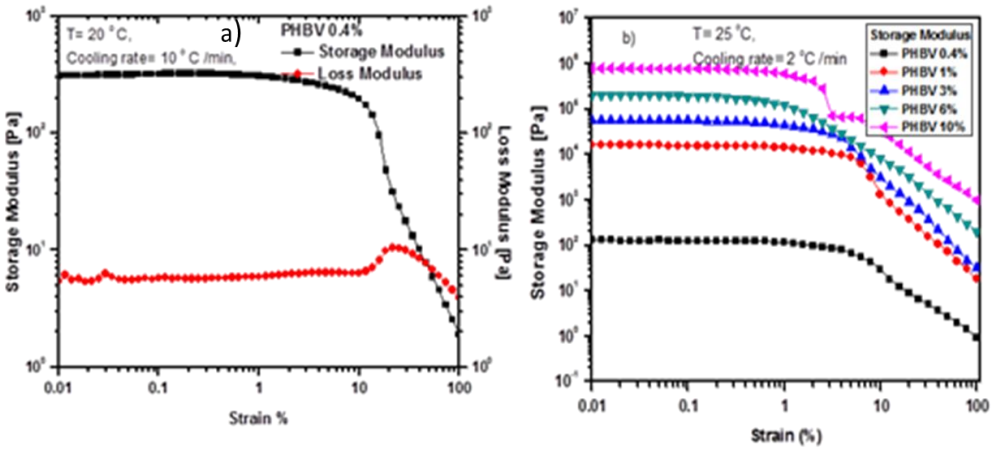

Figure 3.4. a) Overlay of storage and loss modulus as storage modulus as a function strain % for PHBV 0.4% gels. b) Overlay of storage modulus for different polymer concentrations.

3.3.4 Frequency sweep test

Frequency sweep dependence of a PHBV 0.4% gel is shown in figure 3.5. It can be seen that G' is higher that G" over the entire frequency range. Also, G' was independent of frequency over a large range of frequency, while G" showed weak frequency dependence with shallow minimum (at 10 rad/s) in the same range of frequency. K-Carrageenan [7]gelatin gels [8] shows similar minima in G".

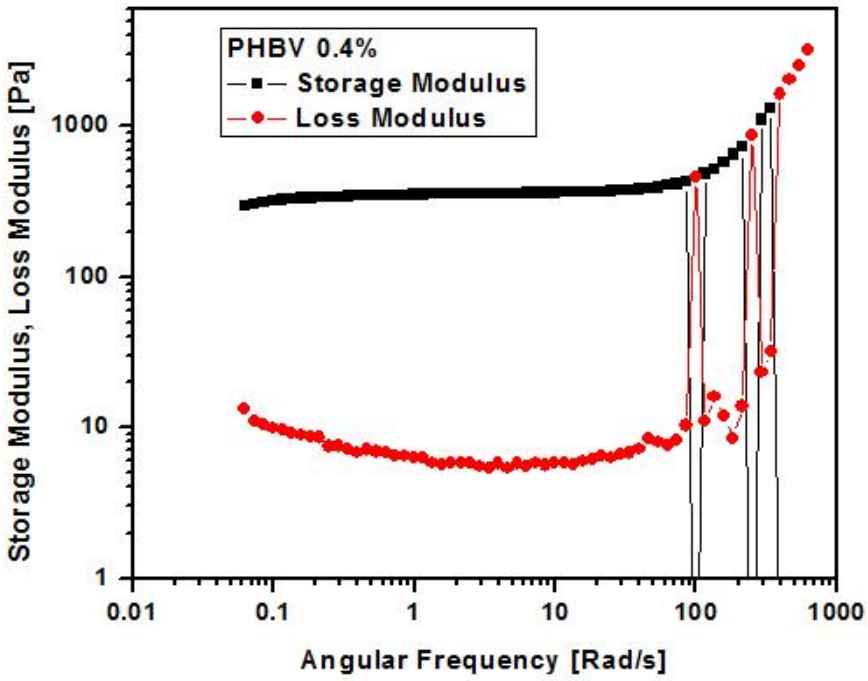

Figure 3.5 Frequency sweep test of PHBV 4% gel at 20 ^{o}C

3.3.5 Isothermal time test

These experiments were designed to provide kinetic data for isothermal phase separation and are analogous to isothermal crystallization experiments performed in differential scanning calorimetry. Isothermal time test of PHBV 3% gels quenched to 50 ^{o}C is shown in figure 3.6. The data suggests that there are possibly three stages of gelation.

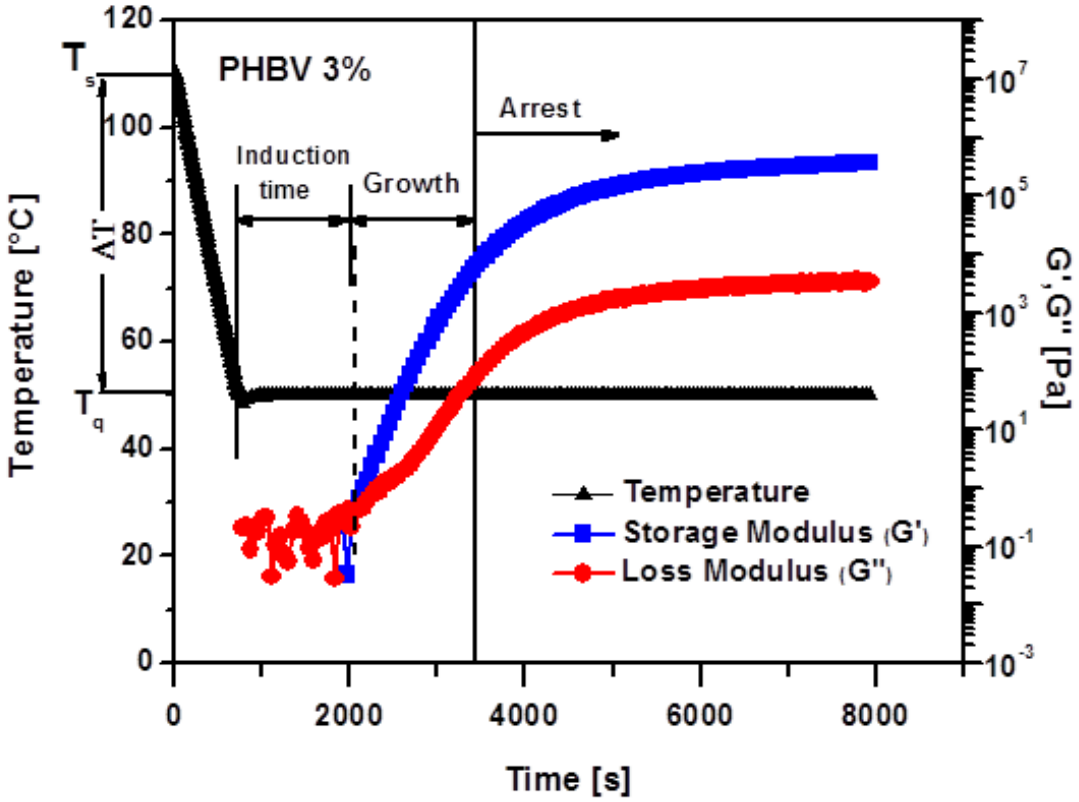

Figure 3.6 Isothermal time test of PHBV 3% gel quenched to 50 ^{o}C

The first stage of gelation shows an initial induction period. During this period, phase separation begins by the formation of stable nuclei. During this time, G" dominates over G' indicating liquid like behavior of the sol. Towards the end of this phase, the network structure starts forming resulting in critical gelation. In the second stage of gelation the network grows rapidly. Both moduli rise with G' rising with more steeply than G" and dominating over G". In the third stage of gelation, the storage and loss moduli rise more slowly and seem to approach a plateau value after a long time. While the rapid rise in stage two reflects the unhindered growth of network (gel) from the sol, the slower increase at longer time in stage three is likely dictated by structural arrest. The temperature difference between solvation temperature T_s and quenching temperature T_q is defined as the degree of undercooling.

$$\Delta T = T_s - T_q$$

Here, ΔT = Degree of undercooling, T_s = Solvation temperature and T_q = Quenched temperature.

Figure 3.7 shows a schematic model of different stages of gelation. In principle, there could be four stages of gelation: nucleation (induction), incipient gelation, rapid gelation and structural arrest. The rheology data shown here cannot differentiate between the first two phases. Hence, we have combined the first two stages into one. Analysis of these three stages of gelation is described in the sections below.

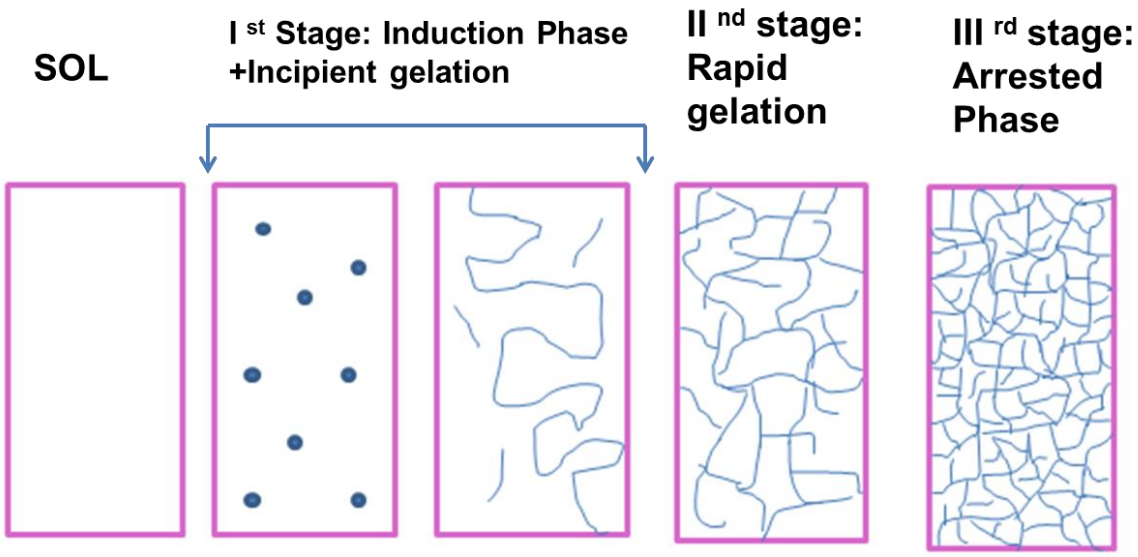

Figure 3.7 Schematic showing different stages of gelation.

3.3.6 Effect of Concentration

Figure 3.8 shows overlay of G' quenched to a constant temperature of 46 ^{o}C for different PHBV concentrations. Lower the concentration higher is the induction time for stage I and slower is the kinetics of gelation in stage II (the moduli rises slowly). As concentration is increased, the rate of gelation increased, moduli rose more steeply with concomitant decrease in the induction time.

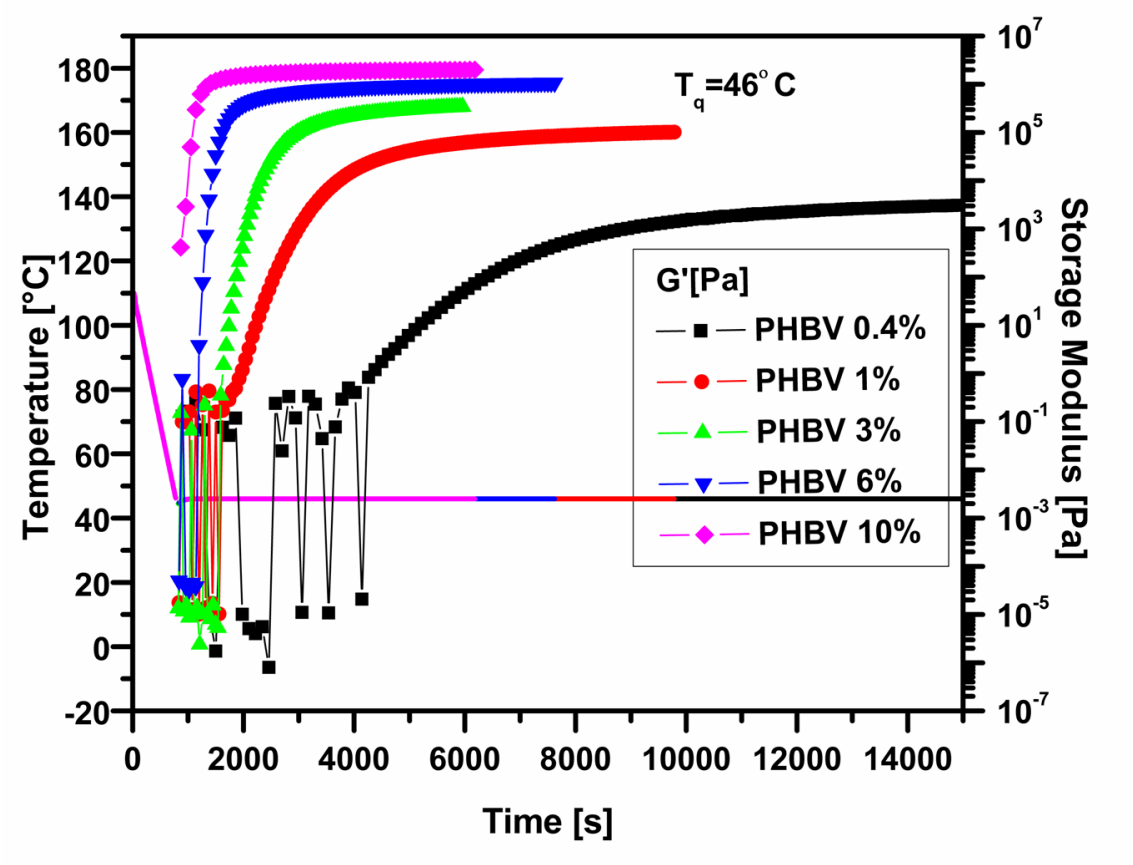

Figure 3.8 Storage modulus vs time at 46 ^{o}C for different concentration

3.3.7 Effect of quenching temperature

Figure 3.9 shows the overlay of storage and loss modulus of 3% gel quenched to different quenching temperatures. We can see that at a higher degree of undercooling, the kinetics of gelation in stage II is fast, while at a lower degree of undercooling the kinetics of gelation is slower. This can be seen via slope of G'. Also, the induction time for the end of stage I increases with decrease in the degree of undercooling.

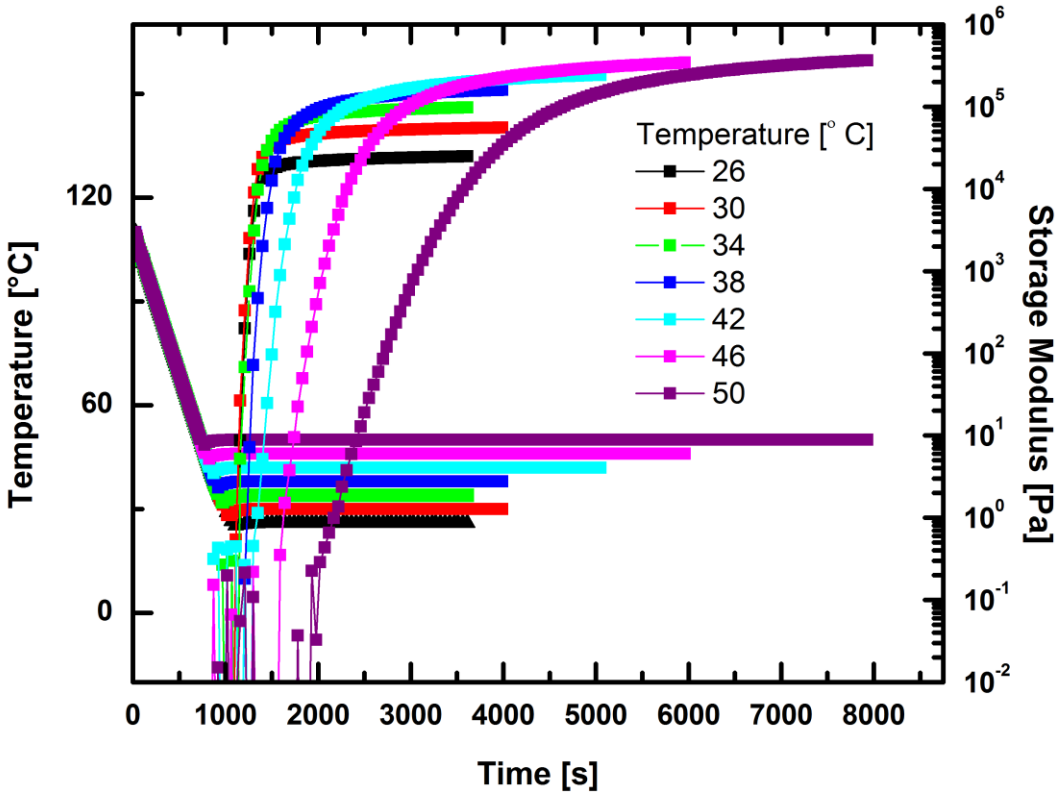

Figure 3.9 Storage modulus of PHBV 3% gel quenched to different temperature.

3.3.8 The first stage of gelation: Induction time

Figure 3.10 shows semi-logarithmic plot of induction time vs. degree of undercooling for PHBV gels of different concentrations quenched to different temperatures. It is clear that for each concentration, the induction time is strongly related to the degree of undercooling. Also, for a given degree of undercooling, the induction time decreases with increase in polymer concentration. Figure 3.10 shows that for any given concentration, the induction time is directly proportional to exponential ($-\Delta T$). This behavior is similar to earlier reports for other systems undergoing first order phase separation phenomena [9] [10]. According to classical theory of first order transition, an exponential dependence of induction time on undercooling suggests that nucleation event kickstarts the phase separation process. The strong dependence of induction time on polymer concentration reflects the increase in nucleation rate with polymer concentration. In other words, the probability of growing stable nuclei increases with polymer concentration.

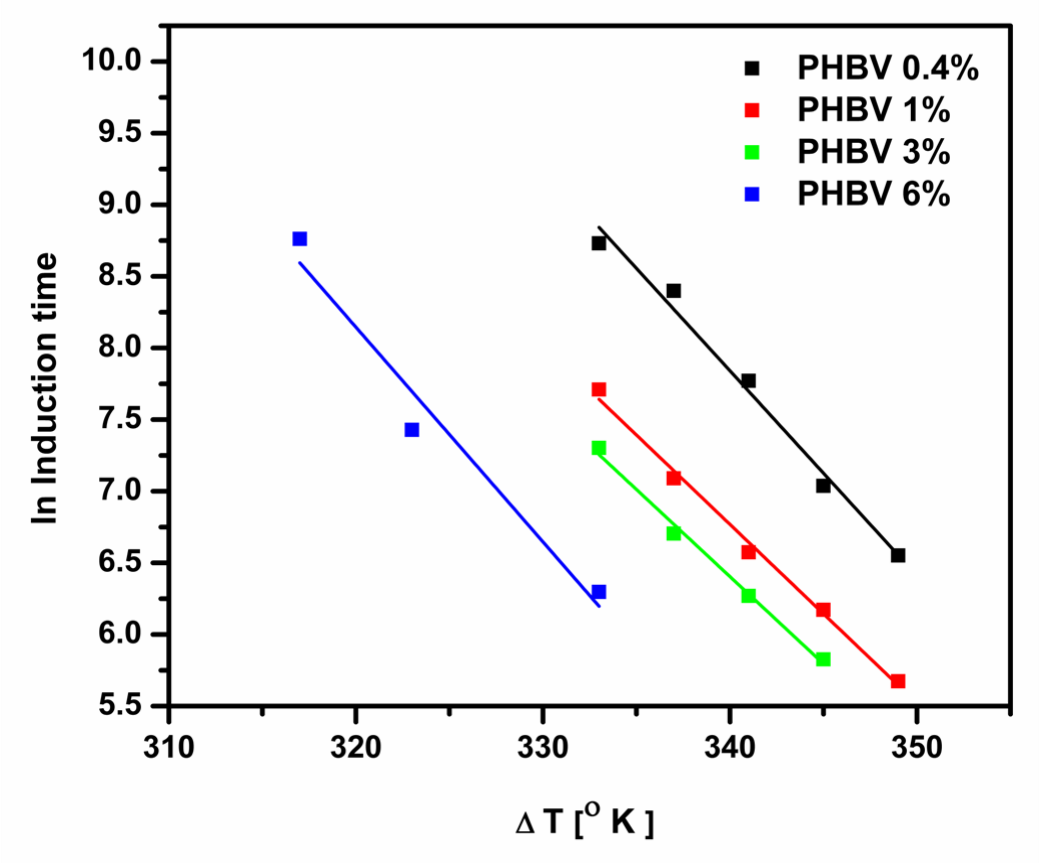

Figure 3.10 Induction time vs. delta T for PHBV gels

3.3.9 The first stage of gelation: Incipient gelation

In order to tailor the properties of gel, it is imperative to find the gel point of the system. In literature, rheological techniques are used to find gel point of the system. It is simplistic to regard that the cross-over point of G' and G" obtained in dynamic mechanical tests (such as small amplitude oscillatory tests) as the gel point of the system. However, it is known that the crossover point is a function of frequency[11]. As crossover point changes with imposed frequency, it is difficult to determine the exact gel point of the system using this criterion. Winter and Chambon [12] have suggested a more rigorous criterion for determination of gel point, popularly known as the Winter-Chambon criteria. According to this criterion, the gel point can be accurately determined as the point at which damping factor during sol-gel transformation becomes frequency independent. This is universal criteria obeyed by physical gels as well as chemical gel systems.

The time where damping factor is independent of frequency is gel time. Two

different experiments can be performed to find out gel time: (i) Time sweep at different frequencies, and (ii) Time Resolved Mechanical Spectroscopy (TRMS). In TRMS, consecutive frequency sweep tests are performed repeatedly one after another on the transient sample [13 14 15]. The advantage of TRMS is that it requires less sample since data for all discrete frequencies can be extracted using one single measurement. Any rheological technique for determination of gel point must take care that the evolving network structure is not ruptured.

To determine gel point for physical gel, the kinetics of gelation must be slow enough so that the material changes its state slowly relative to the measurement timescale. The PHBV samples in this study were was quenched at low undercooling at which the rate of network formation was sluggish compared to the one cycle of consecutive frequency sweep. For example, the time required for each frequency sweep cycle during consecutive frequency sweeps is about 6 min, which is small compared to the gelation time of 335 min for a 10% PHBV sample quenched to 75 ^{o}C (undercooling of 35 ^{o}C). Another criterion used to determine if the material is quasi-stable during measurements is to determine mutation number, which is a dimensionless number that defines how fast the material changes its state in comparison with experimental timescale. It is defined as

$$N_{mu} = \text{Experimental time/Mutation time;}$$

Here, mutation time is the inverse of slope of rate change of storage modulus or loss modulus given as

$$\lambda'_{mu} = \left(\frac{1}{G'}\left|\frac{\partial G'}{\partial t}\right|\right)^{-1} \quad \text{or} \quad \lambda''_{mu} = \left(\frac{1}{G''}\left|\frac{\partial G''}{\partial t}\right|\right)^{-1}$$

Thus, the mutation number is given by

$$N'_{mu} = \frac{\left(\frac{2\pi}{\omega}\right)}{\left(\frac{1}{G'}\left|\frac{\partial G'}{\partial t}\right|\right)^{-1}} \quad \text{or} \quad N''_{mu} = \frac{\left(\frac{2\pi}{\omega}\right)}{\left(\frac{1}{G''}\left|\frac{\partial G'}{\partial t}\right|\right)^{-1}}$$

The mutation number should be <<1 for accurate determination of the gel point. For PHBV 10% gel quenched to 75 ^{o}C the mutation number was determined to be 0.02.

Figure 3.11 shows G' and G" raw data of time resolved mechanical spectroscopy test of PHBV 10% gel at 75 ^{o}C and figure 3.12 shows corresponding raw data of damping factors.

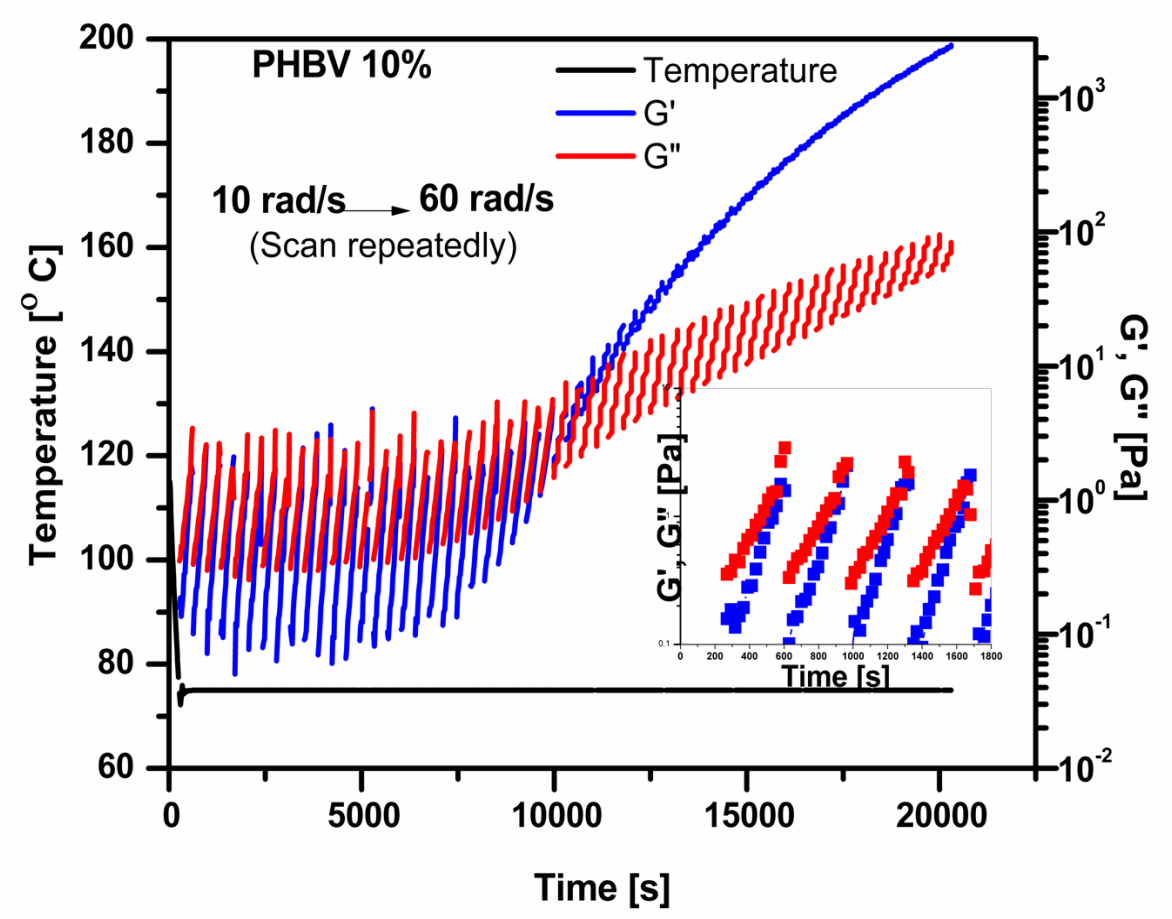

Figure 3.11 Time resolved mechanical spectroscopy data for PHBV 10% gel quenched to 75 ^{o}C. Inset shows zoomed-in initial part of storage and loss modulus vs. time. Each line is a frequency sweep cycle.

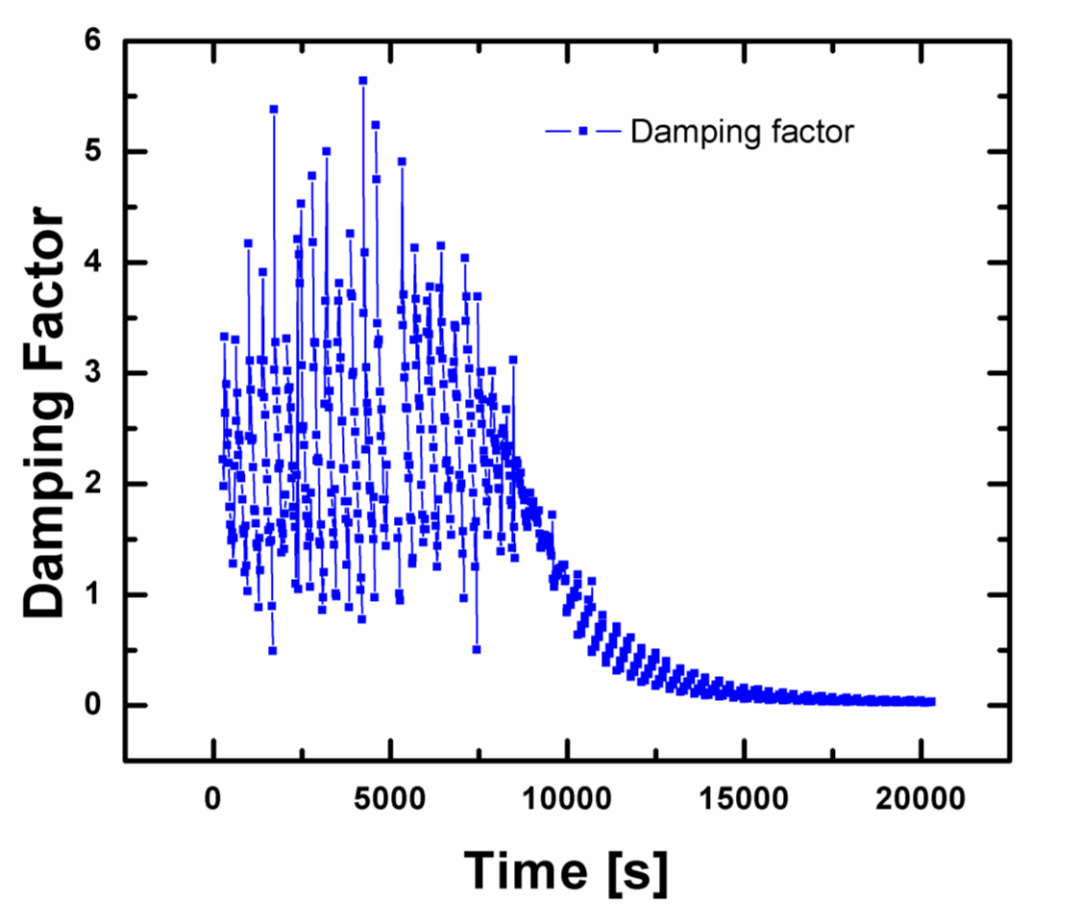

Figure 3.12 TRMS data of damping factor vs time for PHBV 10% gel quenched to 75 ^{o}C.

3.3.9.1TRMS data analysis procedure [13]

TRMS data contains all frequency sweep data gathered in a single file. The following procedure was used for the analysis of TRMS Data.

A) Data sorting

The consecutive frequency sweep data was first sorted at each discrete frequency and then plotted as a function of time. All data sorting was done using Microsoft Excel.

B) Data smoothing

The sorted data was then smoothed using MATLAB software (sgolay method). The smoothed discrete frequency data was plotted at each frequency as a function of time.

C) Data interpolation

Each data point in TRMS is in principle measured at a different state of the material.

The values of viscoelastic materials functions at any intermediate state can be interpolated using fitting functions of discrete frequency sweeps. To get overall materials parameters at any instant of time, the smoothened data was fitted to fitting functions using MATLAB. G' and G" data fitted to higher order polynomial.

D) Plotting

The interpolated values were plotted as function of time for different discrete frequencies.

3.3.9.2 Gel point detection by Winter-Chambon criteria

We followed above procedure for analysis of TRMS data. The fitted damping factor vs. time for discrete frequencies is shown in figure 3.13 below.

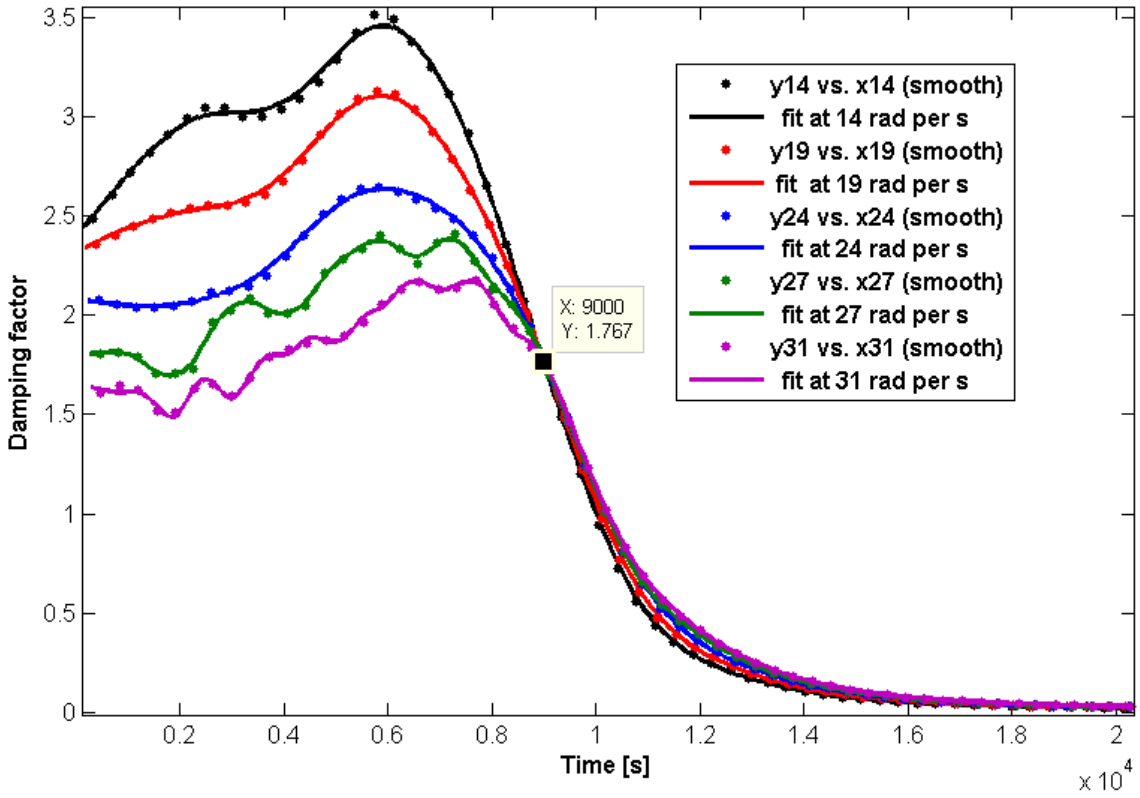

Figure 3.13 Damping factor vs. time for PHBV 10% gel quenched to 75 ^{o}C

The gel point is determined as the point where damping factor becomes independent of frequency. This is also shown in figure 3.14 below

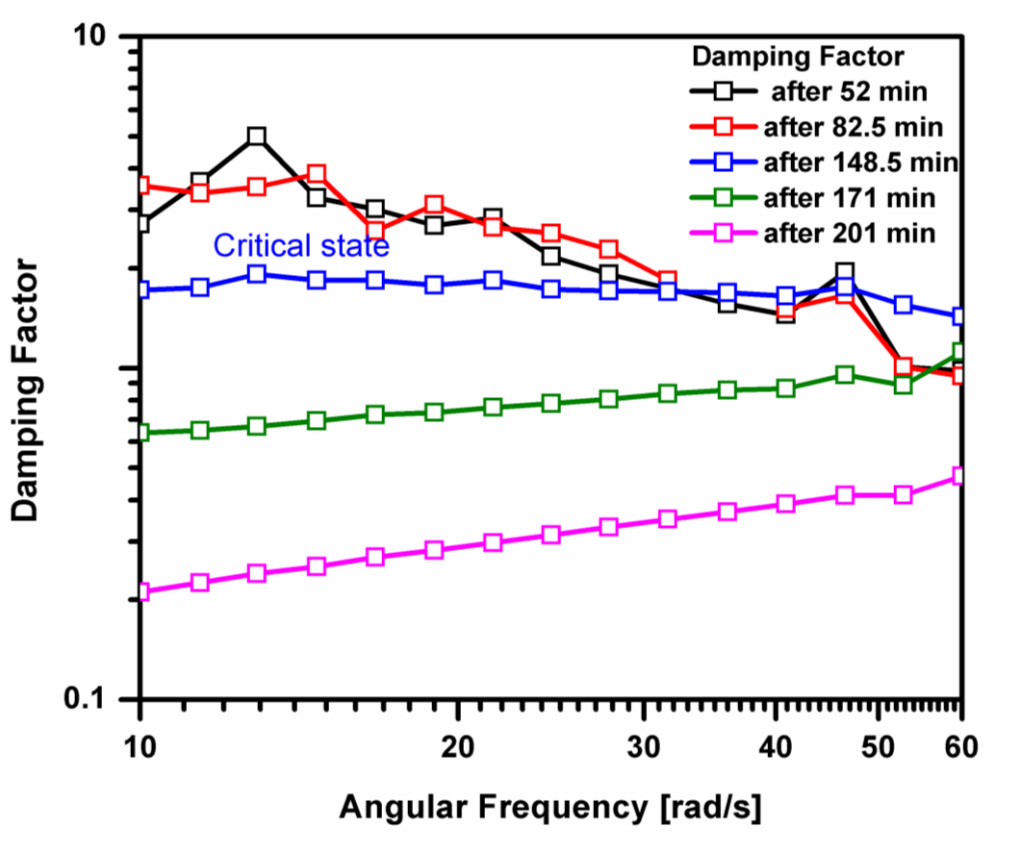

Figure 3.14 Damping factor vs frequency for PHBV 10% gel quenched to 75 ^{o}C.

From these figures, the gel point for the PHBV 10% sample quenched to 75 ºC was determined to be 150 minutes, and same is marked in figure 3.14.

Following Winter and Chambon [16] at critical gel state, the viscoelastic moduli G' and G" scale as ω^n. In other words, the moduli are congruent (have the same slope). At the critical gel state where sample spanning network is formed, the relaxation modulus shows power law behavior given by [16] [17]

$$G(t) = St^{-n};$$

where, G(t) = relaxation modulus, S = gel strength, t = time, and n = relaxation exponent (0<n<1).

This power law behavior of relaxation modulus suggests fractal nature of the gels. The relaxation exponent n is related to fractal dimension of the network structure by the equation n = d/df+2, where df is the fractal dimension and d is the dimensionality

of the system. [18] .

The relaxation exponent ‘n’ and gel strength ‘S’ were determined using following equation respectively for 0<n<1[19].

$$\tan\delta = \tan(\frac{n\pi}{2})$$

$$S = \frac{G'(\omega)}{\omega^n \cos\left(\frac{n\pi}{2}\right)\Gamma(1-\mathrm{n})}$$

For the 10% PHBV gel formed at 75 ^{o}C, the relaxation exponent was obtained as 0.66 and gel strength was 0.14 Pa s^{n}.

In literature, there is a very special case where crossover point of storage and loss modulus in dynamic mechanical experiment and gel point become identical. This happens for gels having n=1/2 [12]. Depending on the of value relaxation exponent, 1) gel point lies before the crossover point if n > 1/2 and gel point lies after crossover point if n < 1/2. In our experiment, we find that the value of relaxation exponent close to 0.66. Thus for the gel considered here, the gel point was found to occur before the crossover point of dynamic moduli in typical isothermal frequency sweep experiments. Indeed it can be seen from the figure 3.10 that the crossover time of dynamic moduli and gel time are not identical.

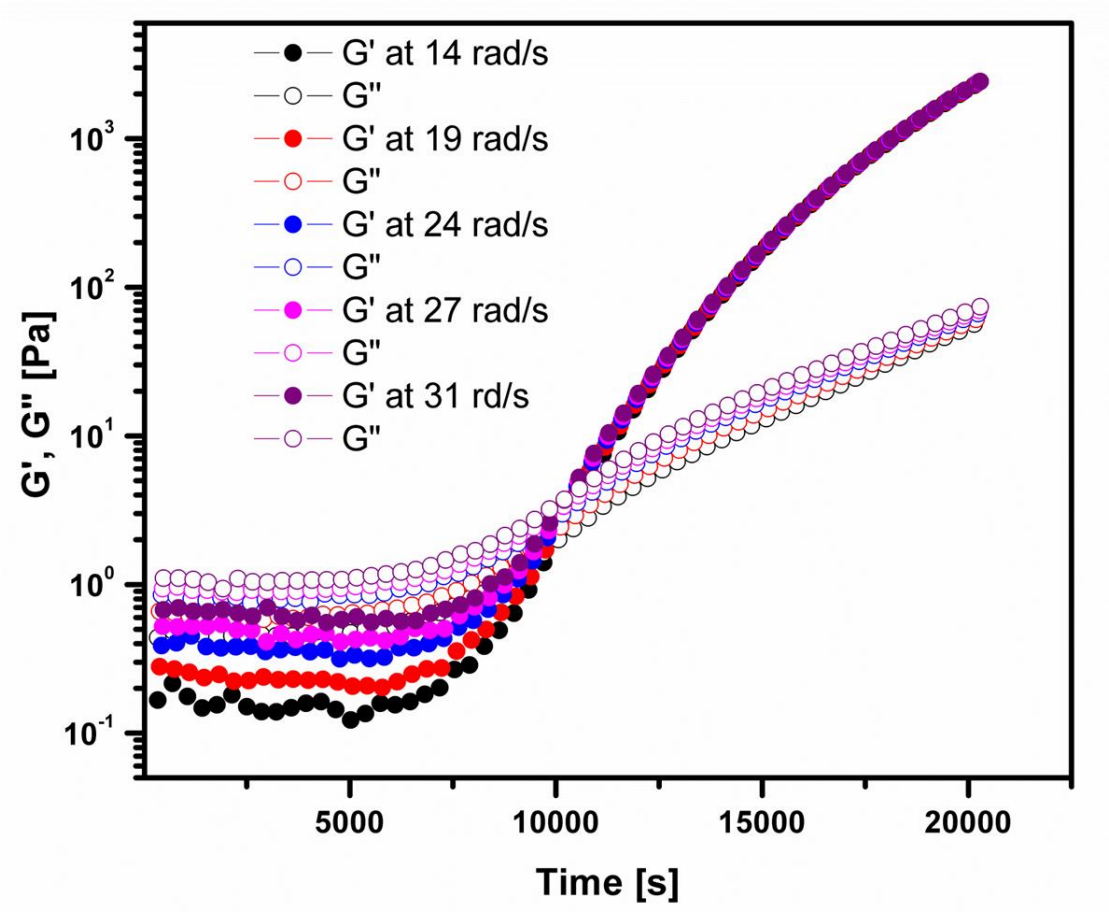

Figure 3.15 G', G" as a function of time for discrete frequencies.

TRMS experiments were also performed for PHBV gel quenched to 60 ^{o}C and is shown in figure 3.16 below.

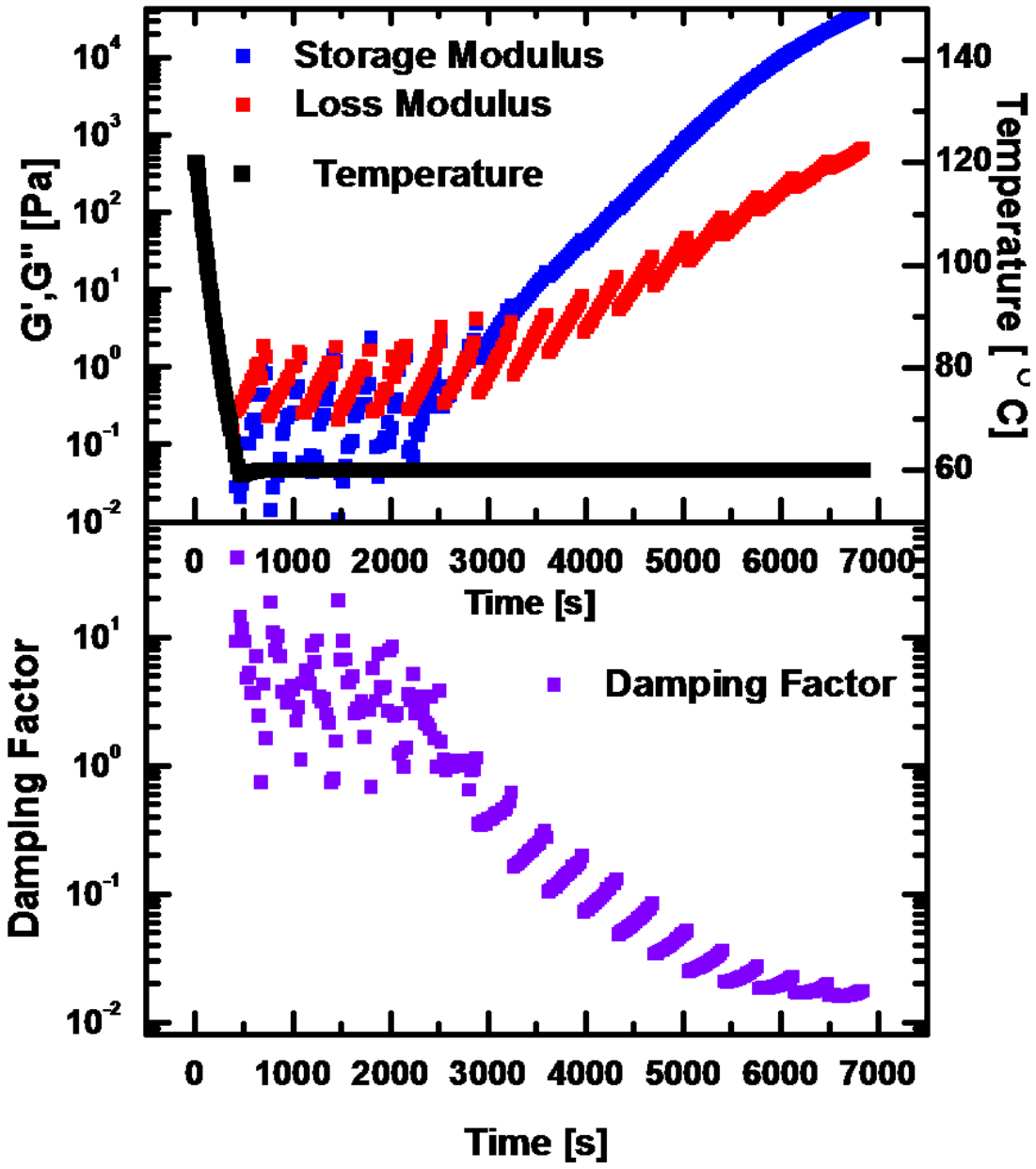

Figure 3.16 TRMS data of PHBV 10% gel quenched to 60 ^{o}C.

The TRMS data was analyzed using above procedure and plot of damping factor vs time is shown in figure 3.17 below.

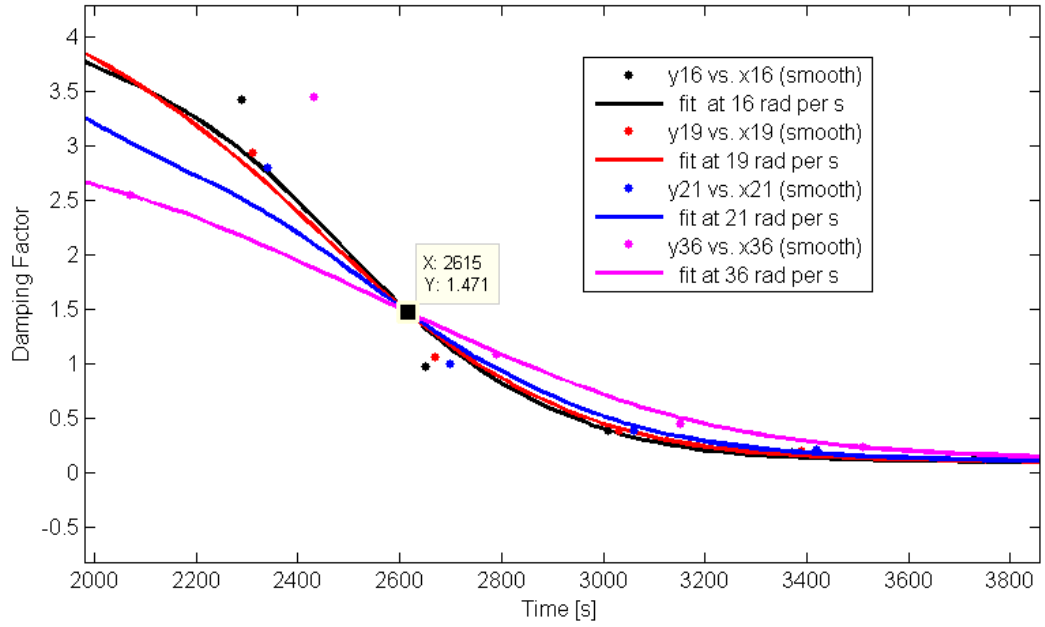

Figure 3.17 Damping factor vs time for PHBV 10% gel quenched to 60 ^{o}C.

The quality of smoothing and interpolation for this case is not as good as for the earlier case. This is due to the fact that the undercooling for this gel is higher, and since the gelation rate increases exponentially with undercooling (as seen from induction time results), therefore the mutation numbers for this case are relatively higher. Nonetheless, the gelation time was obtained to be 43 min and the value of n obtained for this gel was 0.60. Thus, though the concentration of polymer is same i.e. 10%, the gel strength, relaxation exponent and gel time are different compared to the gel formed at 75 ^{o}C. This suggests the gel formation is strongly dependent on quench temperature. The fractal dimension of the network formed during the gelation is 2.5 and 3 for PHBV 10% gel quenched to 75 and 60 ^{o}C, respectively.

3.3.10 The second stage of gelation: Rapid gelation stage

The second stage of gelation was analyzed using an equation similar to Avrami equation. The kinetics of any first-order phase transformation can be described by the empirical Avrami equation [20 21 22]

$$1 - X_t = \exp(-Zt^n)$$

Where, X_t = fractional phase change, Z is the rate of phase change and n is Avrami exponent.

The rapid gelation kinetics can be fitted to an equation similar to Avrami equation in which the fractional phase change is represented by the fractional modulus G(t)/G(∞). Thus, we have

$$1 - [(G(t) - G(0)) / (G(\infty) - G(0))] = \exp(-Zt^n)$$

Here, G(t) is the modulus at time t; G(0) the initial modulus, G(∞) the modulus at infinite time; Z the rate of gelation and n is the Avrami exponent.

Taking double logarithm of above equation on both sides gives,

$$\ln \{-\ln [1-(G(t)-G(0))/(G(\infty)-G(0))]\} = \ln Z + n \ln t$$

The plot of ln {-ln [1-(G (t)-G(0))/(G (∞)-G(0))]} plotted vs. ln t gives the value of Avrami exponent n from the value of slope and the rate of gelation from the intercept. Figure 3.18-3.20 shows the data fitted to Avrami equation for PHBV 1% gel, PHBV 3% gel and 6% quenched to different temperatures. The Avrami exponents were found to be between three and four which suggest the three-dimensional growth of the network structure [23] [24].

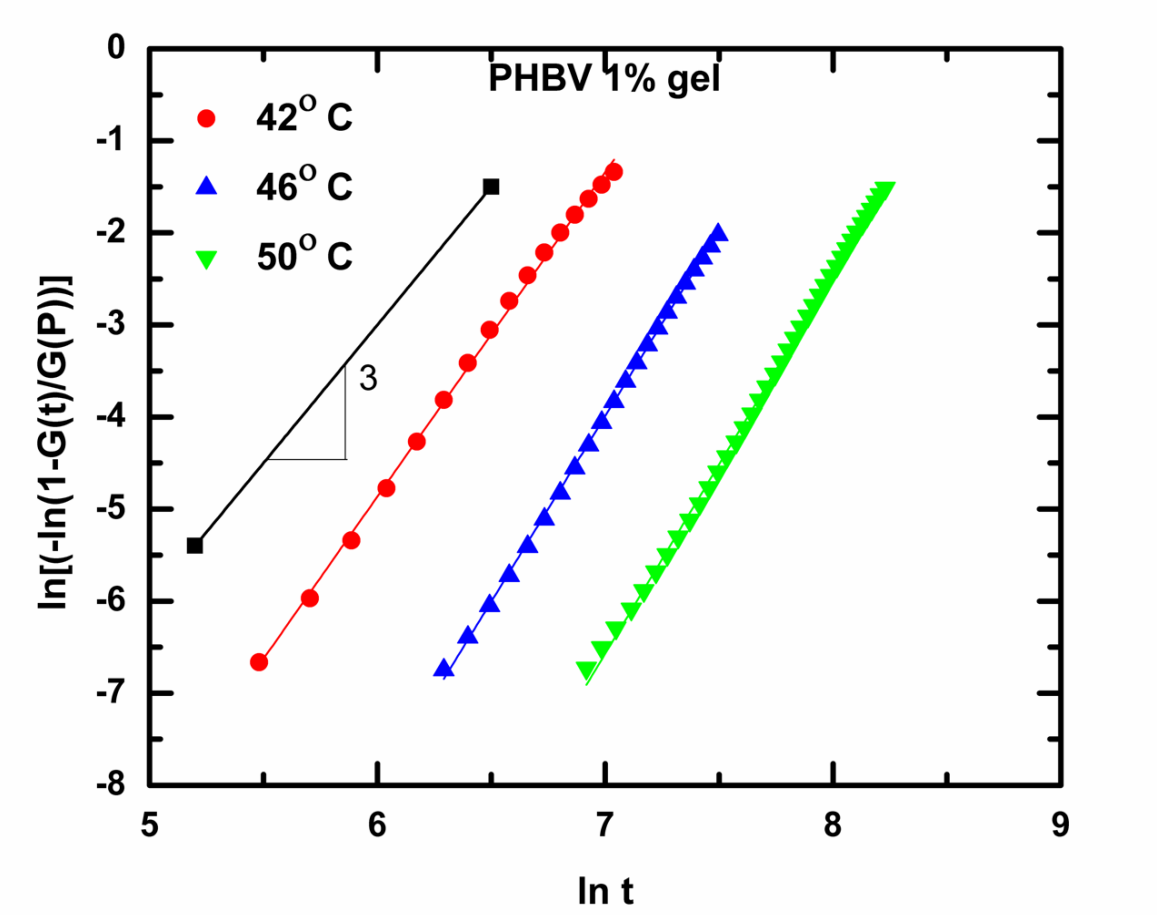

Figure 3.18 Rheological data fitting to an equation similar to Avrami for PHBV 1 % gel quenched to 42, 46 and 50 °C

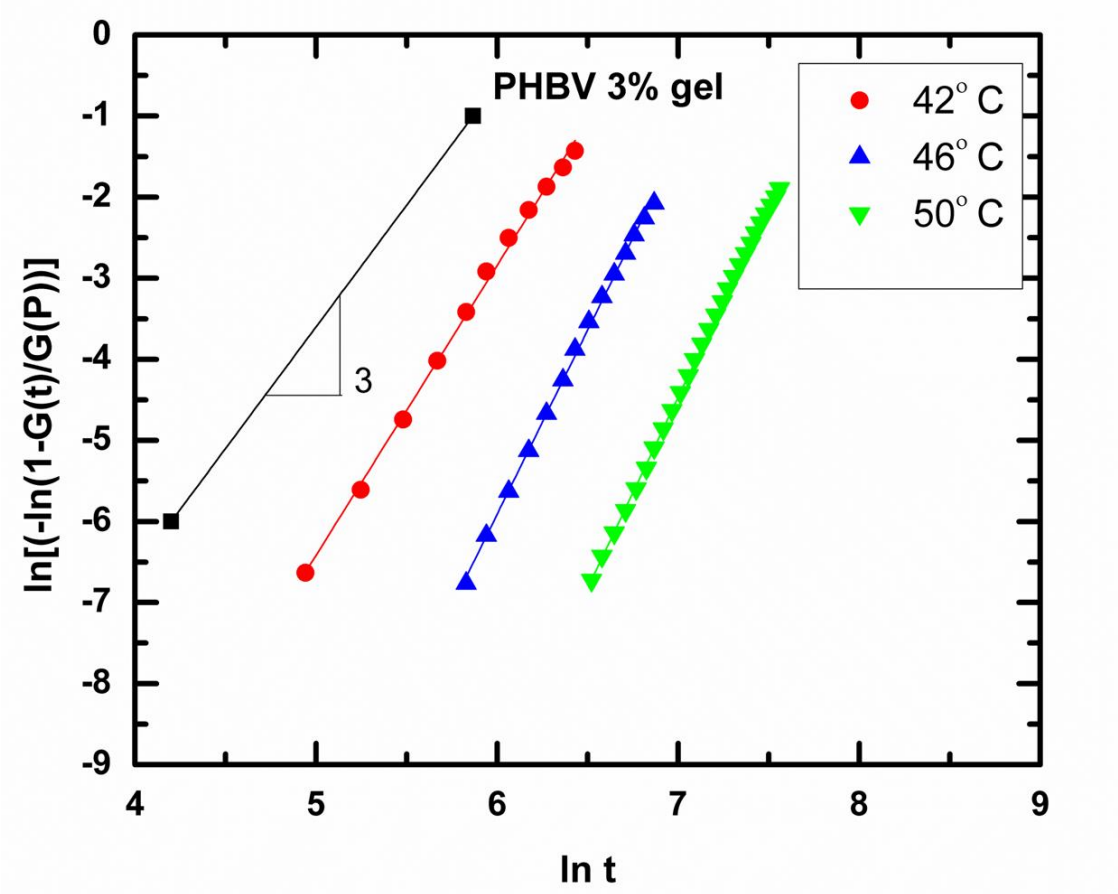

Figure 3.19 Rheological data fitting to an equation similar to Avrami for PHBV 3 % gel quenched to 42, 46 and 50 ^{o}C.

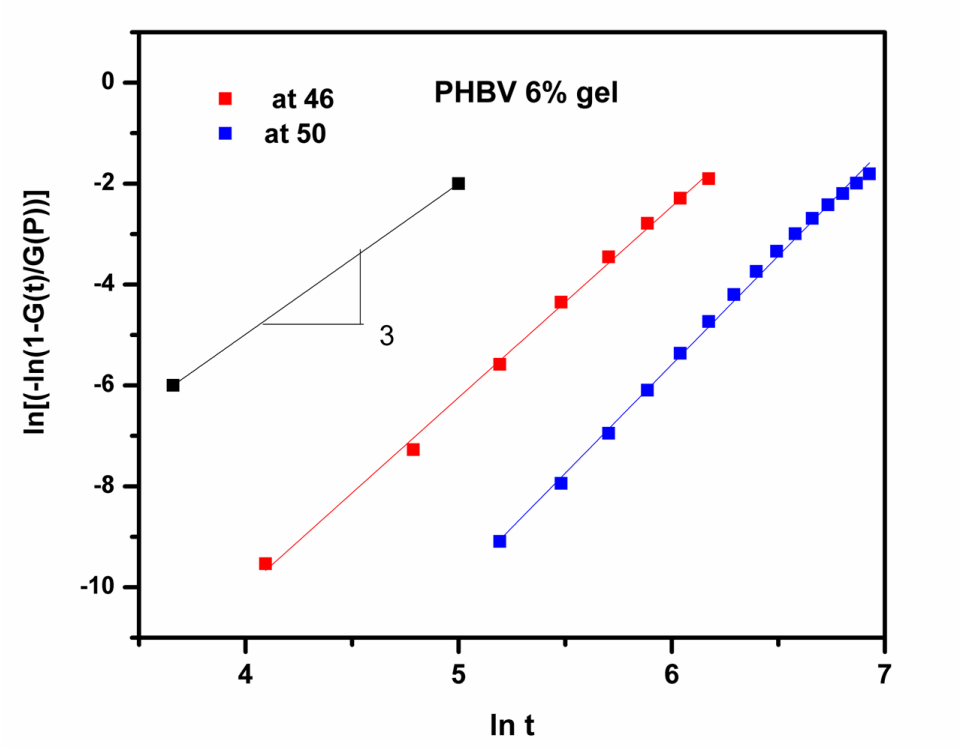

Figure 3.20 Rheological data fitting to an equation similar to Avrami for PHBV 6 % gel quenched to 46 and 50 °C

Table 3.1 Avrami index and Rate for PHBV 1% and PHBV 3% gel at different quench temperature

Sr. No.	Concentration	T (°C) (110 °C - Quench temp)	Avrami Index	Rate Z
1.	PHBV 1%	68	3.4	8.4E-12
		64	3.8	6.2E-14
		60	4.1	4.2E-16
2.	PHBV 3%	68	3.6	2.5E-11
		64	3.9	1.3E-13
		60	4.2	5.7E-16
3.	PHBV 6%	64	3.7	1.2E-11
		60	4.3	2.3E-14

Figure 3.21 below shows the Rate vs Delta T for PHBV 1% , 3% and 6% gel

quenched to 42, 46 and 50 ^{o}C .

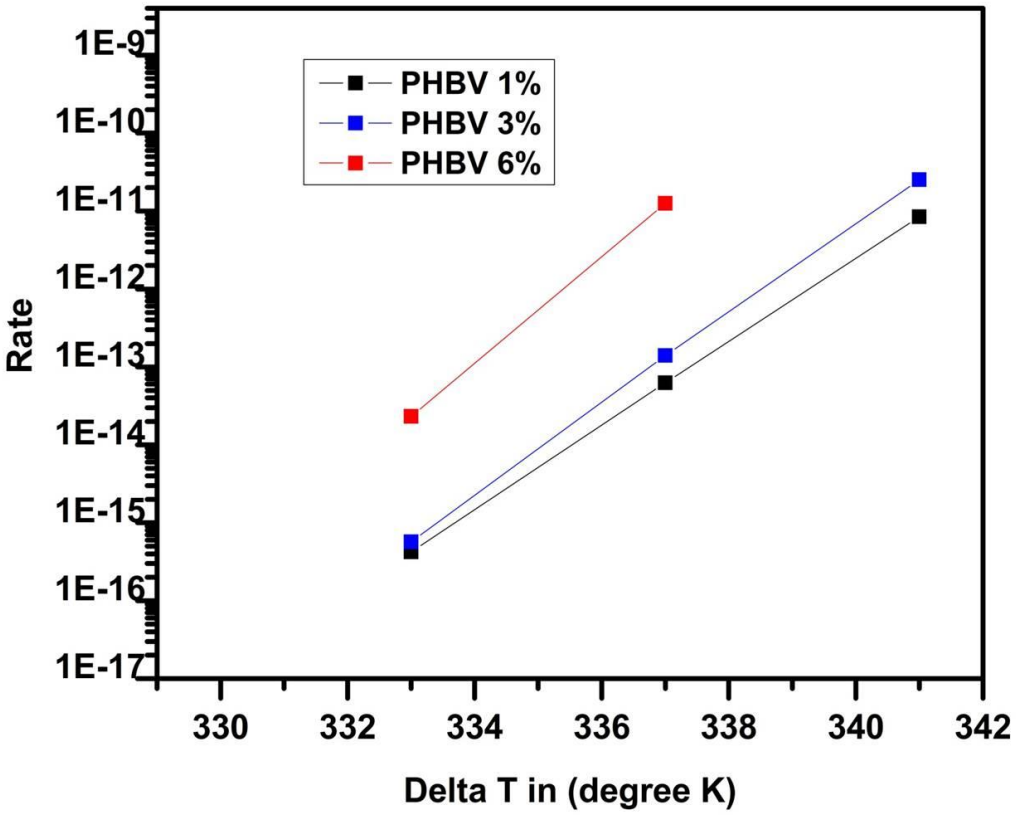

Figure 3.21 Rate Z(T) vs Delta T for PHBV 1%, PHBV 3% and PHBV 6% gel.

Results show that gelation is slow at low undercooling and fast at high undercooling. Indeed, it can be seen that the rate of gelation varies exponentially with undercooling. Comparing the data for 1% PHBV, 3% PHBV and 6% PHBV sols show that the rate of gelation is a strong function of concentration also.

3.4 Conclusions

PHBV gels show thermoreversible sol-gel transition. The incipient gelation regime shows induction times which scale exponentially with degree of undercooling suggesting that phase separation happens most likely by nucleation and growth process. The first stage is also characterized by change of viscoelastic nature of the sample from viscous sol (G" > G') to a cross-over into elastic dominant regime (G' ~ G"). The time for reaching critical gel point during the sol-gel transition was determined using Time Resolved Mechanical Spectroscopy technique and using the

Winter-Chambon procedure. The relaxation exponent of the critical gels were determined to be close to 0.6 suggesting that critical gelation occurs before crossover of G' and G" in isothermal time sweep experiments. The gelation time, relaxation exponent and strength of gel were found to be strong functions of undercooling. The self-similar relaxation modulus showed power law behavior suggesting fractal nature of gel with fractal dimension 3. The second gelation regime showed rapid buildup of dynamic moduli indicating rapid strengthening of the network structure. The kinetics of this regime was analyzed using an Avrami-like equation. The Avrami exponent was found to be between three and four indicating three-dimensional structure of the growing network. The Avrami rate of gelation was found to have exponential dependence on the degree of undercooling, and was also strongly dependent on polymer concentration.

3.5 References

1. Gong, Z., Yang, Y., Huang, L., Chen, X. & Shao, Z. Formation kinetics and fractal characteristics of regenerated silk fibroin alcogel developed from nanofibrillar network. *Soft Matter* **6,** 1217–1223 (2010).

2. Lazaridou, A., Biliaderis, C. G. & Izydorczyk, M. S. Molecular size effects on rheological properties of oat β-glucans in solution and gels. *Food Hydrocolloids* **17,** 693–712 (2003).

3. Gabriele, A., Spyropoulos, F. & Norton, I. T. Kinetic study of fluid gel formation and viscoelastic response with kappa-carrageenan. *Food Hydrocolloids* **23,** 2054–2061 (2009).

4. Djabourov, M., Maquet, J., Theveneau, H., Leblond, J. & Papon, P. Kinetics of gelation of aqueous gelatin solutions. *British polymer journal* **17,** 169–174 (1985).

5. Wyss, H. M. *et al.* Strain-rate frequency superposition: A rheological probe of structural relaxation in soft materials. *Physical review letters* **98,** 238303 (2007).

6. Mohan, P. H. & Bandyopadhyay, R. Phase behavior and dynamics of a micelle-forming triblock copolymer system. *Physical Review E* **77,** 041803 (2008).

7. Meunier, V., Nicolai, T., Durand, D. & Parker, A. Light scattering and viscoelasticity of aggregating and gelling κ-carrageenan. *Macromolecules* **32,** 2610–2616 (1999).

8. Richardson, R. K., Robinson, G., Ross-Murphy, S. B. & Todd, S. Mechanical spectroscopy of filled gelatin gels. *Polymer Bulletin* **4,** 541–546 (1981).

9. Pogodina, N. V. & Winter, H. H. Polypropylene crystallization as a physical gelation process. *Macromolecules* **31,** 8164–8172 (1998).

10. HenningáWinter, H. & others. Rheological expression of physical gelation in polymers. *Faraday Discussions* **101,** 93–104 (1995).

11. Mours, M. & Winter, H. H. Relaxation patterns of nearly critical gels. *Macromolecules* **29,** 7221–7229 (1996).

12. Winter, H. H. Can the gel point of a cross-linking polymer be detected by the G′–G ″crossover? *Polymer Engineering & Science* **27,** 1698–1702 (1987).

13. Tanaka, T. *Experimental Methods in Polymer Science: Modern Methods in Polymer Research and Technology*. (Academic Press, 2000), H H Winter M Mours Chapter 5.

14. Mours, M. & Winter, H. H. Time-resolved rheometry. *Rheologica Acta* **33,** 385–397 (1994).

15. Henningá Winter, H. Rheological expression of physical gelation in polymers. *Faraday Discussions* **101,** 93–104 (1995).

16. Winter, H. H. The critical gel. in *Structure and Dynamics of Polymer and Colloidal Systems* 439–470 (Springer, 2002).

17. Winter, H. H. & others. Soft polymeric materials near the transition from liquid to solid state. *Korea-Australia Rheology Journal* **11,** 275–278 (1999).

18. Tan, L., Liu, S., Pan, D. & Pan, N. Gelation of polyacrylonitrile in a mixed solvent : scaling and fractal analysis. *Soft Matter* **5,** 4297–4304 (2009).

19. Winter, H. H. Polymer gels, materials that combine liquid and solid properties. *Mrs Bulletin* **16,** 44–48 (1991).

20. Avrami, M. Kinetics of phase change. I General theory. *The Journal of Chemical Physics* **7,** 1103–1112 (1939).

21. Avrami, M. Kinetics of phase change. II transformation-time relations for random distribution of nuclei. *The Journal of Chemical Physics* **8,** 212–224 (1940).

22. Avrami, M. Granulation, phase change, and microstructure kinetics of phase change. III. *The Journal of chemical physics* **9,** 177–184 (1941).

23. Hiemenz, P. C. & Lodge, T. P. *Polymer Chemistry: The Basic Concepts*. (Taylor & Francis, 1984).

24. Hay, J. N. Application of the modified avrami equations to polymer crystallisation kinetics. *Polymer International* **3,** 74–82 (1971).

Chapter 4

Sol -Gel transition kinetics of PHBV gel under non-isothermal conditions

Temperature-dependent evolution of the network structure during gelation was probed by using rheology. The initial incipient gelation stage was analyzed for Winter-Chambon criteria to determine sol-gel transition. The rapid gelation stage under non-isothermal condition was analyzed using an equation similar to modified Avrami equation. Effect of heating and cooling rate and concentration on gelation kinetics was presented in this chapter.

4.1 Introduction

Temperature-Induced Phase Separation (TIPS) has been used for the preparation of macroporous membranes and scaffolds [1] [2]. Porous biocompatible scaffolds of biopolymers such as PLA, PLA-PLLA blends [3], PCL[4], Chitosan [5], PHHX[6], and PU[7] have been prepared via TIPS process. For scaffold preparation, solutions are quenched to low temperature, and solvents are evaporated or freeze-dried to form the scaffolds. In the TIPS process, thermal energy drives liquid-liquid phase separation to form polymer rich and polymer lean phases followed by crystallization in the polymer-rich phase [8]. The final structure of scaffolds depends on the kinetics of phase separation and crystallization [9]. Structure formation in non-isothermal TIPS process depends on quench rate, the concentration of polymer and type of solvent[10]. Hence a study of structure formation during non-isothermal gelation is crucial for determining the final morphology of the scaffold.

While several characterization techniques can be used to study structure formation during sol-gel transition under non-isothermal conditions, rheological methods have been widely deployed for the same purpose for various gels. For example, TIPs process has been investigated using rheology to study gelation of gelatin , maltodextrin and k-Carignan mixed gels [11] , methylcellulose solutions[12] and pectin gels[13] .

In this chapter, the study of non-isothermal gelation kinetics of PHBV sol using small amplitude oscillatory experiments is described. As described in the earlier chapters, PHBV forms UCST type of gels in chlorobenzene upon quenching to lower temperatures. First, initial incipient gelation kinetics is analyzed using the Winter-Chambon criteria. Next, the rapid gelation stage is analyzed using an equation similar to modified Avrami equation. Also, the effect of heating and cooling rate and concentration is presented in this chapter.

4.2 Materials and methods

4.2.1 Materials

Polyhydroxybutyratevalerate (PHBV) random block copolymer (Mw = 4,10,000 g/mol) was procured from Goodfellow, UK. The HV content is 2%. The melting point of PHBV is 160 ^{o}C, and glass transition is 1^{o}C. The solvent chlorobenzene procured from Merck Chemicals, India. The boiling point of chlorobenzene is 130 ^{o}C.

4.2.2 Gel preparation

PHBV solutions with different concentration (0.4, 1, 3, 6 and 10%w/v) were prepared in chlorobenzene. The PHBV solutions are prepared using a hot oil bath at 130 ^{o}C. Upon cooling, the PHBV solutions form a translucent gel. PHBV gels were stored at low temperatures and used when required.

4.2.3 Rheology

Small amplitude oscillatory experiments were performed under non-isothermal conditions. A stress-controlled Anton Paar MCR 301 rheometer with cup and bob geometry was used for the experiments. The various rheological parameters such as storage modulus, loss modulus, damping factor, etc. were determined from the raw data using the in-built software of the rheometer. All experiments were performed in the linear viscoelastic regime so that the network formed during gelation does not break.

4.2.4 Temperature sweep test

Small amplitude oscillatory shear temperature sweep tests were performed at a constant strain amplitude of 0.05% and a constant frequency of 10 rad/s. These tests were performed for different PHBV concentration (0.4, 1, 3, 6 and 10 w/v) at cooling rates of 0.5, 1 and 2 ^{o}C/min. The cooling and heating rates were chosen such that the thermal fixture of the cup and bob geometry of the rheometer ensures linearity of time-temperature relation. The experimental protocol for this test is shown in figure 4.1. The main purpose of this test is to record the changes in linear viscoelastic properties of the material during controlled heating and cooling protocol.

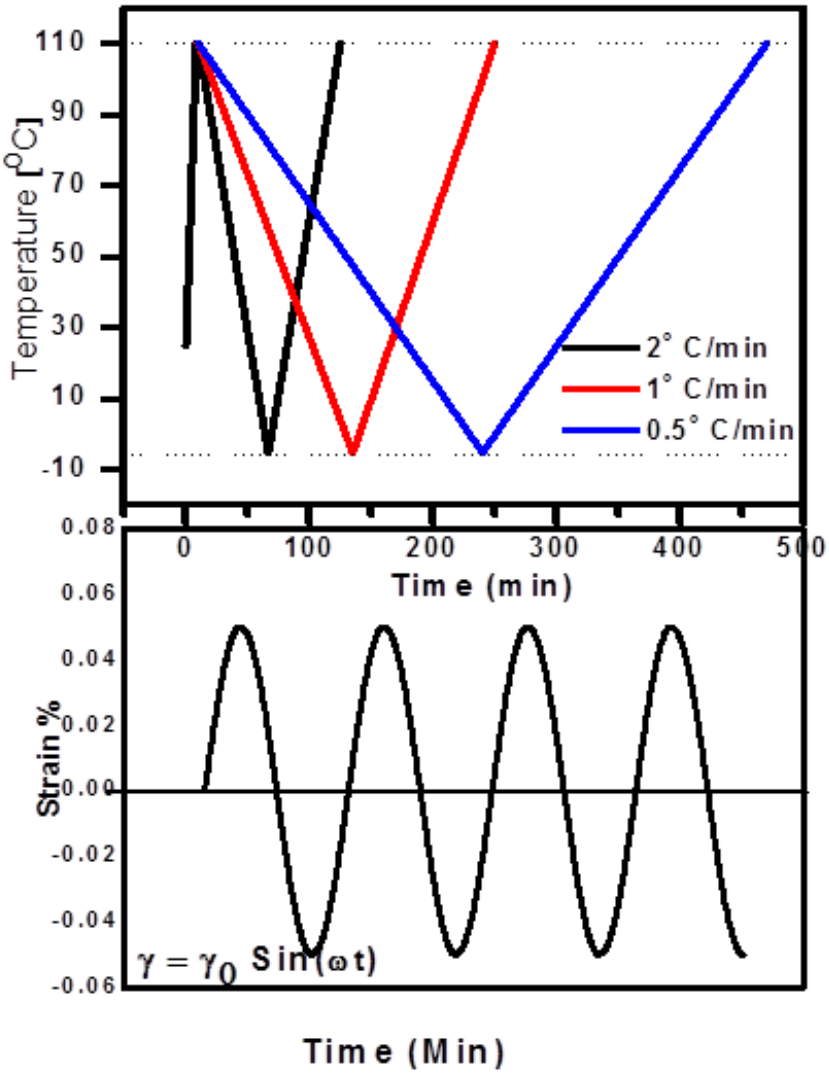

Figure 4.1 Experimental protocol for temperature sweep test at different heating and cooling rate.

4.2.5 Time resolved mechanical spectroscopy

The time resolved mechanical tests were performed under non-isothermal conditions in order to find sol-gel transition temperature. The gel is melted in a cup at 115 ^{o}C to convert it to sol. The sol was cooled down to 6 ^{o}C at 1 ^{o}C/min. During this cooling, quick frequency sweep tests with frequency ranging from 10 rad/s to 60 rad/s at 0.15% strain were performed on the sol. The time required for each frequency sweep is equal to the time to cool down sol by 6 ^{o}C in 6 min i.e., the frequency sweeps were done six times faster than the rate of change in temperature. In other

words, each frequency sweep cycle was performed under nearly isothermal conditions. The protocol was continued till the material completely transformed from sol state to gel state.

4.2.6 Differential scanning calorimetry

Differential scanning calorimetry studies of PHBV gel were performed on TA Instruments DSC Q100. Gel sample was crimped in a hermetically sealed aluminum pan. Non-isothermal heating and cooling cycles were conducted on the sample under inert nitrogen atmosphere. The gel was heated and cooled with 1 ^{o}C/min. PHBV melt pressed film was subjected to thermal analysis for comparative purpose. This sample was heated and cooled at 10 ^{o}C/min.

4.3 Results and discussion

4.3.1 Temperature sweep test

The results of a representative temperature sweep test for PHBV 3% gel are shown in figure 4.2. The evolution of storage and loss moduli as a function of temperature when subjected to cooling and heating rate of 1^{o}C / min are shown in Figure 4.2 a). The DSC thermogram for the same sample during cooling and heating scans at 1^{o}C / min are shown in figure 4. 2 b.

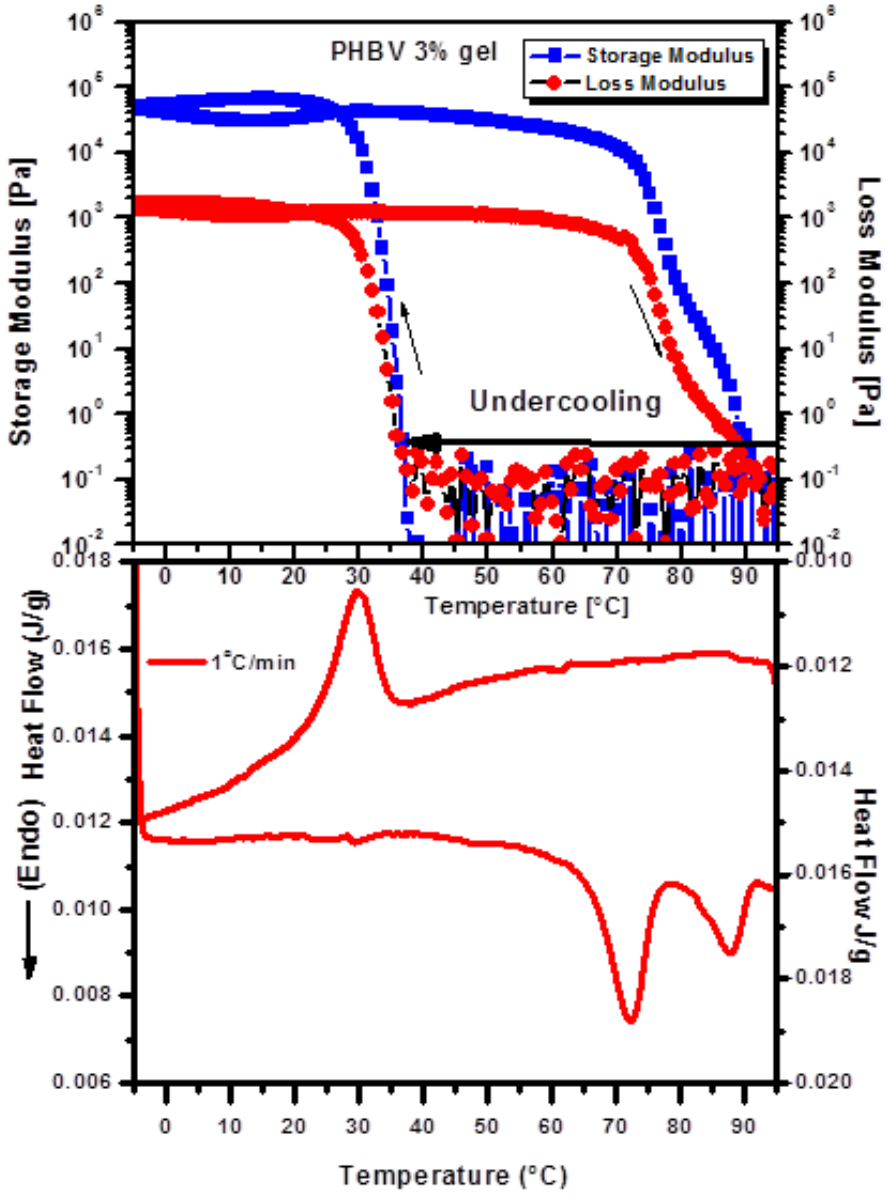

Figure 4.2 a) Storage modulus and loss moduli as a function of temperature for PHBV 3% gel subjected to cooling and heating rates of 1^{o} C/min, b) DSC heating and cooling scans for the same sample at the same heating and cooling rates.

Fig 4.2 a shows that initially at high temperature (>100 ^{o}C), the storage modulus (G'), and loss modulus (G") values are low and the data shows fluctuations since the torque value is below the minimum resolution limit of the rheometer. The sample is a sol and the rheological behavior is expected to be dominated by viscous nature of the sol. This is the first regime of gelation in which incipient phase

separation begins as discussed in the previous chapter. As the temperature decreases, a point comes when G' crosses over G" (G'>G") indicating the beginning of gelation. Each temperature in the figure also represents a degree of undercooling, which is the difference between solvation temperature and the said temperature. For undercooling higher than the cross-over point, both moduli rise rapidly indicating build-up of network structure. This is the second stage of gelation described in the previous chapter. At still higher undercooling, a stage is reached where both moduli start growing much more slowly indicating arrested phase separation. Upon reheating, the gels show a breakdown of the network as indicated by a significant drop in the both the moduli. Interestingly, the drop in moduli shows hints of a two-step process as indicated by a distinct shoulder. The decrease in moduli is seen to occur at a temperature much higher than that where rapid increase in moduli was observed during the cooling cycle. Thus, there is considerable hysteresis in the evolution of viscoelastic moduli during the sol-gel transition. This suggests that the transition is associated with a first-order transition.

Figure 4.2 b shows DSC results of PHBV gels upon cooling from 110 ^{o}C. The data shows an exothermic peak in the temperature range in which G' and G" increase. This peak may be related to the exotherm associated with liquid-liquid phase separation of the sol or with crystallization of PHBV from the polymer-rich phase. Upon heating the gel, we observed a bimodal melting peak in DSC with a temperature corresponding to two-step drop in G' and G". This bimodal melting peaks may be attributed to melting, recrystallization, and melting of lower stability crystals[14]. For comparison, DSC was done on a PHBV melt pressed film as illustrated in figure 4.3 below. The film showed similar melting-recrystallization-melting behavior. It can be seen from the DSC graph of figure 4.2b; there is hysteresis in heating and cooling scan which is also indicative of a first order transition process. Thus, the network formation detected rheologically is correlated with phase separation or crystallization or combination of both. These physical phenomena are first order in nature and capable of creating a sample spanning network. The double melting phenomenon and the corresponding two-stage moduli decrease suggest that the evolution of moduli is likely dictated by crystallization of PHBV.

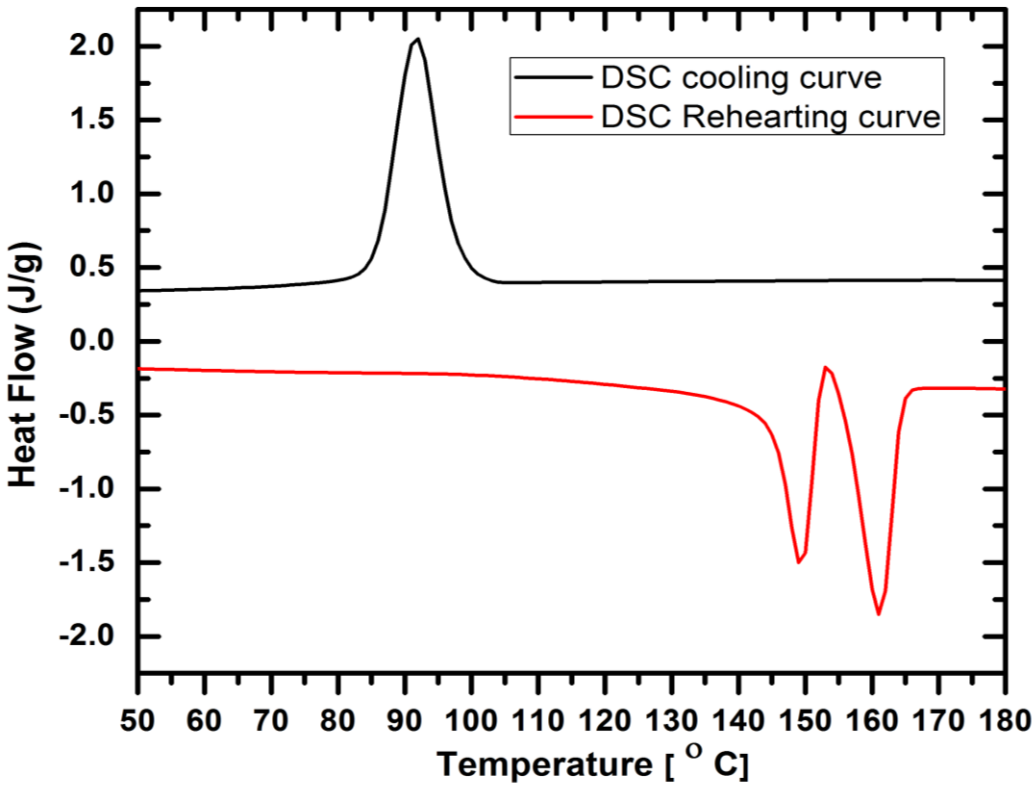

Figure 4.3 DSC thermogram of PHBV melt pressed film.

4.3.2 Time resolved mechanical spectroscopy (TRMS)

In TRMS, frequency sweep on the sample is repeated one after the another during heating and cooling cycles to probe the sol-gel transition. TRMS data of PHBV 10% gel cool and heated with 1 ^{o}C/min is shown in figure 4.4. The raw data was analysed using the procedure of smoothening, fitting and interpolating which was described in detail in the previous chapter.

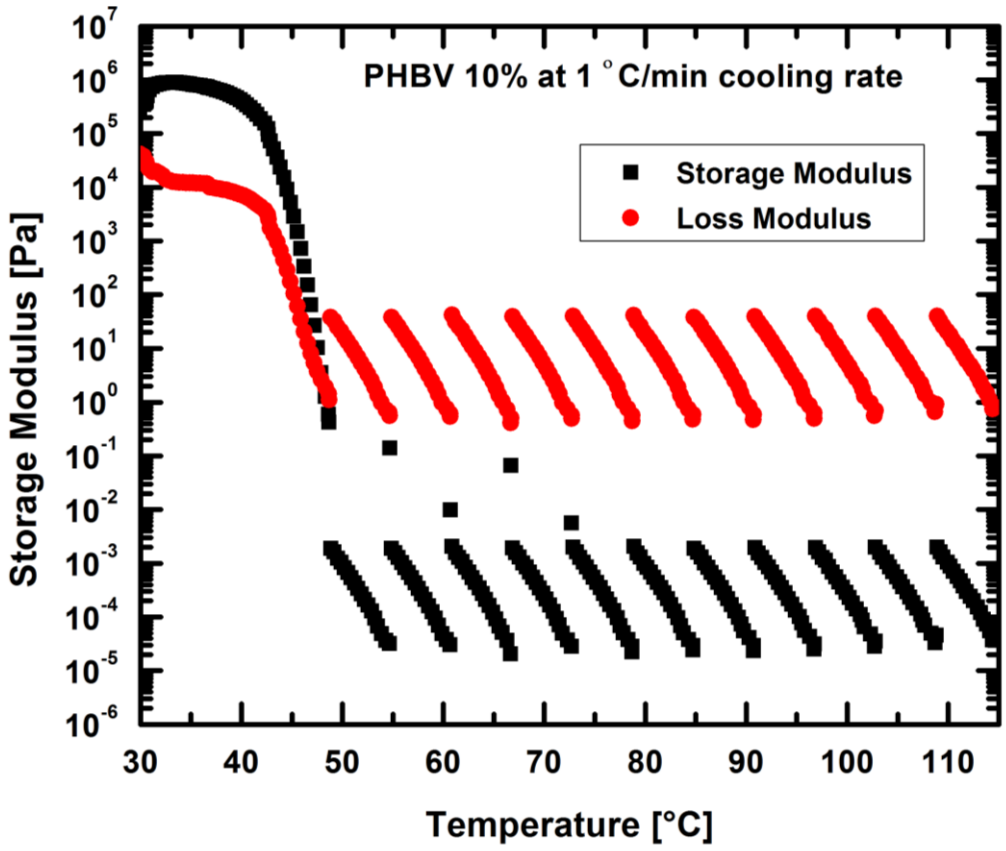

Figure 4.4 Time resolved mechanical spectroscopy test for PHBV 10% gel with 1 ^{o}C/min heating and cooling rate

The TRMS data file contains data at all frequencies as a function of temperature. Since the experiments are temperature dependent. The temperature scale can be converted to the time scale. The data at each discrete frequency as a function of time is separated. Figure 4.5 below shows the damping factor vs. time data for discrete frequencies. It can be seen that the damping factor becomes independent of frequency at a certain time.

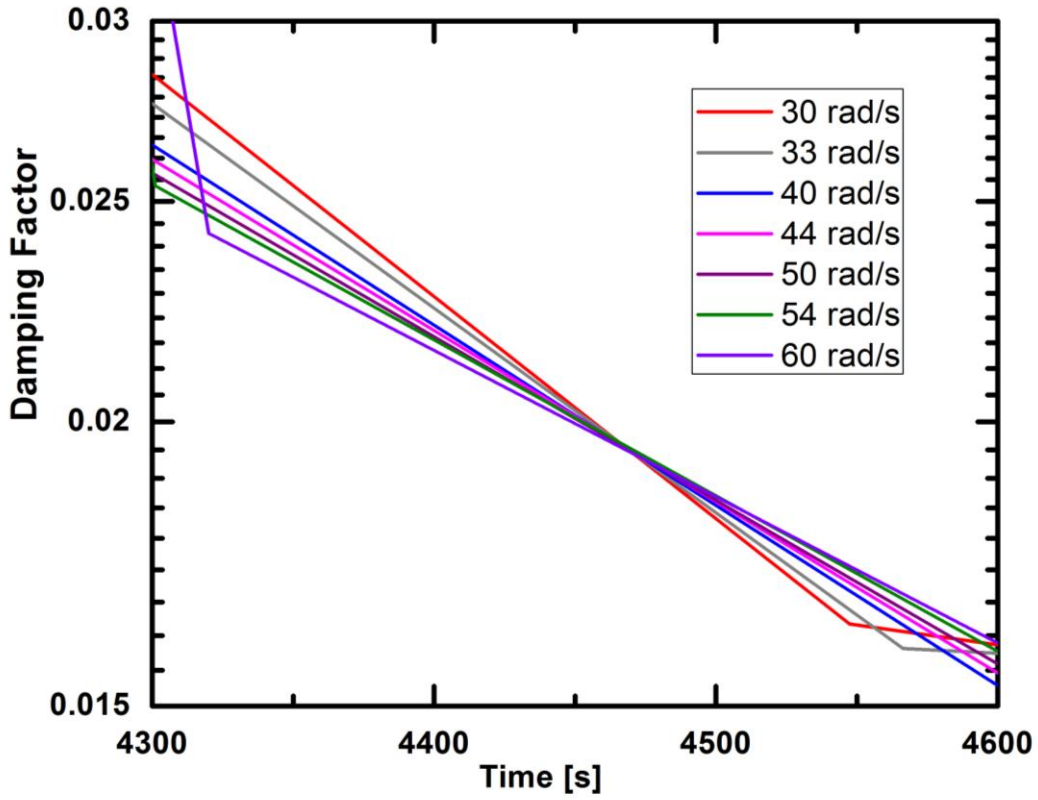

Figure 4.5 Damping factor vs. temperature for PHBV 10% gel

This is the gel point of the system and the temperature corresponding to this time is the sol-gel transition temperature. The gel time is 4467s (74.5 min) and sol-gel transition temperature is 40.5 ^{o}C. As discussed earlier in chapter 3, the value of relaxation exponent and gel strength is calculated from damping factor. The relaxation exponent is found to be 0.01 and strength of gel is around 33300 Pa.s$^{0.01}$. The low value of relaxation exponents and high value of gel strength indicates that the gels are stiff. The low value of relaxation exponent, which is much less than 0.5, suggests that gelation happens after the crossover point of G' and G". Figure 4.6 below illustrates storage and loss modulus as a function of time for discrete frequencies. As can be seen from the figure 4.5, the cross-over time of storage and loss modulus is around 4225 s while the gel time is around 4467 s. As discussed in the earlier chapter, the validity of TRMS procedure depends on whether the mutation number is less than 1. In this TRMS experiment, the mutation number was ~0.001, which is much less than 1.

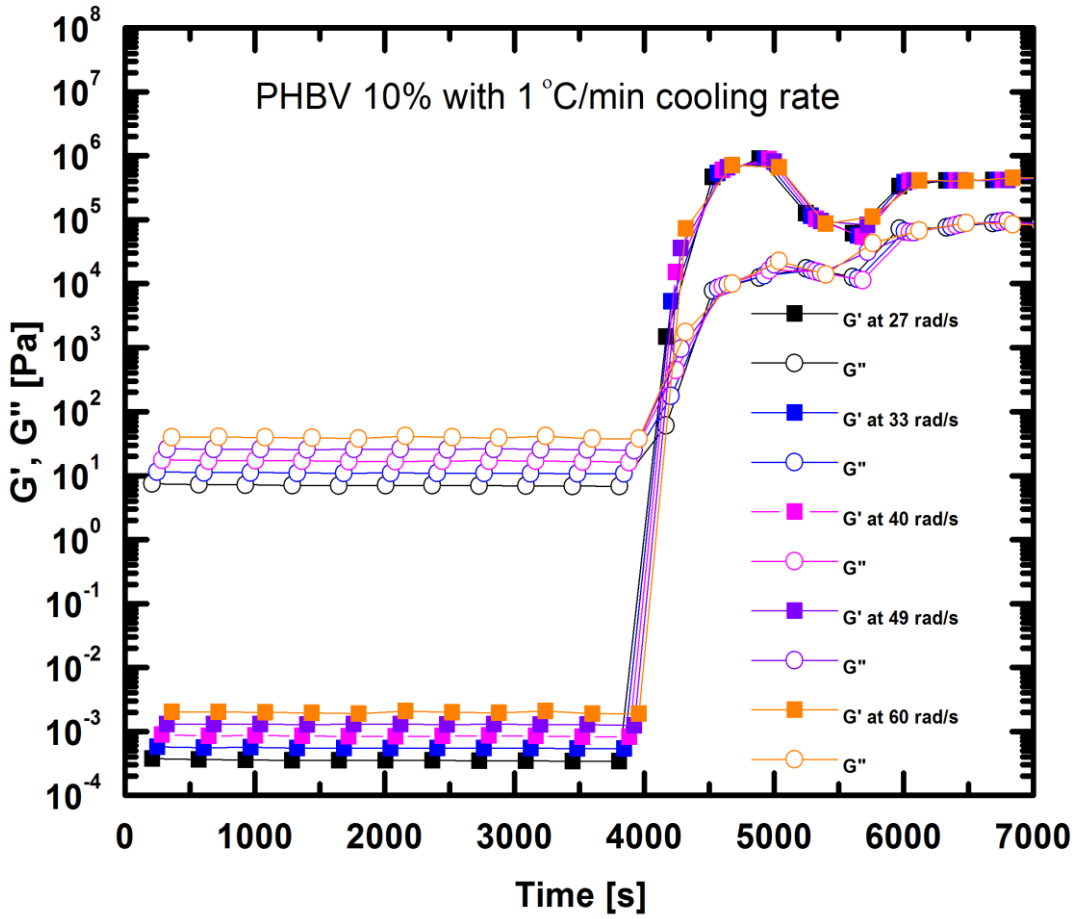

Figure 4.6 Storage and loss modulus as function of frequency for discrete frequency.

It is of interest to compare the non-isothermal gelation results with isothermal results discussed in the earlier chapter. As was discussed in Chapter 3, the gelation time at 75 ^{o}C was about 151 min, whereas the gelation time at 60 ^{o}C was about 43 min. The relaxation exponents were 0.66 and 0.60 at 75 ^{o}C and 60 ^{o}C, respectively. In comparison, non-isothermal gelation occurs at 40 ^{o}C and in about 74 min, and the gel has a much lower exponent. Thus, gelation in non-isothermal conditions occurs at higher undercooling and consequently, the gels are much stiffer than those formed under isothermal conditions.

4.3.3 Effect of concentration

Effect of concentrations at constant heating and cooling rate of 0.5 ^{o} C/min is shown in figure 4.7.

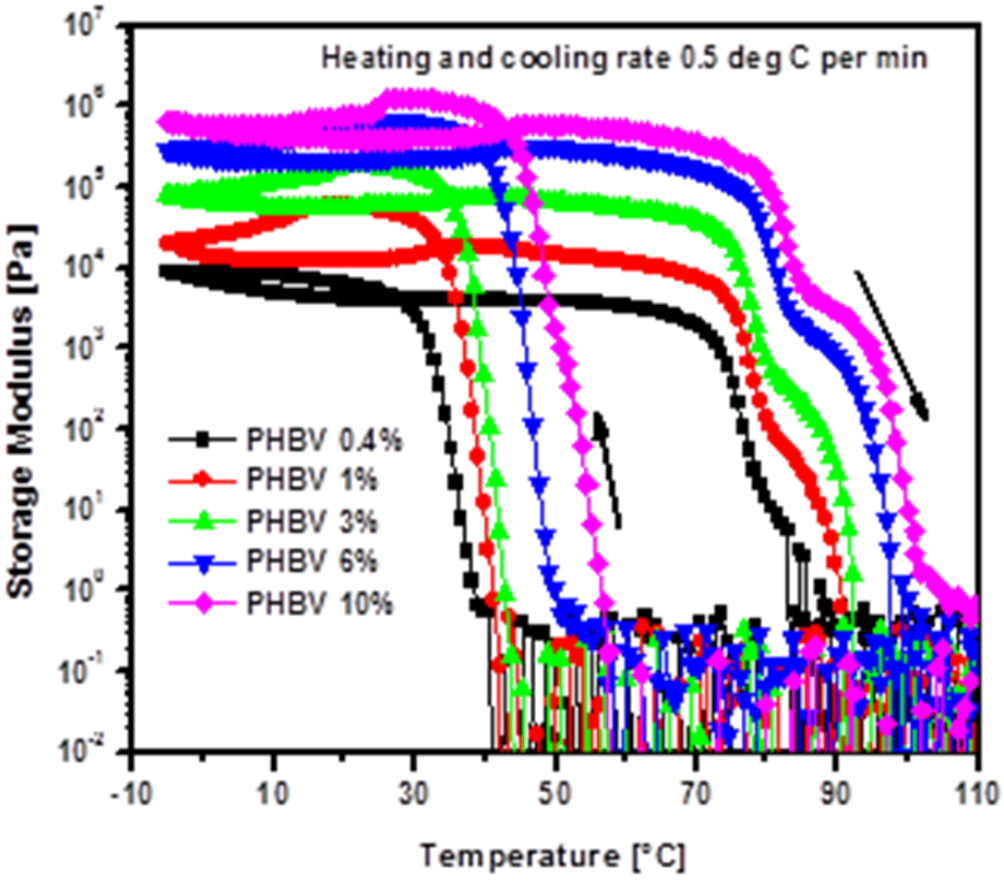

Figure 4.7 Overlay of storage modulus as a function of temperature for PHBV 0.4, 1, 3, 6 and 10%

The cooling cycle shows that lower the polymer concentration, lower are the temperatures at which sol-gel transitions occur during cooling and heating cycles. All heating cycles showed two-step melting.

4.3.4 Effect of cooling and heating rate

The heating rate and cooling rate dependence of sol-gel transition for PHBV 3% gels are shown in figure 4.8 for heating and cooling rates of 0.5, 1 and 2^{o}C/min. Cooling cycles show that the degree of undercooling for structure formation increases with the cooling rate. The heating cycles showed a two-step decrease in moduli for the heating rates of 0.5 and 1^{o}C/min. However, only one step decrease was seen for the 2^{o}C/min heating rate. This is possibly due to insufficient time available for imperfect crystals formed during the faster cooling rate to reorganize and form more

perfect crystals (crystals with greater order such as those having thicker lamellae).

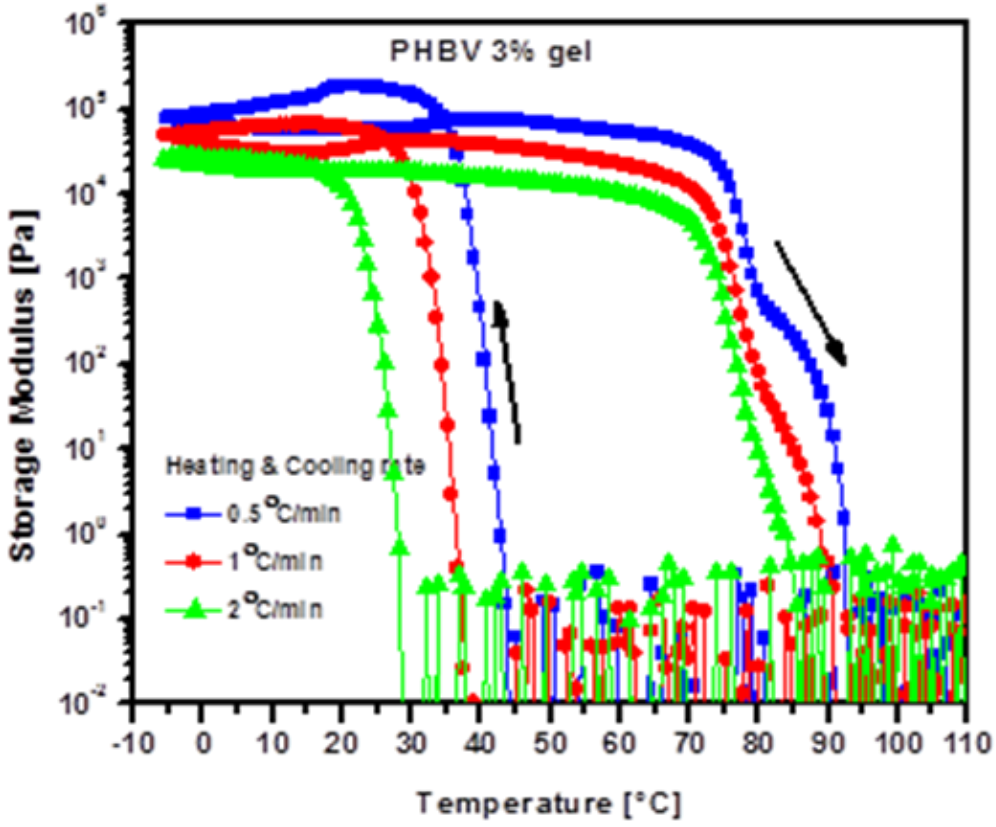

Figure 4.8 Storage modulus of PHBV 3% gel as a function of temperature with heating and cooling rate 0.5, 1, and 2°C/min

4.3.5 Analysis of rapid gelation stage

The rapid growth of moduli (stage II) at lower temperatures for PHBV 3% gel formed under different cooling rates is analyzed using the modified Avrami type model. As discussed in the earlier chapter, the isothermal crystallization process has been very well described by the Avrami equation

$$1 - X_t = e^{-Zt^n}$$

On the other hand, the modified Avrami equation is widely used to study non-isothermal crystallization kinetics [15]. The modified Avrami equation is given by

$$1 - X_t = e^{-Z_t\left(\frac{|T_0 - T|}{\emptyset}\right)^n}$$

and is similar to the Avrami equation. In this equation, the temperature scale is converted to time scale by using the following formula,

$$t = \frac{|\ T - T0\ |}{\phi}$$

Where, ϕ = cooling rate, T= temperature at time t and T_0 = Initial temperature where crystallization begins. In this work, we use an equation similar to the modified Avrami equation for fitting the non-isothermal rheology data.

The rheological equivalent of the Avrami equation is

$$1 - \left(\frac{G(t) - G(0)}{G(P) - G(0)}\right) = e^{-Z_t\left(\frac{|T_0 - T|}{\emptyset}\right)^n}$$

Where,

$\left(\frac{G(t) - G(0)}{G(P) - G(0)}\right)$ is the fractional modulus,

Z_t = rate of phase change

n = Avrami index,

T_0 = temperature at which network structure starts forming,

G(P) = plateau modulus,

G(0) = initial modulus,

G(t) = modulus at time t,

Taking double logarithm on both sides, we get,

$$ln\left(-ln\left\{1-\left(\frac{G(t)-G(0)}{G(P)-G(0)}\right)\right\}\right)=\ln Z_t+n\ln\left(\frac{|T_0-T|}{\emptyset}\right)$$

Hence, plot of ln{-ln (1-[(G(t)-G(0))/(G(P)-G(0))]} vs. ln [(|T0-T|/ϕ)] gives value of Avrami exponent n from slope, and rate can be determined from the intercept. Figure 4.9 shows data for PHBV 3% gel fitted to the modified Avrami equation for the different cooling rates. The inset in the figure shows the corrected rate as a function of cooling rate.

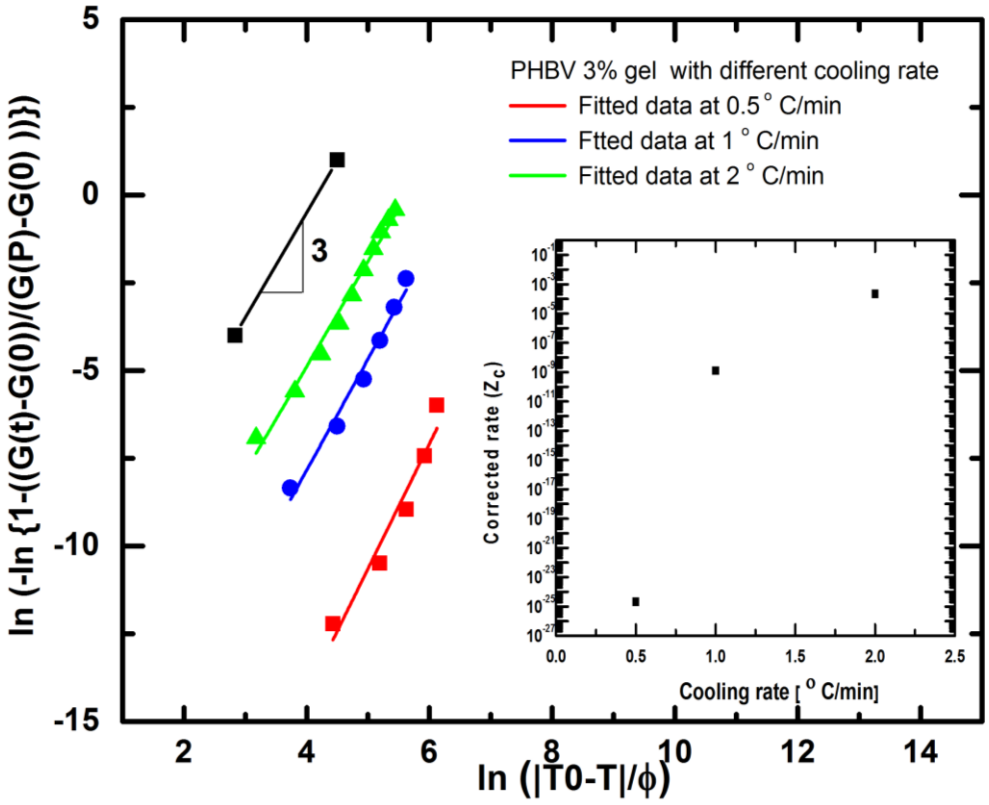

Figure 4.9 PHBV 3% gels non-isothermal data fitted to modified Avrami equation. The inset shows corrected rate (Z_c)vs. Cooling rate for PHBV 3% gel

The slope of the graph gives value of Avrami exponent close to 3 [16] [17] suggesting three-dimensional growth of polymer network. The rate is determined from the

intercept of the above graph. suggested that rate of phase change in a non-isothermal process needs to be appropriately corrected for cooling rate[18]. The rate is corrected using following formula,

$$lnZ_c = \frac{\ln Z_t}{\emptyset}$$

The corrected rate as a function of cooling rate is shown in the inset figure 4.9. It can be seen from the figure 4.9, the rate increases with increase in cooling rate.

3.4 Conclusions

The temperature sweep tests show three stages of gelation in non-isothermal process. In the first stage the state of the sample remains sol as the undercooling increases. At a certain undercooling, which depends on polymer concentration and rate of cooling, the sol starts to convert into a gel. This transition is characterized by crossover of storage and loss moduli, and approximately demarcates the end of the first stage of gelation.

In the second stage of gelation, the viscoelastic moduli increase rapidly. The rapid kinetics of network growth is captured by a rheological equivalent of the empirical Avrami equation that is suitably modified to describe the non-isothermal process. The Avrami exponent was found to be close to 3 suggesting three- dimensional growth of the network. The rate of gelation was found to increase with cooling rate. The third stage of gelation is characterized by slowly rising moduli. In the reverse heating cycle, the gel reverses into sol at a temperature that is higher than the temperature at which gelation happened. The hysteresis of sol-gel transition suggests its first order nature. The conversion into sol is characterized by rapid decrease in the viscoelastic moduli. This decrease occurs in an apparent two-step process. Comparison of rheology data with DSC data shows that gelation is accompanied by an exotherm while liquefaction is accompanied by two endotherms. This suggests that the rheological features are correlated with crystallization of the polymer from the solution. The two melting peaks arise because of the melting-recrystallization-remelting processes. The gel time, transition temperature, relaxation exponent and strength of the gel formed in non-isothermal process are different than for a gel formed under isothermal conditions. In particular, gels formed under non-isothermal conditions are stiffer.

4.5 References

1. Lloyd, D. R., Lim, G. B. & others. Microporous membrane formation via thermally-induced phase separation. VII. Effect of dilution, cooling rate, and nucleating agent addition on morphology. *Journal of membrane science* **79,** 27–34 (1993).

2. Hua, F. J., Kim, G. E., Lee, J. D., Son, Y. K. & Lee, D. S. Macroporous poly (L-lactide) scaffold 1. Preparation of a macroporous scaffold by liquid–liquid phase separation of a PLLA–dioxane–water system. *Journal of biomedical materials research* **63,** 161–167 (2002).

3. La Carrubba, V., Pavia, F. C., Brucato, V. & Piccarolo, S. PLLA/PLA scaffolds prepared via Thermally Induced Phase Separation (TIPS): tuning of properties and biodegradability. *International Journal of Material Forming* **1,** 619–622 (2008).

4. Guarino, V., Guaccio, A., Guarnieri, D., Netti, P. A. & Ambrosio, L. Binary system thermodynamics to control pore architecture of PCL scaffold via temperature-driven phase separation process. *Journal of biomaterials applications* **27,** 241–254 (2012).

5. Roh, I. J. & Kwon, I.-C. Fabrication of a pure porous chitosan bead matrix: influences of phase separation on the microstructure. *Journal of Biomaterials Science, Polymer Edition* **13,** 769–782 (2002).

6. Tsujimoto, T., Hosoda, N. & Uyama, H. Fabrication of porous poly (3-hydroxybutyrate-co-3-hydroxyhexanoate) monoliths via thermally induced phase separation. *Polymers* **8,** 66 (2016).

7. Martinez-Perez, C. A. *et al.* Porous biodegradable polyurethane scaffolds prepared by thermally induced phase separation. *Journal of Advanced Materials (Special Edition)* **1,** 5–11 (2006).

8. Lloyd, D. R., Kim, S. S. & Kinzer, K. E. Microporous membrane formation via thermally-induced phase separation. II. Liquid—liquid phase separation. *Journal of Membrane Science* **64,** 1–11 (1991).

9. Graham, P. D. & McHugh, A. J. Kinetics of Thermally Induced Phase Separation in a Crystallizable Polymer Solution. *Macromolecules* **31,** 2565–2568 (1998).

10. Martínez-Pérez, C. A., Olivas-Armendariz, I., Castro-Carmona, J. S., García-Casillas, P. E. & others. Scaffolds for tissue engineering via thermally induced phase separation. *Advances in Regenerative Medicine: InTech* 275–294 (2011).

11. Eleya, M. O. & Turgeon, S. L. Rheology of κ-carrageenan and β-lactoglobulin mixed gels. *Food hydrocolloids* **14,** 29–40 (2000).

12. Kobayashi, K., Huang, C. & Lodge, T. P. Thermoreversible gelation of aqueous methylcellulose solutions. *Macromolecules* **32,** 7070–7077 (1999).

13. Fu, J. T. & Rao, M. A. Rheology and structure development during gelation of low-methoxyl pectin gels: the effect of sucrose. *Food Hydrocolloids* **15,** 93–100 (2001).

14. Lai, M. *et al.* The morphology and thermal properties of multi-walled carbon nanotube and poly (hydroxybutyrate-co-hydroxyvalerate) composite. *Polymer International* **53,** 1479–1484 (2004).

15. Zhang, Z., Xiao, C. & Dong, Z. Comparison of the Ozawa and modified Avrami models of polymer crystallization under nonisothermal conditions using a computer simulation method. *Thermochimica acta* **466,** 22–28 (2007).

16. Sperling, L. H. *Introduction to physical polymer science*. (John Wiley & Sons, 2005).

17. Hiemenz, P. C. & Lodge, T. P. *Polymer Chemistry: The Basic Concepts*. (Taylor & Francis, 1984).

18. Jeziorny, A. Parameters characterizing the kinetics of the non-isothermal crystallization of poly(ethylene terephthalate) determined by d.s.c. *Polymer* **19,** 1142–1144 (1978).

Chapter 5

Dynamic Light Scattering on Gels

Dynamic light scattering experiments are performed during the transformation from sol state to gel state under isothermal conditions. We have used similar experimental protocols for rheological and dynamic light scattering experiments on PHBV 1% gel under isothermal conditions in order to understand the structural and mechanical changes associated with gelation. PHBV sols were quenched to 42 and 50 ^{o} C and autocorrelation function vs. lag time was determined for a various time during sol-gel transition under isothermal condition. The autocorrelation function data during sol-gel transformation correlated with rheological data.

5.1. Introduction

Dynamic light scattering (DLS) is widely used for studying thermal motions of particles (scatterers) in solution. Temporal data of scattering intensity due to mobile scatterers is used to determine diffusion coefficient and size of the scatterers as summarized below. DLS has been used to study dynamics of various systems such as gels[1 2 3 4], suspensions[5 6 7 8], microphase separation[9], etc.

The raw data of DLS is used to determine the autocorrelation function using the Siegart relation[10 11]

$$g_{2(\tau)} = B[1 + \beta|g_1(\tau)|^2$$

Here, the electric field correlation function $g_1(\tau)$ for monodisperse scatterers is related to lag time τ and by the following equation [12 13] ,

$$g_1(\tau) = e^{-\Gamma\tau}$$

Where,

$$\Gamma = Dq^2$$

D = Diffusion coefficient and q = scattering vector,

The scattering vector is given by

$$q = \frac{4\pi n \sin\frac{\theta}{2}}{\lambda}$$

Where n = refractive index,

θ = scattering angle,

λ = wavelength of the laser.

The hydrodynamic radius of the scatterers can be determined from the diffusion coefficient using Stoke-Einstein equation :

$$D = \frac{K_B\, T}{6\pi\eta R}$$

Where,

K_B = Boltzmann constant.

T = Temperature,

η = Viscosity of solvent,

R= Size (effective radius) of the scatterers.

5.2 Materials and methods

Ludox (30 % silica particles dispersed in water) was procured from Sigma Aldrich, USA. PHBV is procured from Good fellow UK; toluene and chlorobenzene is procured from Merck chemicals India. Chlorobenzene, toluene and deionized water were filtered thrice using 0.2 micrometer PTFE filter in order to remove dust and suspended contaminants. PHBV 1% gel was prepared as per the procedure given in section 3.2.2.

5.2.1 Dynamic light scattering setup in CSIR-NCL

A home-built experimental setup for DLS is shown in figure 5.1.

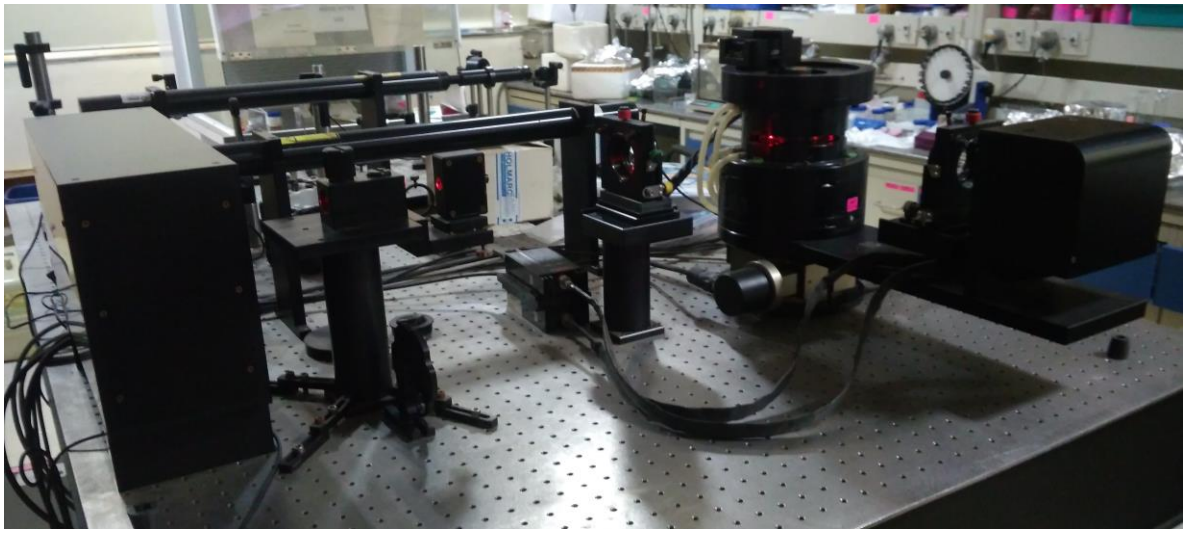

Figure 5.1 Dynamic light scattering setup in CSIR-NCL

A Helium-Neon Laser with wavelength 632 nm (32mW) was used for the experiment. This laser beam was split into two laser beams using a beam splitter. A glass VAT containing filtered toluene solution acts as the sample holder. The toluene solution has a refractive index close to the glass of the VAT. The VAT is heated and cooled with an external water circulatory system (Julabo). The sample is taken in a glass cuvette and kept inside the VAT. The two laser beams were aligned to intersect inside the sample cuvette so as to create a scattering volume. Due to Brownian motion, the scatterers in the sample diffuse inside the scattering volume and consequently, the recorder records fluctuations in scattered light intensity. The temporal fluctuations lead to a speckle pattern as a function of time. Figure 5.2 below shows a schematic of fluctuations of light intensity as a function of time.

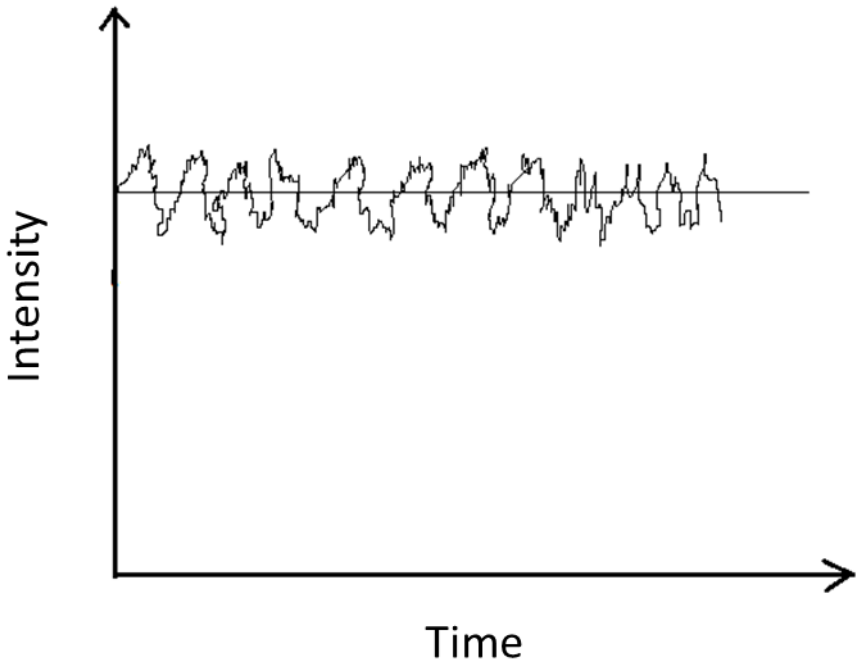

Figure 5.2 Intensity fluctuations as a function of time

The digital correlator, which is a signal comparator, correlates the intensity within time interval t and t+dt. In autocorrelation, correlator compares the signal with itself. Over short time duration, the intensity fluctuations are correlated. However, the fluctuations decorrelate for long time duration. The decay in autocorrelation gives a

time constant, which is related to the diffusion coefficient of the scatterer, and hence its size.

5.2.2 Dynamic light scattering experiment on Ludox

As standard calibration procedure, 3D DLS experiment was performed on Ludox (30% colloidal silica of 12 nm size dispersed in water) at room temperature and 50 ^{o} C. Approximately 200 microliters of colloidal silica solution dispersed in 5 ml of filtered DI water was taken in the DLS cuvette. The sample was then placed in the VAT for measurements. The scattered light intensity was measured at 90 ^{o} scattering angle and recorded for 1 minute. The sample was scanned thrice. The normalized intensity autocorrelation function was fitted using Matlab subroutine. The diffusion coefficient and hydrodynamic radius were calculated by fitting the decay of autocorrelation function as described earlier.

5.2.3 Dynamic light scattering (3D DLS) on PHBV gels

PHBV gels were prepared in the cup geometry of Physica MCR 301 rheometer. This allowed us to have good control on thermal history of gelation. The gels were prepared as follows. Silicone oil was poured into the cup and the DLS cuvette containing the sample was dipped in the oil. The cuvette was covered tightly with Teflon tape. The sample was heated to 110 ^{o} C in order to convert gel into sol. The sol was then cooled at 5 ^{o} C /min to a temperature 10 ^{o} C higher than quenched temperature. Once solution reached this temperature, the cuvette was quickly transferred into the 3D DLS VAT, which was already preheated and maintained at the quench temperature. DLS experiment was commenced. The scattered light intensity was measured at the scattering angle of 90 ^{o}. The cuvette was continuously rotated clockwise at 0.5 rpm during measurement. Intensity fluctuation raw data was recored continuously till the material completely transformed from the sol state to gel state. Data analysis was done for raw data collected over 1 min interval, and this was repeated for different time intervals during gelation such as 10 min, 20 min, 30 min, 60 min, 90 min, 120 min and 150 min. The correlator correlates the scattering light intensity and gives the autocorrelation function. The autocorrelation data was normalized with initial data for comparison. The experimental data were fitted to three modes of exponential decay function.

5.2.4 Rheology (Isothermal Time Test)

Rheology of PHBV 1% gel was studied using cup and bob geometry of Physica MCR 301 rheometer. The gel was melted in a cup at 110 ^{o} C, cooled at 5 ^{o} C/ min and quenched to 42 ^{o} C. Small amplitude oscillatory shear test was performed as a function of time using 0.05% strain amplitude and 10 rad/s angular frequency. The time-dependent evolution of viscoelastic moduli was measured as a function of time.

5.3 Results and discussions

5.3.1 Dynamic Light Scattering on Ludox sample

The autocorrelation function as a function of lag time is shown in figure 5.3 for three samples of the standard Ludox solution. The autocorrelation data for all three samples match well. The autocorrelation function can be fitted to a single exponential decay function suggesting monodispersity of particle size. The particle size calculated from the autocorrelation decay using Stokes-Einstein equation (12.6 nm) matched well with the particle size of the sample supplied by the manufacturer. Thus, the 3D DLS equipment was well calibrated.

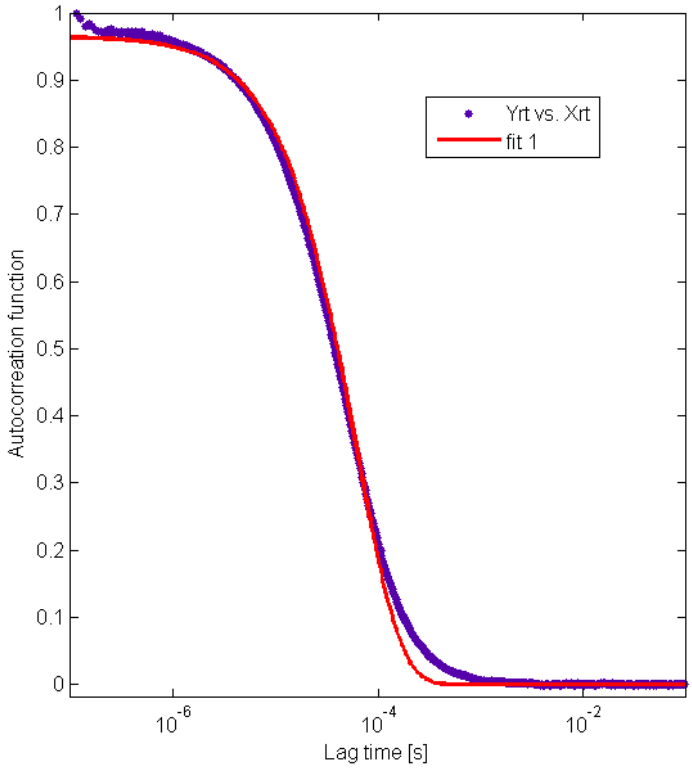

Figure 5.3 Autocorrelation function vs lag time for Ludox particle

5.3.2 Correlation of dynamic light scattering and rheology

As discussed in the earlier chapters, there are three regimes of gelation: the initial induction phase and incipient gelation phase (I), the rapid gelation phase (II) and the arrested phase (III). Figure 5.4 a shows the autocorrelation function vs. lag time during sol-gel transformation and figure 5. 4b shows viscoelastic moduli as a function of time during isothermal time sweep test for PHBV 1% gel quenched to 42 ^{o} C.

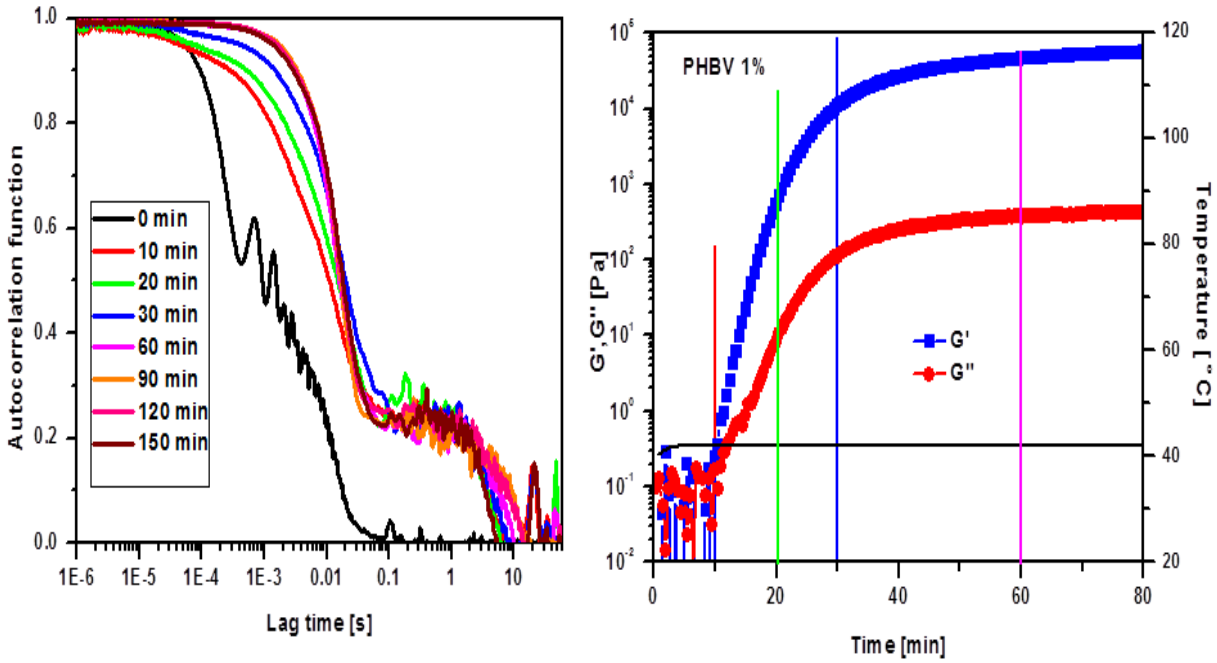

Figure 5.4 PHBV 1% gel at 42^{o}C a) Autocorrelation functions vs. lag time during gelation, b) Rheology of the isothermal test during gelation. (Note: the vertical color lines on the time axis in figure 5.4b correspond to the times where autocorrelation function was measured and shown in figure 5.4a

It can be seen from figure 5.4b that immediately upon quenching to 42 ^{o}C, the sample is in sol state. The moduli fluctuate significantly since the measured torque is below resolution limit of the transducer. Corresponding to this time in figure 5.4 a, the autocorrelation function decays completely indicating rapid diffusive motion of the structural units in the sol, which correlates with the predominantly viscous nature of the sample. After 10 min from reaching quench temperature, figure 5.4b shows

crossover of G' and G" indicating incipient gelation and formation of sample spanning network structure. Correspondingly in the DLS data at this time, a delay in the autocorrelation function can be observed together with the appearance of a distinct plateau, which is a clear signature of gelation. The delayed decay of autocorrelation function indicates growth of scattering entities. Between 10 min and 30 min, rapid rise in the viscoelastic moduli suggests fast growth of the network structure. This is the regime II of gelation. After about 40 min, the growth rate of viscoelastic moduli G' and G" decreases suggesting arrest of the network structure. This is the third regime of gelation (III). As can be seen in figure 5.4 a, the decay time of the autocorrelation function increases in regime (II) of gelation and continues till about 60 min, which suggests increase in sluggishness of motion of the network. Thus, as the network grows and strengthens, its dynamic rearrangement also slows down. Beyond 60 min, figure 4a shows that the autocorrelation function also does not change suggesting that the network structure gets arrested.

The autocorrelation data in figure 5.4a could be fitted to a three-mode exponential decay function with three time constants corresponding to a fast mode, an intermediate mode, and a slow mode. The fits are shown in figure 5.5 below.

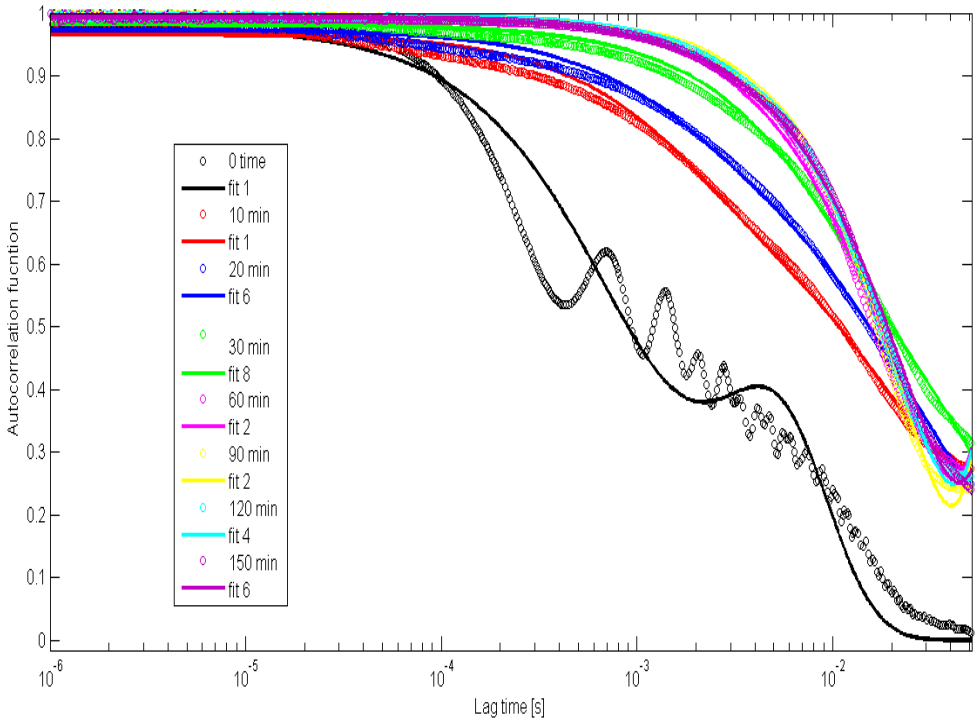

Figure 5.5. Fitting of autocorrelation function with a 3-time constant exponential

decay function $F(\tau) = a*\exp(-b*\tau) + c*\exp(-d*\tau)+e*\exp(-f*\tau)$, where a-e are fitting constants with b, d and f being decay time constants and a, c and e are preexponential factors.

Similar results were obtained for PHBV 1% gel formed at quench temperature of 50 ^{o} C. Figure 5.6 shows the autocorrelation function and isothermal rheological data for this gel. At shorter times below 20 min, the viscoelastic response shows predominantly viscous behavior while the autocorrelation function decays rapidly. After 20 min, the viscoelastic moduli grow rapidly while the time constant of decay of autocorrelation function increases with waiting time. It also shows an intermediate plateau before decaying fully. The height and width of the intermediate plateau does not seem to change with waiting time in a consistent manner. After long time beyond 150 min, the autocorrelation function does not change any further. Also, the viscoelastic moduli almost reach a plateau value.

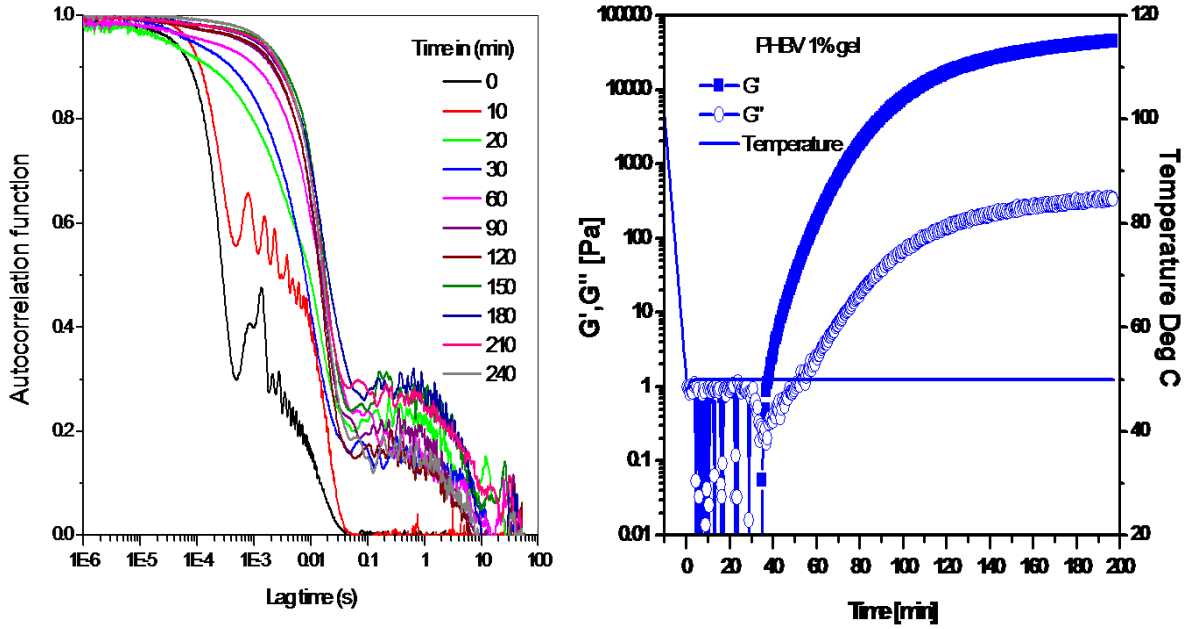

Figure 5.6 PHBV 1% gel at 50 ^{o}C. a) Autocorrelation functions vs. lag time during gelation, b) Rheology of the isothermal test during gelation

The autocorrelation data for this gel can also be fit to a three mode exponential decay

function and the fits are shown in figure 5.7.

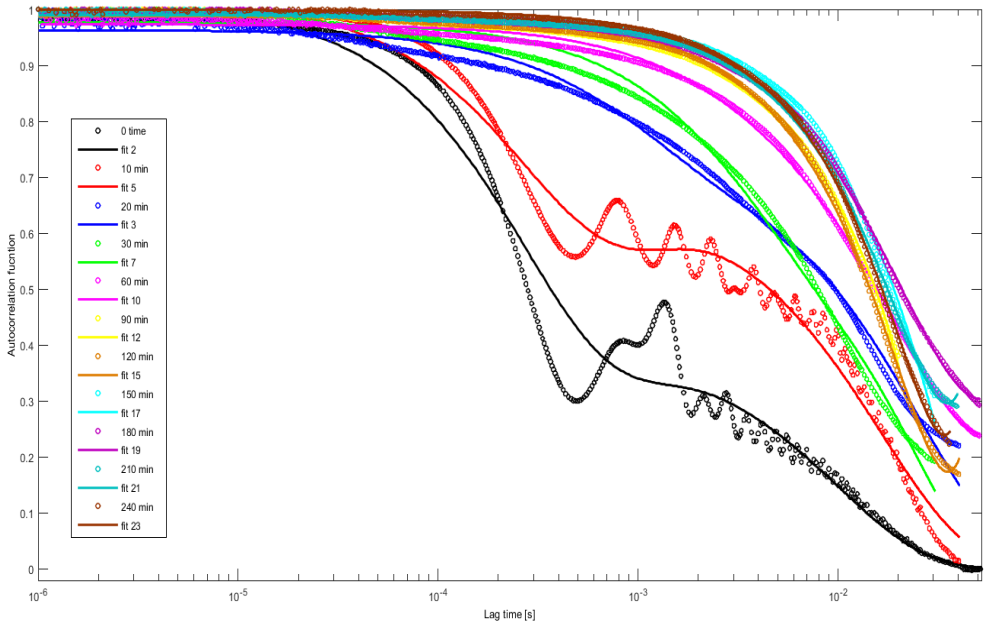

Figure 5.7 PHBV autocorrelation data fitted to three mode exponential decay function

5.3.4 Kinetics of gelation

Figure 5.8 shows the comparison of isothermal time sweep data for PHBV 1% gel quenched to 42 and 50 ^{o} C. As expected, the kinetics of gelation for the PHBV 1% gel quenched to 50 ^{o} C is slow as compared to the gel formed by quenching at 42 ^{o} C .

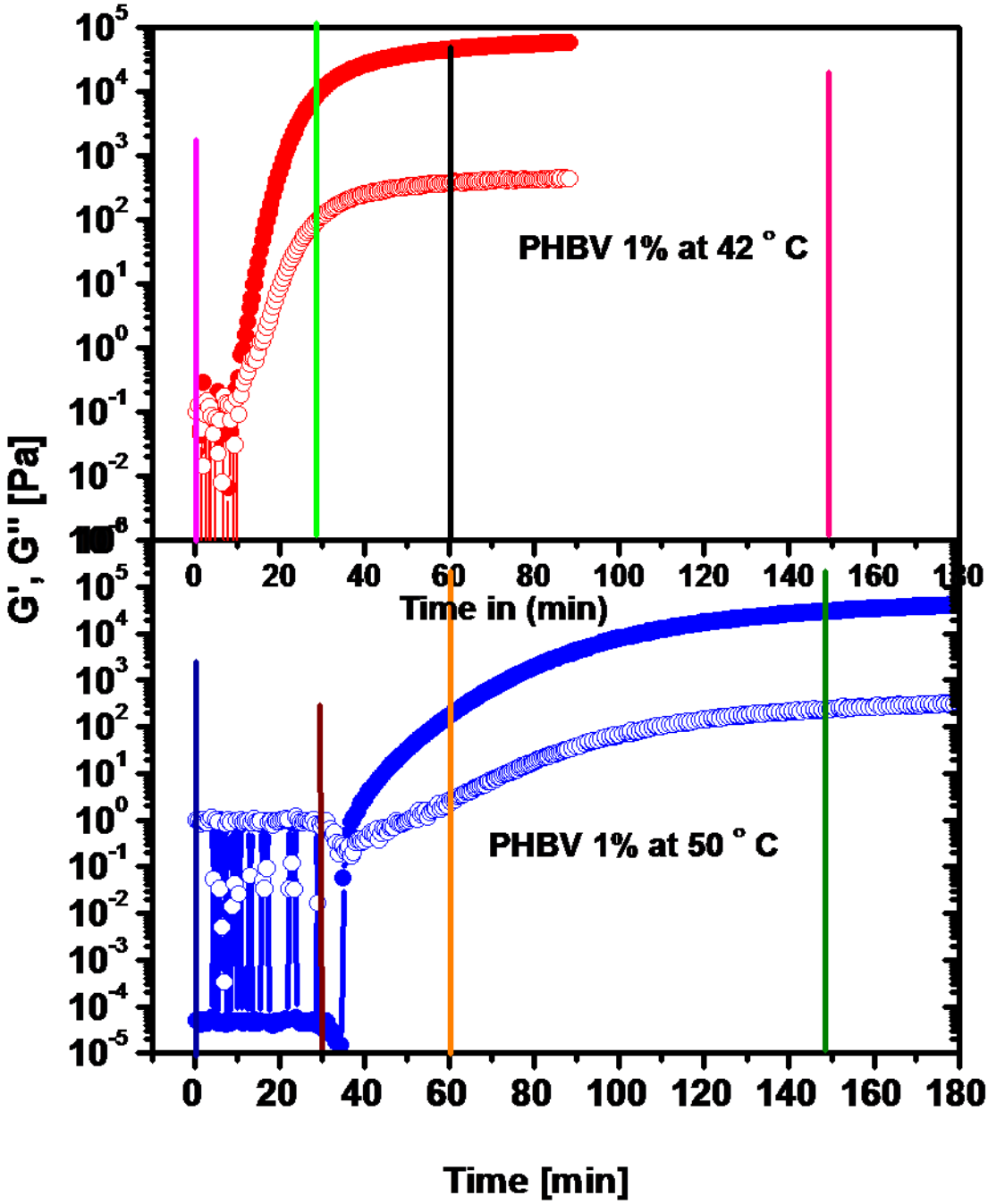

Figure 5.8 G', G" vs. time for PHBV 1% gel quenched to a) 42 °C and b) 50 °C

Figure 5.9 shows comparison of autocorrelation functions for the PHBV 1% gels quenched to 42 and 50 °C at different time intervals after quenching. The colors of

the lines used to depict autocorrelation functions in figure 5.9 correspond to the vertical lines shown in figure 5.8 for demarking the different time intervals for the respective quench temperatures.

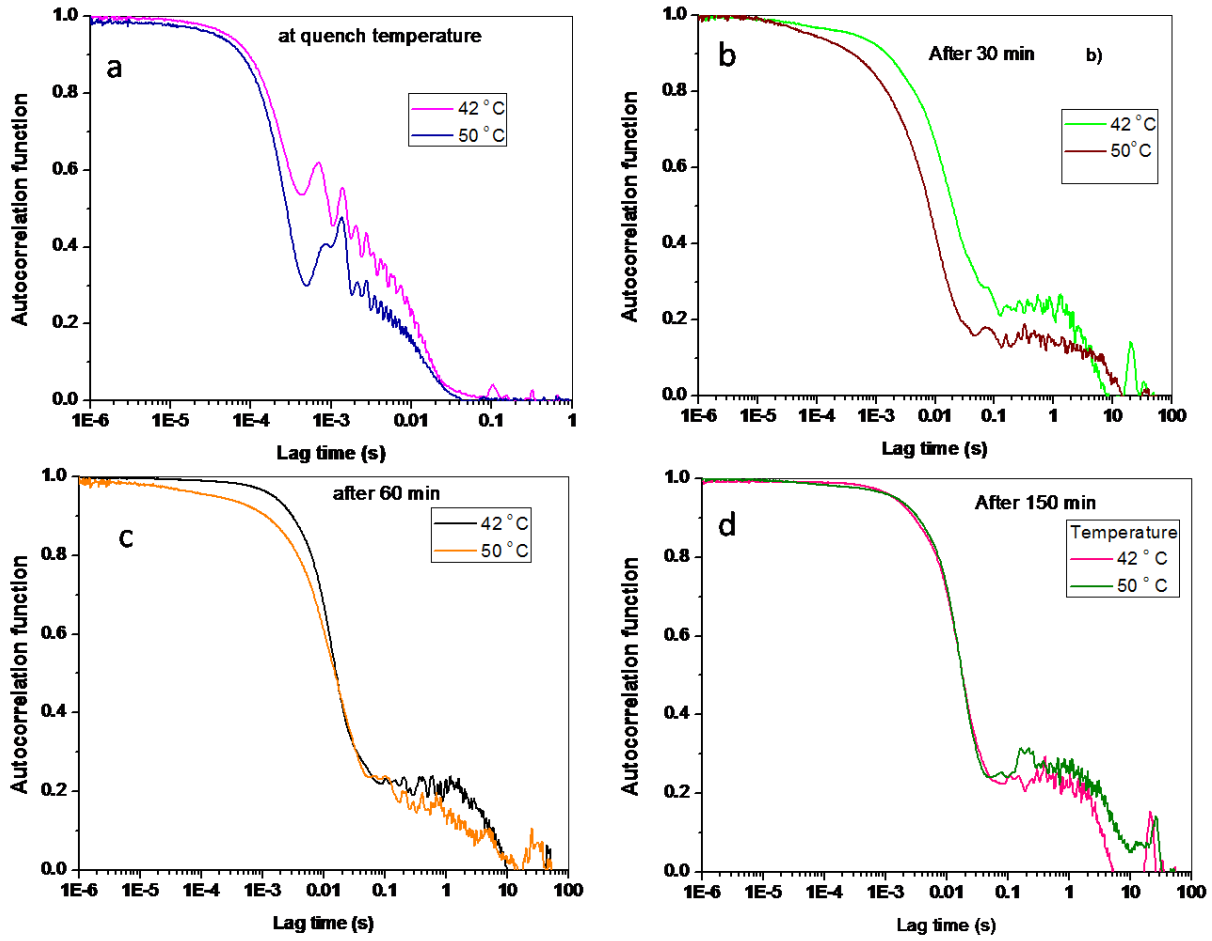

Figure 5.9 Comparison of the autocorrelation function of PHBV 1% gel quenched to 42 and 50 ^{o} C during gelation after a) 0 time, b) 30 min, C) 60 min and d) 150 min

It can be observed from figure 5.9 that immediately upon quenching the autocorrelation function for the PHBV gel formed by quenching at 50 ^{o}C decays slightly faster compared to the gel formed by quenching at 42 ^{o}C. After 30 min, the autocorrelation function for PHBV 1% gel formed at 42 ^{o}C shows delayed decay compared to the gel formed at 50 ^{o}C . After 60 min, the moduli of PHBV gel formed at 42 ^{o}C increase very slowly i.e., the phase separation in this gel has been arrested (regime III), while for the PHBV gels formed at 50 ^{o}C its moduli are still growing i.e.,

the gelation is in regime II. Correspondingly, the decay time constant of autocorrelation function for the gel formed at 42 ^{o}C has stopped increasing and is higher than the decay time constant for the gel formed at 50 ^{o}C. Eventually after 150 min, where the network growth is arrested for both gels, it can be observed that the autocorrelation functions for both gels match and there is no further change in them due to the arrested motion of the network.

5.4 Conclusions

Dynamic light scattering experiments were performed on PHBV gels during isothermal gelation experiments. PHBV 1% gel was quenched to two temperatures, 42 ^{o}C and 50 ^{o}C. DLS data was acquired continuously and analysed for different waiting times. The same gels were also subjected to isothermal dynamic oscillatory time sweep tests in the linear viscoelastic regime. The 3D-DLS equipment was calibrated using a dilute suspension of monodisperse 12 nm silica particles. The data for this sample shows a single exponential decay in the autocorrelation function, which upon analysis by Stokes-Einstein equation gave a particle size that matched the size provided by the manufacturer. DLS data for the PHBV sample during sol-gel transition showed three characteristic features in the three regimes of gelation. In regime I, where the viscoelastic data shows a predominant viscous behavior, the DLS data correspondingly showed one-step decay of the autocorrelation function with small time constant. At longer times, when gelation occurs in regime II, the viscoelastic moduli grow rapidly and the autocorrelation function shows an intermediate plateau in decay while at the same time the time constant for decay increases with waiting time. At still longer time, when the viscoelastic moduli show very slow growth in regime III, the autocorrelation function no longer changes. Thus, there is reliable correlation between the gelation regimes, the corresponding changes in viscoelastic moduli and the DLS data.

5.5 References

1. Shibayama, M., Fujikawa, Y. & Nomura, S. Dynamic light scattering study of poly (N-isopropylacrylamide-co-acrylic acid) gels. *Macromolecules* **29,** 6535–6540 (1996).

2. Tosh, S. M., Marangoni, A. G., Hallett, F. R. & Britt, I. J. Aging dynamics in gelatin gel microstructure. *Food Hydrocolloids* **17,** 503–513 (2003).

3. Djabourov, M., Lechaire, J.-P. & Gaill, F. Structure and rheology of gelatin and collagen gels. *Biorheology* **30,** 191–205 (1993).

4. Cipelletti, L., Manley, S., Ball, R. C. & Weitz, D. A. Universal aging features in the restructuring of fractal colloidal gels. *Physical review letters* **84,** 2275 (2000).

5. Kroon, M., Wegdam, G. H. & Sprik, R. Dynamic light scattering studies on the sol-gel transition of a suspension of anisotropic colloidal particles. *Physical Review E* **54,** 6541 (1996).

6. Van Megen, W. & Pusey, P. N. Dynamic light-scattering study of the glass transition in a colloidal suspension. *Physical review A* **43,** 5429 (1991).

7. Urban, C. & Schurtenberger, P. Characterization of turbid colloidal suspensions using light scattering techniques combined with cross-correlation methods. *Journal of colloid and interface science* **207,** 150–158 (1998).

8. Hassan, P. A., Rana, S. & Verma, G. Making sense of Brownian motion: colloid characterization by dynamic light scattering. *Langmuir* **31,** 3–12 (2014).

9. Osaka, N. *et al.* Micro- and Macrophase Separations of Hydrophobically Solvated Block Copolymer Aqueous Solutions Induced by Pressure and Temperature. *Macromolecules* **39,** 5875–5884 (2006).

10. Furukawa, H. & Hirotsu, S. Dynamic light scattering from static and dynamic fluctuations in inhomogeneous media. *Journal of the Physical Society of Japan* **71,** 2873–2880 (2002).

11. Kätzel, U., Vorbau, M., Stintz, M., Gottschalk-Gaudig, T. & Barthel, H. Dynamic light scattering for the characterization of polydisperse fractal systems: II.

Relation between structure and DLS results. Particle & Particle Systems Characterization **25,** 19–30 (2008).

12. Pecora, R. Dynamic light scattering: applications of photon correlation spectroscopy. (Springer Science & Business Media, 2013).

13. Li, J., Ngai, T. & Wu, C. The slow relaxation mode: from solutions to gel networks. Polymer journal **42,** 609 (2010).

Chapter 6

Recommendations for further work

6.1 Oscillations in autocorrelation function

Figure 6.1 below show PHBV 1% data at 50 ^{o}C . Initial autocorrelation data of PHBV 1% gel at 50 ^{o}C shows oscillations in autocorrelation function

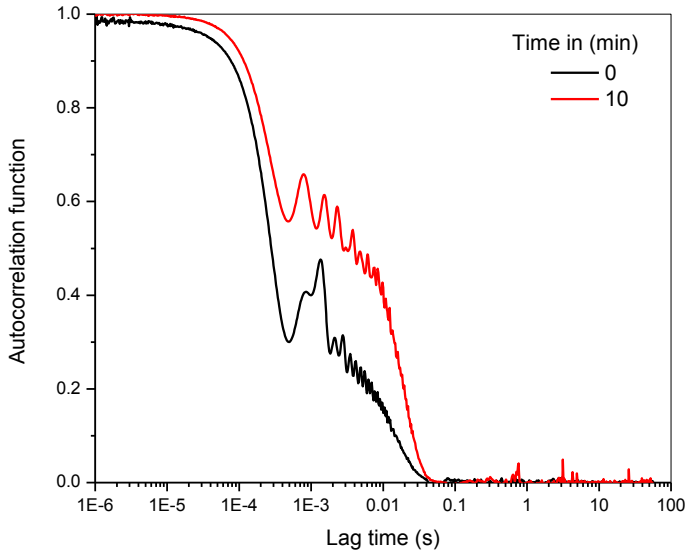

Figure 6.1: autocorrelation function of PHBV 1% gel at 50 ^{o}C

We performed the DLS experiments at 50 ^{o}C on Ludox sample. The autocorrelation function of the Ludox sample at 50 ^{o}C shown in figure 6.2 below. The autocorrelation functions do not show any oscillations

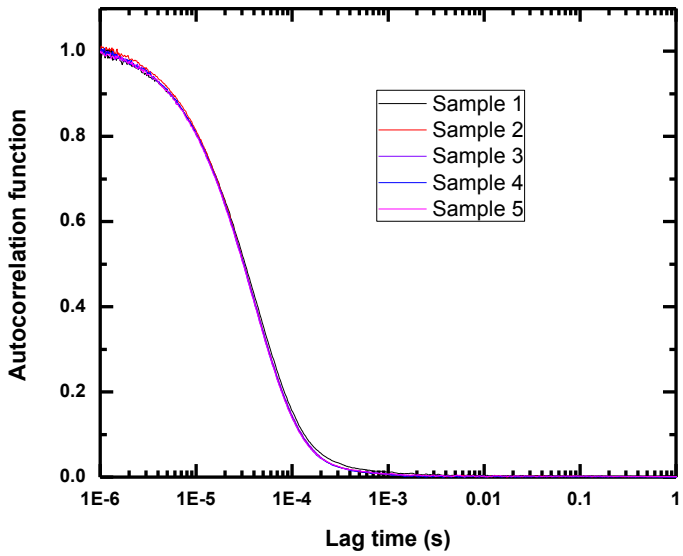

Figure 6.2 Autocorrelation function of Ludox sample at 50 ^{o}C.

The DLS data at high temperature do not show any oscillations in autocorrelation function. These oscillations may be response from the sample. It is proposed to do the systematic study on PHBV gels at different scattering angles on these gels to find out the origin of these oscillations.

List of Publications

1. Bile acid hydrazides: gelation, structural, physical and spectroscopic properties., Dr. Vandana Pore, SandipAglave, Prashant Patil, ShrikantPharande, New Journal of Chemistry, 2015,39, 453-460.

2. Characterization of copolymer Poly (hydroxybutyrate-co-hydroxyvalerate) produced by HalomonasCampisilas its biodegradability and potential application."Prashant Patil, Dr. Jyoti P. Jog, Snehal Kulkarni, PradnyaKanetkar, SmitaNilegaonkar, Seema Sarnaik, Pranav Khshirsagar, Bioresource Technology, 102, 2011, 6625-6628.

3. Poly (4-methyl, 1-pentene)/MWNT nanocomposites Prashant Patil, Dr. Jyoti P. Jog, Dr. Santosh Wanjale, e- Polymers, 2008, 079, 1-13.

Oral/Poster Presentations

1. Thermoreversible gelation in PHBV, Prashant Patil, Dr. Ashish Lele, Dr. Jyoti Jog. Macro 2015, IACS, Kolkata.

2. “Gelation in PHBV solutions” in XVIth International congress on rheology" , 5th August 2012 to 10th August 2012 held at Lisbon Portugal.

3. "Electrospun scaffolds of PHB” in Advanced Polymeric Materials, 2010 held at Central Institute of Plastics Engineering and Technology, Bhubaneswar.